Investigation of cervical remodeling during pregnancy with *in vivo* Raman spectroscopy

By
Christine Mary O'Brien

Dissertation
Submitted to the Faculty of the
Graduate School of Vanderbilt University
in partial fulfillment of the requirements
for the degree of
DOCTOR OF PHILOSOPHY
in
Biomedical Engineering
January 31, 2018
Nashville, Tennessee

Approved:

Anita Mahadevan-Jansen, Ph.D.

Jeff Reese, M.D.

E. Duco Jansen, Ph.D.

James C. Slaughter, Dr. P.H.

Dineo Khabele, M.D.

Brett Byram, Ph.D.

For my family, friends, teachers, and mentors.

ACKNOWLEDGMENTS

This work was made possible due to the support from the following funding sources: NIH R01 HD081121, NIH R01 CA095405, NIH HD 044741, the NSF Graduate Research Fellowship (CO), predoctoral fellowship grant no. T32-HL7751-15 (EV), and CTSA award no. UL1TR000445 from the National Center for Advancing Translational Sciences (NCATS).

I would like to thank my PhD advisor, Dr. Anita Mahadevan-Jansen, for training me in the field of Biophotonics and specifically Raman spectroscopy, and for providing me with freedom to explore my own ideas and passions. I would also like to thank my unofficial co-advisor, Dr. Jeff Reese, for training me in the field of Reproductive Biology and for similarly allowing me to take on additional responsibilities beyond that of my PhD work. Dr. Reese treated me as his own lab member and spent a large amount of time helping to develop my writing and grantsmanship skills. Dr. Chris Slaughter deserves thanks for working with me consistently throughout my PhD to develop tailored multivariate statistical analysis methods for this work. He was extremely patient when explaining complex ideas and I am certain that this work is greatly improved from his help. Dr. Dineo Khabele provided Obstetrics & Gynecology expertise, as well as her experience as a physician-scientist working with Raman spectroscopy in the application of cervical dysplasia. Dr. Duco Jansen provided guidance on laser-tissue interaction including help with Monte Carlo modeling and maximum permissible exposure calculations. Dr. Brett

Byram gave helpful feedback on my work from the perspective of ultrasound, the current gold standard of cervical assessment during pregnancy.

Beyond my PhD committee, I'd like to thank the Biophotonics Center and Reese Lab for being caring and close-knit communities and places where it was a joy to come to work. Specifically I'd like to thank Ms. Amy Rudin who helped me recruit and measure all of the pregnant patients at One Hundred Oaks and for her assistance with everything pertaining to IRB. Dr. Elizabeth Vargis has served as a role model and scientific mentor throughout my PhD and my work would not have been possible without the foundational studies that she conducted. I was incredibly lucky to have received a large portion of my training from Dr. Isaac Pence, who was patient, encouraging, smart, and selfless. He continues to provide guidance, advice, and humor, and I consider him a great friend. I'd like to thank Dr. Jennifer Herington who I was fortunate to spend a large amount of time working with and who helped me learn reproductive biology, helped me work through complex ideas and data interpretation in the mouse studies, and introduced me to research methods pertaining to uterine contractility. She spent countless hours reading through my manuscripts, served as a sounding board, and also as a mentor and great friend as I navigated the last few years of my PhD. Dr. BC Paria helped teach me how to design well controlled experiments and helped with data interpretation from his expertise in reproductive biology. He also provided endless entertainment. Ms. Naoko Brown stayed up many late nights and early mornings to help me perform mouse experiments. She went out of her way to help me including ordering supplies, breeding and transporting mice to and from the animal facility, and performing cervical tissue dissections. I could not have

performed any of the mouse studies without her help and am grateful for both her skills and her friendship. Stan Poole provided expertise with the biomechanical testing system on which he frequently performed maintenance to keep our experiments going strong. He also provided assistance in installing the stepper motors for the biomechanics experiments. Oscar Ayala provided his expertise in statistical analysis, Raman mapping with the Renishaw system, and engaged in helpful discussion throughout my PhD. John Nguyen assisted in autofluorescence analysis and imaging, and provided feedback on my manuscripts and experimental design. Dr. Giju Thomas provided his medical expertise in data interpretation for the human pregnancy projects and served as a sounding board when writing introduction and discussion sections of those manuscripts. Dr. Quyen Nguyen helped train me at the beginning of my PhD and provided critical feedback on my experimental design. Dr. Chetan Patil served as a mentor for the majority of my PhD and provided useful discussions regarding Raman data, recommending trying out least squares analysis, and gave me advice about research and career choices. I'd also like to thank Ms. Jean Alley for her help regarding grant and fellowship submissions, reimbursements, ordering, help with budgets, organizing speakers, and extracurricular events.

Many physicians and women's health providers at Vanderbilt Medical Center have helped me conduct this research. Dr. Kelly Bennett provided her expertise, funds, and patients to ensure the success of the prenatal and labor studies. Dr. J Newton rallied resident support of the project and provided critical feedback on how this project could be better integrated into standard obstetric care. He also contributed to our grants and manuscripts beyond what was expected and provided expertise on high risk pregnancies.

Dr. Mack Goldberg helped us recruit and measure nearly half of the patients in the labor study and significantly contributed to the design and testing of the speculum-free Raman spectroscopy probe. Dr. Sarah Hall assisted with recruiting laboring patients even though she was an anesthesiology resident and had very little extra time to spare. She met with us weekly to discuss data and plan out recruitment strategies. Ms. Tammy Keown helped recruit and measure colposcopy patients during early work investigating detection of cervical dysplasia with Raman spectroscopy, aided in preliminary concepts for the speculum-free design with a senior design team, and continued helping with testing and constructive feedback of the speculum-free probe.

I had the opportunity to mentor many students during my time at Vanderbilt, including Ellen Yeats, Katherine Cochran, Laura Masson, Jen Bateman, Kevin Qin, Becca Williams, and Dr. Nishant Ganesh Kumar. Working with these students was one of my favorite parts of my PhD; they made my projects better, brought up critical questions, designed clever solutions to problems, and helped make work fun. Many of these students taught me during this process, particularly Dr. Nishant Ganesh Kumar. I feel lucky to have mentored and worked with him during his time at Vanderbilt as a Medical Student. His joint experience as a biomedical engineer and medical professional strengthened our projects and helped generate new ideas and improvements on existing approaches.

I had the privilege to work with Dr. Doug Morgan and Ms. Charlotte Cherry Buehler on an exciting global health project focused on point-of-care gastric cancer detection. They taught me about gastric cancer and took me on two trips to Santa Rosa de Copan, Honduras to measure patients using our optical approach undergoing upper

endoscopy. This work solidified my desire to work on problems in low resource settings and I am grateful for the opportunities, training, and trust they put in me during this project.

Last I'd like to thank my family and friends for their constant support. My parents encouraged my curiosity from a young age and provided endless opportunities for my education and continued success. My sister Emily has always been my cheerleader, and has reminded me of my abilities and strengths during times of doubt. My friends kept me laughing during the hardest times of my PhD and helped make Nashville a home away from home. I'd like to especially thank Dr. Kelsey Mayo, Dr. Rebekah Griesenauer, Dr. Amy Shah, Dr. Kristin Poole, and Amy Creecy for their support and encouragement throughout my PhD. Finally I'd like to thank my fiancé Will, who followed me to Nashville without any job, picked me up from lab many late nights, and makes me smile every day.

TABLE OF CONTENTS

LIST OF FIGURES

LIST OF TABLES

LIST OF ABBREVIATIONS

LPS- lipopolysaccharide

RU486- mifepristone

MMP- Matrix metalloproteinase

HA- hyaluronic acid

RS- Raman spectroscopy

WT- wild type

PP- post-partum

Cox-1- cyclooxygenase 1

KO- knock out

PTB-preterm birth

sPTB- spontaneous preterm birth

BMI- body mass index

CHAPTER 1

INTRODUCTION

1.1 Objective

The goal of this doctoral research project is to develop a method to aid in monitoring the health status of the cervix in pregnant women for guiding patient care. This work used *in vivo* Raman spectroscopy to measure biochemical changes that occur in the cervix as it prepares for delivery and during post-partum repair.

1.2 Specific aims

The leading cause of infant morbidity and mortality is preterm birth (PTB), defined as a birth before 37 weeks of gestation. An estimated 15 million PTBs occur globally every year, which costs the United States alone approximately $26 billion. Current methods for predicting PTB have a maximum accuracy of 50% even when multiple tests are combined. These poor outcomes are ultimately due to an incomplete understanding of the cascade of events leading to labor and parturition.

All cases of spontaneous PTB, regardless of etiology, require cervical ripening for vaginal delivery of a fetus. Despite its critical role, cervical remodeling during pregnancy and labor is not well understood. Prior work has established that cervical remodeling occurs weeks prior to uterine contractions, and therefore may be an ideal target for investigation of early physiologic events in the labor process.

Alterations in cervical biochemistry must precede the vast mechanical changes (cervical thinning and dilation) that occur during parturition. Known biochemical constituents that significantly change include (but are not limited to) collagen, hydrophilic glycosaminoglycans, prostaglandins, and hydration level, resulting in decreased tensile strength and increased elasticity of the cervix; however, the exact mechanisms of how these molecular alterations affect mechanical properties is currently unknown. A tool that could non-invasively, longitudinally evaluate cervical remodeling on a molecular level could aid in a deeper understanding of the mechanisms involved in cervical maturation and consequently identify early indicators of PTB.

To address this need, we use Raman Spectroscopy (RS), an inelastic light scattering method that is capable of non-invasively extracting a biochemical fingerprint of *in vivo* cervical tissue. Raman spectra are sensitive to tissue hydration, collagen content and structure, lipids, proteins, and individual amino acids such as phenylalanine, all of which are known to be important factors in the cervical remodeling process.

We hypothesize that Raman spectroscopy can provide new information about cervical maturation by longitudinally probing dynamic biochemical changes within the *in vivo* pregnant cervix. The following aims were proposed to address this hypothesis:

Specific Aim 1: Evaluate Raman spectral signatures from normal pregnant patients during pregnancy. a) Pregnant patients classified as normal were recruited. A fiber optic probe-based RS system was used to acquire spectra from patients during their prenatal visits. A statistical model was developed to analyze the Raman spectral changes as a function of gestational age, with the goal of characterizing Raman spectral changes during pregnancy.

b) Pregnant patients that were admitted to the Labor and Delivery Unit at Vanderbilt University Medical Center for scheduled labor induction were recruited. Raman spectra were measured

from the cervix every four hours until the fetal membranes ruptured or the patient or provider determined measurements should not be continued. At each time point that Raman spectra were acquired, cervical length via ultrasound and Bishop score was measured. These measures were correlated with Raman spectra, and a statistical model was used to analyze spectral changes over the course of labor.

Specific Aim 2: Characterize the contributions of individual biochemicals on Raman spectra from the *in vivo* pregnant cervix. Raman spectra of the main biochemical components known to makeup cervical tissue were measured in their pure form. A linear least squares model was developed to estimate the contribution each biochemical component has on spectra acquired from *in vivo* cervix tissue. It was applied to spectra measured from pregnant human and mouse cervices acquired in Aims 1 & 3 to determine how the biochemical contributions of each substance changes during pregnancy.

Specific Aim 3: Identify Raman spectral differences between wild type and abnormal pregnancy mouse models and correlate results to extracellular matrix remodeling and mechanical properties. Raman spectra of wild type mice were acquired throughout gestation. We then evaluated complementary mouse models with abnormal parturition phenotypes: induced preterm labor (lipopolysaccharide (LPS) injection and mifepristone injection), and delayed parturition (cyclooxygenase-1 null). Biochemical and structural properties for each mouse model were examined by biomechanical testing and standard collagen assays, and results were correlated with Raman spectral data.

The overarching goal of this proposal was to use Raman spectroscopy to further our understanding of cervical remodeling during pregnancy. This technique has the unique ability to measure biochemical information non-invasively, over the course of pregnancy and labor. RS

has the potential to unveil information that has not been detectable with previous methods. New knowledge about this elusive process could allow for more targeted diagnostic and therapeutic strategies for handling preterm birth, and ultimately reduce the unacceptably high rates of infant morbidity and mortality.

1.3 Summary of chapters

Following the introductory chapter, Chapter 2 contains relevant background information on the biology and anatomy of the cervix, known physiology governing cervical remodeling during pregnancy and post-partum repair, review of current clinical and research tools under development for cervical assessment during pregnancy[1], and a review of the theory, instrumentation, and prior biomedical applications of *in vivo* Raman spectroscopy.

Chapter 3 presents the use of Raman spectroscopy to measure cervical remodeling in a mouse model of delayed parturition, Cox-1 null mice[2]. *In vivo* Raman spectra are compared to *ex vivo* assays including biomechanical testing, collagen, progesterone, and hydration assays, as well as correlations between *in vivo* Raman spectra and *ex vivo* mechanical results. This work demonstrates the use of Raman spectroscopy as a research tool for improved understanding of how the cervix remodels in normal and abnormal mouse models of pregnancy.

In Chapter 4, the first report of using *in vivo* Raman spectroscopy for monitoring cervical remodeling in pregnant women is presented. Sixty-eight women were measured longitudinally throughout prenatal care and post-partum, and specialized statistical analysis methods were developed for visualization and analysis of the high dimensional data set. Biochemical contributors to the Raman signal were tracked over time, and the impact of patient variables such as prior pregnancy and body mass index were investigated.

Chapter 5 describes the development of an optical probe that can be used to measure the cervix of pregnant patients without the need for a speculum. In our previous work measuring cervical remodeling in patients, we noted that the speculum examinations that were performed for cervical visualization and subsequent Raman probe placement are often uncomfortable and sometimes painful for patients, particularly during pregnancy when the lower reproductive tract is under additional load from the fetus. Furthermore, Obstetrics providers do not commonly perform speculum examination in this population, and the incorporation of a speculum exam into obstetric care adds time and complexity to their workflow. Thus, the newly built device is designed to be inserted via digital examination in conjunction with standard cervical checks, minimizing added time and discomfort for the patient and provider by integrating Raman measurements with standard Obstetrics care.

Chapter 6 presents the results from Raman spectral measurement of the cervix in laboring patients. Sixteen patients were enrolled and measured every two to four hours during labor prior to rupture of membranes. Changes in Raman spectra were tracked as a function of hours until delivery using generalized linear models.

Chapter 7 summarizes and integrates the work presented in this dissertation, presents recommendations for future research and clinical translation endeavors, and describes the contributions of this work to science and society.

Appendix I presents a work in progress of Raman spectroscopy investigation of two mouse models of preterm birth: inflammation induced with LPS, and progesterone withdrawal induced with mifepristone. The appendix includes results to date and recommendations for completion of this project.

Appendix II includes supplementary figures from chapter 3.

CHAPTER 2

BACKGROUND

Text partially adapted from:

CM O'Brien, E Vargis, BC Paria, KA Bennett, A Mahadevan-Jansen, and J Reese. "Raman spectroscopy provides a noninvasive approach for determining biochemical composition of the pregnant cervix *in vivo*." Acta Paediatrica 103.7 (2014): 715-721.

2.1 The problem: preterm birth

Fifteen million babies were born prematurely in 2010, of which, 3.1 million died as a result of preterm birth as shown in Figure 2.1 [3]. As of 2013, a tenth of all babies born in the United States were premature[4]. For those babies that survive, PTB causes a myriad of short-term and long-term morbidities, including underdeveloped lungs, brain, and gastrointestinal tract, and elevated risk for infection. In fact, PTB, low birth weight, and infant respiratory distress syndrome account for the most expensive hospital costs and longest length of stay compared to all other diagnoses including cancer [5], and contribute to the $26 billion spent on PTB-related medical costs annually in the United States [6].

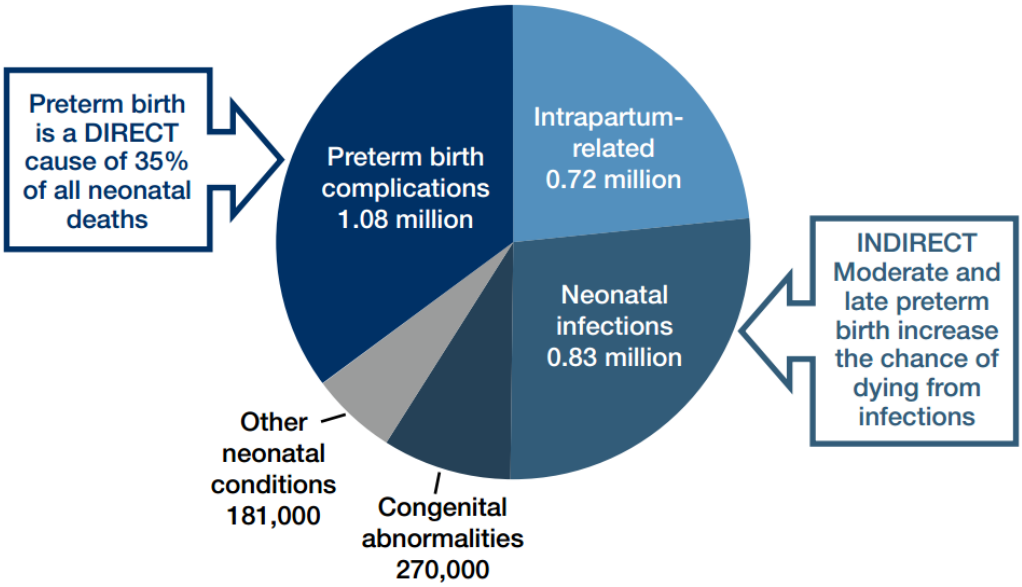

Figure 2.1. Causes of the estimated 3.1 million neonatal deaths in 2010. Of note, preterm birth is a direct cause of 35 % of all neonatal deaths. Ref. 3.

The human fetus needs at least 39 weeks to complete development and be ready to live without medical assistance outside of the womb; therefore, prolonging gestation to term (39 weeks) is important to ensure health of the fetus. The American Congress of Obstetricians and Gynecologists recently changed the definition of term from 37 weeks to 39 weeks gestation, and have new classifications for "late preterm" (34-36 6/7 weeks) and "early term" (37-39 weeks) [7]. Preterm birth syndrome is traditionally classified into two groups: indicated and spontaneous preterm birth. Indicated preterm birth is initiated by the patient's healthcare provider due to complications in the mother or fetus. This proposal focuses on spontaneous preterm birth (sPTB), which is an unexpected, spontaneous delivery. Over half of all sPTB cases have unknown causes [8].

A variety of risk factors for PTB have been identified, including previous preterm birth, non-white race, poor nutrition, drug use, and many others [9,10]. Cervical insufficiency is an additional risk factor in which the cervix cannot withstand forces of pregnancy and ripens prematurely.

Although a plethora of risk factors exist for PTB, over half of sPTB cases do not fall within any specific high-risk category, making the management of this syndrome difficult [11].

The physician's goals in managing a patient with symptoms of labor before 37 weeks therefore are to: 1) Diagnose true preterm labor; 2) Identify treatable etiologies of preterm labor; and 3) Enact measures to halt preterm labor. Tocolytic agents are one way of delaying labor although all such agents have side effects, and no tocolytic can delay delivery indefinitely. However, increasing gestational age by even a few days can have a monumental impact on improving neonatal outcome [12]. In addition to tocolytics, corticosteroids have been used to improve respiratory and other outcomes in preterm infants by increasing production of surfactant by the infant's alveoli. Surfactant reduces the surface tension of alveoli, requiring a lower pressure difference to inflate and deflate the lungs, ultimately making it easier for the infant to breathe [13]. Finally, antibiotics are commonly prescribed in case the patient has a subclinical infection, shown to be correlated with sPTB in many cases [13]. The efficacy of the aforementioned pharmaceutical agents' increases when administered early, pointing to the need for recognizing early signs of PTB [12]. Being able to diagnose and "treat" preterm labor as early as possible is the greatest chance that preterm neonates have to be healthy.

Various clinical methods have been explored to estimate PTB risk, including monitoring uterine activity with a tocodynamometer, following salivary estriol levels, measuring cervical length using transvaginal ultrasound, calculating cervical Bishop score via digital examination (Table 2.1), screening cervicovaginal fluids for the presence and quantification of fetal fibronectin (fFN) and inflammatory markers, and rapid testing of inflammatory markers in amniotic fluid [14-22]. Combined cervical length and fFN measurements have yielded relatively high sensitivity and specificity [23] for predicting sPTB, however, these studies report large ranges

of findings and have low positive predictive value [23]. Furthermore, these methods provide little information regarding the etiology of preterm labor [24]. Therefore, early detection of sPTB risk should ideally include clues to the cause of preterm labor, as well as provide quantitative risk assessment.

Table 2.1. Bishop score rubric

Bishop Score to Assess Likelihood of Successful Induction of Labor				
Physiological Findings	Rating			
	0	1	2	3
Cervix				
Position	Posterior	Mid	Anterior	-
Consistency	Firm	Medium	Soft	-
Effacement (%)	0-30	40-50	60-70	≥80
Dilation (cm)	0	-1	-2	≥5
Fetal Head				
Station (cm)	-3	-2	-1	1

2.2 The cervix

While labor and parturition are coordinated processes involving many systems and organs for proper function, the cervix may be an ideal target to investigate for early signs of PTB. Regardless of etiology, all instances of sPTB with vaginal delivery require passage through the cervix (Figure 2.2). This fact is not trivial, as the cervix is a rigid structure with little elasticity at the beginning of pregnancy, incapable of dilating a few millimeters, let alone multiple centimeters. Ultrasound measurements of cervical length have demonstrated that cervical ripening occurs weeks prior to uterine contractions [25], supporting investigation of cervical remodeling to determine PTB risk.

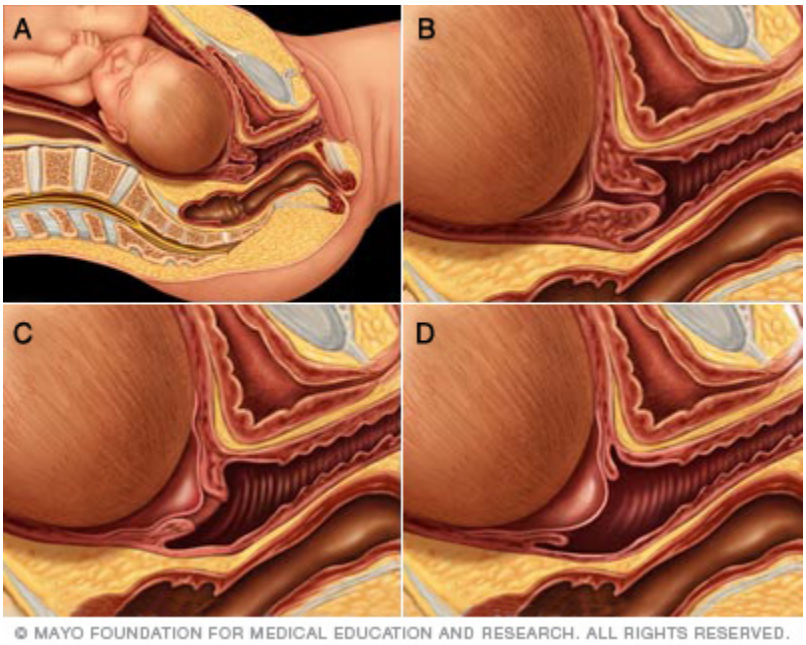

Figure 2.2. Schematic of cervical effacement and dilation throughout labor. (Image courtesy of Mayo Foundation for Medical Education and Research)

Anatomically, the cervix is a cylindrical shaped organ located at the bottom-most part of the uterus. The cervix extends into the vagina, and has a canal termed the endocervical canal through which a baby descends during delivery (Figure 2.3). The outer portion of the cervix is termed the ectocervix. The cervix has an inner diameter on the order of millimeters, and is typically ~4.5 cm in length [26]. The angle between the uterus and the cervical canal (termed the uterocervical angle) aids in distributing the fetal load and prevents forces from gravity being aligned with the endocervical canal.

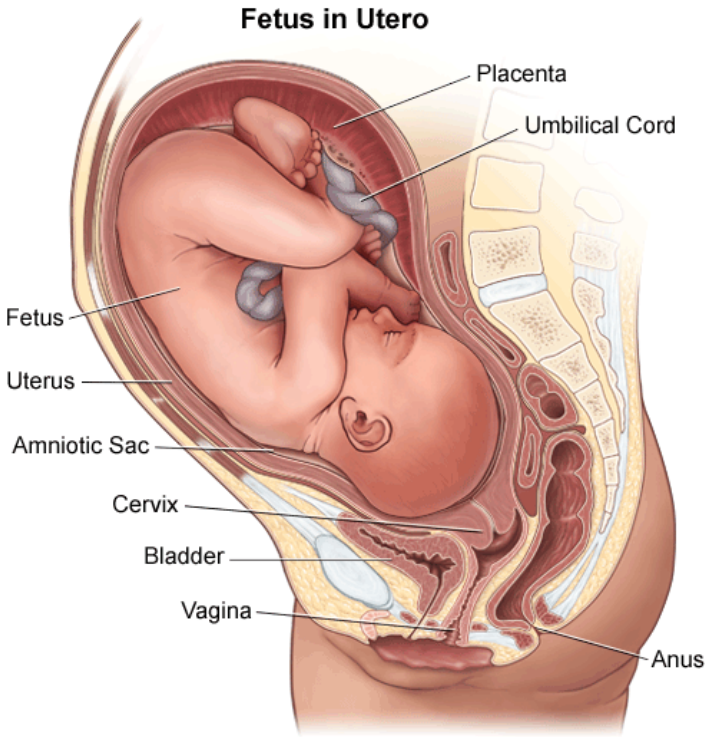

Figure 2.3. Illustration of the reproductive organs during pregnancy. (Courtesy of Stanford Children's Health)

The cervix consists mainly of a dense extracellular matrix that is infiltrated by fibroblasts, immune cells, blood vessels, and a small amount of smooth muscle estimated to comprise 10-15 % of the stroma [27-29]. The functional role of the smooth muscle is currently under debate, as the cells are distributed throughout the cervix and rarely form bundles, potentially limiting contractile power [30]. However, a new hypothesis proposes that the smooth muscle in the cervix serves as a sphincter, helping to keep the cervix closed until term[31]. The most abundant component of the ECM is fibrillar collagen, accounting for 90% of the matrix proteins in the cervix. Collagens type I and III make up 70% and 30% of collagen proteins respectively. The majority of the tensile strength in the cervix comes from collagen cross-links, specifically strong trivalent pyridinoline and weak divalent nonpyridinoline cross-links. Strong cross-links are prevalent in non-gravid cervix tissues and correspond with high stiffness[32]. Elastin, another load-

bearing fibrillar protein, is found most densely around the external os[29]. Reports from human cervical tissue dissections found few elastin fibers in the stroma or at the internal os which had higher smooth muscle content[29]. Matricellular proteins facilitate collagen fiber assembly and fibrillogenesis[33], and mice with null mutations of matricellular proteins such as thrombospondin 2 have increased cervical extensibility and increased expression of matrix metalloproteinase 2 (MMP)[34]. All five glycosaminoglycans (GAGs) including the unsulfated GAG hyaluronan, and sulfated GAGs chondroitin sulfate, dermatan sulfate, heparin sulfate, and keratin sulfate are found in the cervix extracellular matrix and aid in binding water, adding to the viscoelasticity of cervix tissue[35,36]. In the non-pregnant cervix, the mean hydration is 75.5%, whereas pregnant cervix tissues are 81% hydrated[37]. The outside of the cervix is lined with squamous epithelium while the endocervical canal is lined with mucus-secreting columnar epithelium[28] which serve as barriers to infection. Their junction is termed the squamo-columnar junction.

The hormonal environment affects the extracellular matrix and biomechanical properties of the cervix tissue, as demonstrated by variations in internal os diameter during the female menstrual cycle[38]. Further evidence was recently reported in wild type ovarectomized female mice which were treated with either estrogen or progesterone[39]; mice treated with progesterone had significantly greater maximum stiffness, strength, and yield stress compared to mice injected with estrogen or mice without treatment[39,40]. In addition, the hormone relaxin promotes cervical growth by stimulating epithelial cell and fibroblast growth and by preventing apoptosis[41]; animals with relaxin deficiencies have significantly reduced wet weight and cervix circumference at term compared to controls[42].

2.3 Cervical remodeling during pregnancy

Current understanding of cervical changes during pregnancy is limited compared to our knowledge of other aspects of uterine biology, particularly in cases of cervical insufficiency and PTB. It is known that the normal process of cervical remodeling consists of four distinct stages with variable lengths between patients (Figure 2.4) [43]. In the first stage, termed "softening," the cervix has increased distensibility due to hydration and vascularity increase as well as collagen reorganization [43]. The next stage, "ripening," involves increased accumulation of glycosaminoglycans, resulting in a further increase in cervix tissue hydration and collagen solubility [29]. The third stage is called "cervical dilation" is characterized by rapid changes in mechanical properties caused by MMPs acting on the extracellular matrix. After the delivery of the fetus, the cervix immediate begins the "repair" phase which includes inflammatory wound healing response. Collagen remodeling occurs in all phases of cervical maturation, and has been identified as the most important constituent governing mechanical strength in the cervix [44,45]. A firm relationship has been established between the extent of collagen cross-linking and tensile strength in the pregnant mouse cervix [46] and human cervix tissues [37,47,48].

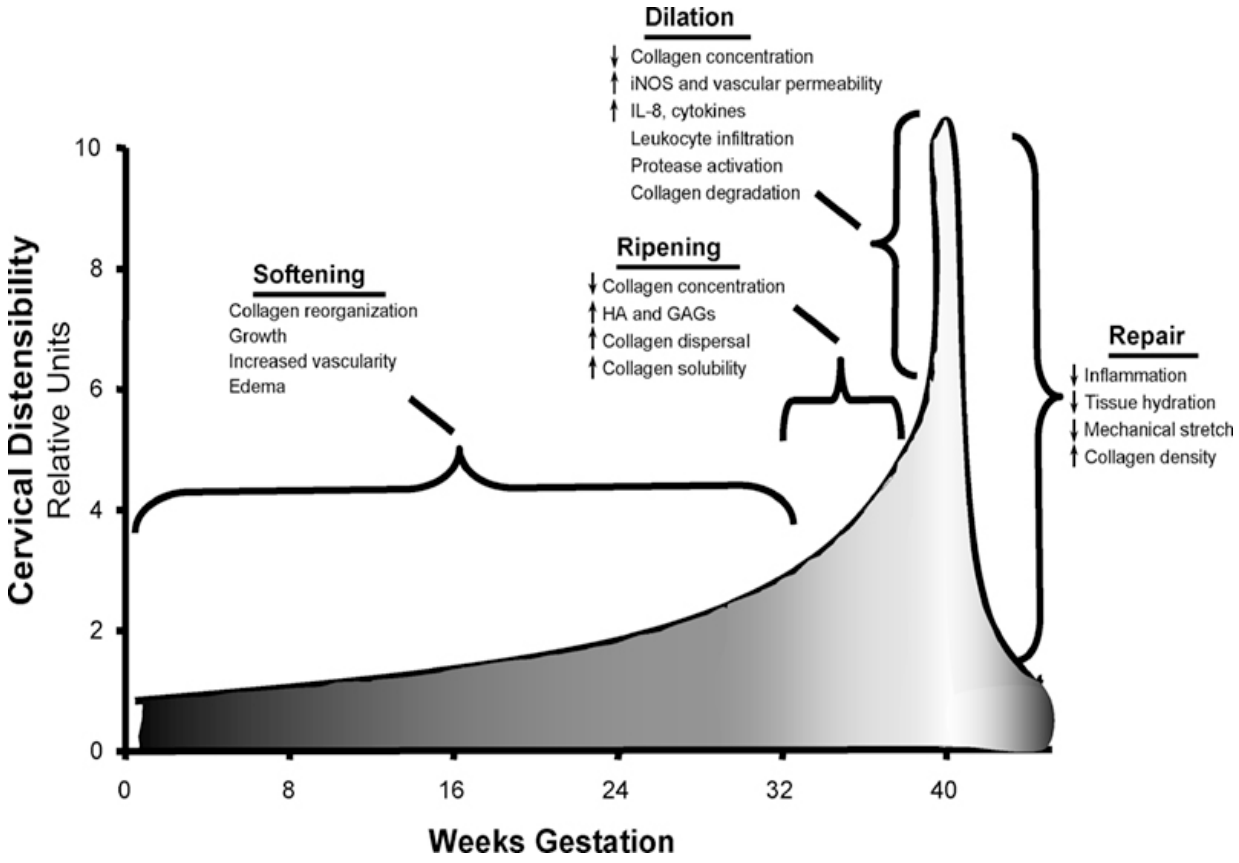

Figure 2.4. Plot representing biochemical changes and distensibility over pregnancy. Ref. 41.

2.3.1 The softening phase

In women, increased cervix distensibility occurs within a month of conception, whereas in mice it occurs by day 12 of a 19.5 day pregnancy[49]. In early pregnancy, estrogen levels are low and progesterone levels are high. Immature fibrillar collagens are synthesized but the enzymes that facilitate cross-linking are down regulated, and increased levels of MMPs reduce levels of existing maturely cross-linked collagens[32,46], contributing to the reduced stiffness observed in the softening phase. In mouse studies, collagen content and hydration levels were the same as non-gravid tissues, however collagen solubility was significantly higher on day 12,

indicating that the increased distensibility observed in this phase is primarily due to changes in the types of collagen cross-links[49].

2.3.2 The ripening/dilation phase

The majority of cervical remodeling studies are performed in mice, and due to the short timeframe of the dilation phase most reports group the ripening and dilation phases together. Decreases in progesterone and increased estrogen transition the cervix into the ripening phase, where collagen fibers become dispersed and the cervix hydration significantly increases (Figure 2.5). This increased hydration is thought to be caused by elevated levels of hyaluronan (HA), hydrophilic molecules that are upregulated during the ripening phase[50,51]. In early mouse pregnancy, HA contributed to 17% of the total GAGs in the cervix, whereas during the ripening phase HA comprised 71% of the total GAG content[51]. Macrophages, neutrophils, and monocytes are observed in the ripening phase, and were previously thought to increase matrix metalloproteinases (MMPs) and degrade the extracellular matrix; however, high levels of inflammatory genes and MMPs are not observed[52]. The mucosal epithelia proliferate during the ripening phase and serve as protective barrier by secreting antimicrobials, cytokines, and attracting inflammatory cells to fight potential pathogens (Figure 2.5) [35,36]. Further study specifically targeting the dilation phase is needed.

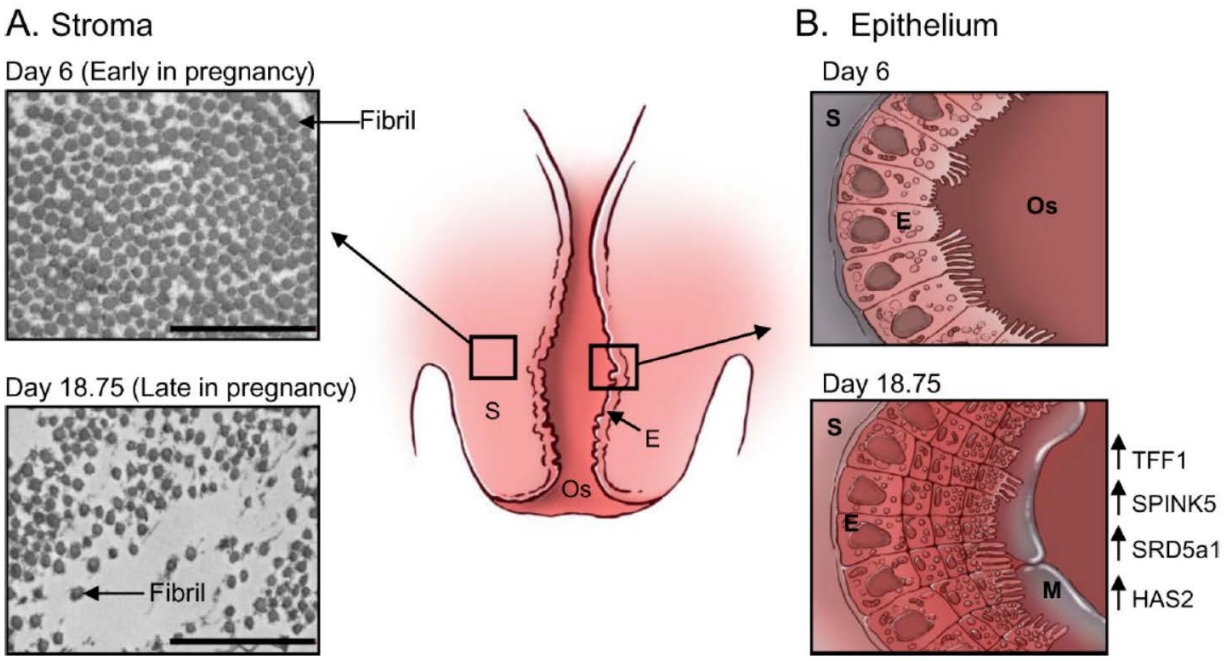

Figure 2.5. Schematic depicting extracellular matrix changes in the mouse cervix during pregnancy, adapted from Ref. 34.

2.3.3 The repair phase

Studies in mice and women indicate that the repair phase is similar to a wound healing process. Immune cells infiltrate the cervix and become activated, and a variety of proinflammatory genes are expressed [52-54]. Microarray analyses have also identified upregulation of matrix cross-linking and collagen synthesis genes, as is expected to help the cervix regain its strength [55,56]. Longitudinal studies are lacking to observe the process of cervical repair over time.

2.3.4 Preterm cervical remodeling

Preterm birth has multiple causes[24] and investigations in animal models of pregnancy have shown that cervical remodeling physiology in progesterone withdrawal-mediated and inflammation-induced preterm birth are both distinct physiological processed compared to

term[57-61] (Figure 2.6). Cervix tissues from mice with inflammation induced preterm birth (LPS treated[57,61]) have infiltration of neutrophils[57] and M1 and M2 macrophages[61], elevated levels of inflammatory cytokines and MMPs[57,58,61,62], and a dispersed, losely packed collagen matrix with no change in tissue wet weight. Mice in the progesterone withdrawal treatment group have increased monocytes[57], increased tissue wet weight, and increased expression of MMP-8.

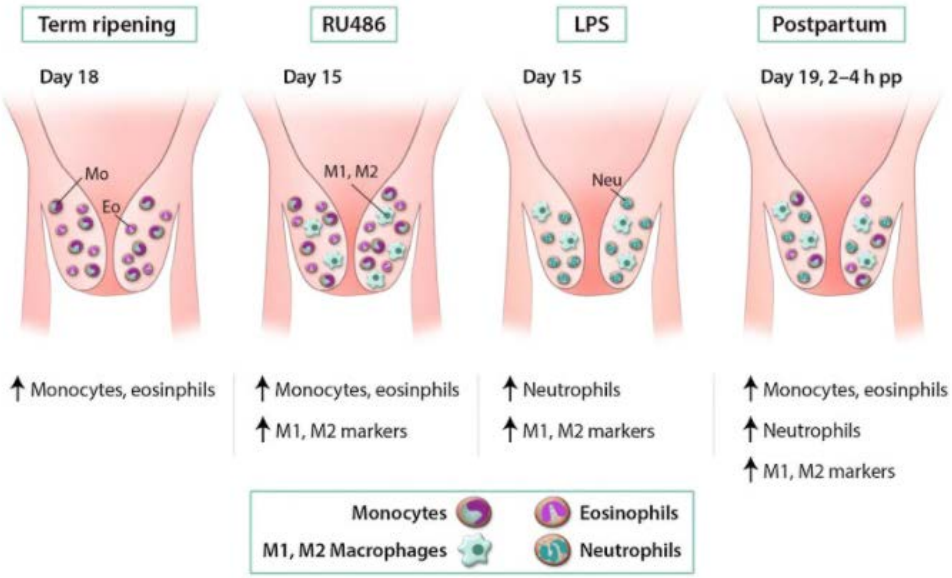

Figure 2.6. Schematic depicting immune cell population in the mouse cervix during term, preterm labor, and post-partum, adapted from Ref. 35.

2.4 Novel methods to study cervical remodeling

Clinical methods that have been explored as ways to estimate risk for preterm birth include cervical length by ultrasound, cervical Bishop score, fetal fibronectin screening, measuring salivary estriol levels and monitoring uterine contractions [14-17,63]. Of all these methods, cervical length measures have demonstrated the highest accuracy for predicting preterm delivery. However, reports vary considerably across different studies [64]. Furthermore, none of these methods provide biochemical information that could be vital in characterising the

microstructural and molecular processes that govern cervical remodeling and determine the etiology of preterm labor.

In addition to clinically used methods, researchers have identified other technologies that can evaluate the cervix to accurately predict preterm birth. These methods employ optical, ultrasonic, mechanical, and electrical phenomena to non-invasively interrogate state of the cervical tissue (Table 2.2). An in-depth review of these methods can be found in Feltovich et al. [65].

Table 2.2. Developing technologies for analysis of the pregnant cervix

Technique	Collagen structure?	Tissue hydration?	Tissue elasticity/ stiffness?
Electrical Impedance		✓	
Acoustic Attenuation		✓	
Elastography			✓
Backscattered power loss	✓		
Mechanical testing			✓
Near-infrared spectroscopy		✓	
Second harmonic generation	✓		
Laser-induced fluorescence	✓		
Raman Spectroscopy	✓	✓	✓

2.4.1 Electrical Methods

Electrical methods have classically been utilized for investigating myometrial contractions, but the assessment of fundamental electrical properties are now being applied to help understand the pregnant cervix. Electrical impedance is a measure of the resistance to electrical flow and is specific to the material being evaluated. This property was measured in the cervix of pregnant women and a correlation was found between the electrical impedance and

cervical hydration state [66]. While this is a promising method to measure cervical hydration, it is limited in its ability to monitor other biochemical and structural changes occurring in the cervix during pregnancy.

2.4 2 Acoustic Methods

Ultrasound is a well-established clinical technique traditionally used to track the progress of fetal development and quantify the progression of pregnancy. Multiple research groups are developing techniques that aim to capture new information using ultrasound. For example, signal attenuation in transvaginal ultrasound images of the cervix has been shown to correlate with cervical hydration level, exploiting the increasing hydration of cervical tissue in preparation for parturition [67]. Backscattered power loss, a variation of ultrasound, measures acoustic scatterers, such as collagen, from different steering angles and the detected signal can provide information regarding the alignment of scatterers within the sample. This method has demonstrated that preferential alignment, presumably of collagen, is present in the cervix and that it may be able to detect slight alterations in collagen alignment associated with cervical remodeling [68].

Finally, ultrasound-based elastography probes the mechanical properties of tissue by comparing images acquired before and during deformation to estimate stiffness of the tissue [69]. Studies comparing induction patients revealed that those patients who had successful induction had a significantly higher elasticity index, indicating softer tissue, than patients with unsuccessful induction [69]. While ultrasound provides valuable structural information about the pregnant cervix, these methods have limited spatial resolution and cannot elucidate the biochemical and molecular dynamics that might provide insight into the parturition process.

2.4.3 Mechanical Methods

Direct mechanical testing of the pregnant cervix has been conducted using two main methods. Researchers have developed an aspiration device that estimates cervical stiffness by measuring the pressure required to displace cervical tissue by a pre-set amount and results from this work have demonstrated the ability to detect decreasing levels of stiffness over the course of pregnancy [70]. Other groups have developed cervical dilators that measure cervical resistance index, which is the force required to dilate the cervix by a total of 8mm [71]. Significant differences in cervical resistance index, between non-pregnant patients without abnormal obstetric history and non-pregnant patients with history of spontaneous mid-trimester abortions have been reported.

Some investigators have developed mathematical models to specifically understand the mechanical changes that occur in the *in vivo* cervix during pregnancy and parturition. These models could potentially use indirect measures of mechanical properties collected from other optical, acoustic, electrical and mechanical methods to model the changes that occur during pregnancy. Such models could allow individual patient parameters to be used to predict patient outcome and assess risk of preterm birth [48,72]. These methods offer important biomechanical information, but cannot be used to monitor molecular changes that may help to determine new information regarding the cervical remodeling process.

2.4.4 Optical Methods

Three primary methods have been explored to study preterm birth using optical techniques. The collascope, a device that excites collagen and measures light-induced autofluorescence, can monitor the state of collagen in the cervix during pregnancy [73]. Collagen is

a natively fluorescent protein, with insoluble collagen having higher fluorescent intensity than soluble collagen[73]. Because collagen solubility increases as the cervix ripens, the intensity of light-induced fluorescence changes with advancing gestation [73-75]. This technique has been applied in mice as well as humans and results have shown that fluorescence intensity decreases as parturition approaches [73-75].

In addition to being an intrinsically fluorescent protein, collagen type 1 is capable of second harmonic generation and can produce a strong signal with very little background if excited at the appropriate wavelengths. This technique has been used to study the cervix of pregnant mice *in vivo* and has been demonstrated in *ex vivo* human cervical samples. It is capable of producing high resolution images of cervical collagen and the results have verified that the collagen networks in the cervix become increasingly disorganised with advancing gestation [76,77].

Near-infrared spectroscopy has been used to monitor haemoglobin, water and optical scatterers in the pregnant cervix, by measuring the diffuse reflectance of light at various near-infrared wavelengths. From these measurements, the researchers calculate the optical properties that can be used to estimate concentrations of biological absorbers, such as haemoglobin and water, and determine the relative density of structural interfaces encountered such as cells and collagen [78,79]. Preliminary studies found increasing values for light scattering and haemoglobin over the course of pregnancy and observed an increase in cervical hydration during cervical ripening with misoprostol [78,79].

2.5 The need

Incomplete understanding of cervical remodeling and the parturition process is the culprit behind unacceptably high prevalence, morbidity, and mortality caused by preterm birth. This prevents us from developing effective diagnostics and therapeutic interventions because we do not know what their targets should be. Therefore, if we hope to improve these outcomes we must expand our understanding of these events. Unfortunately, classically used basic science methods have not yet been able to solve this problem, partially due to their invasive nature. Few methods have offered the ability to monitor cervical changes over time within the same subject, while fewer have been capable of probing the biochemical micro-environment that evolves during pregnancy. Thus, there is a need for new approaches that can track these biochemical markers *in vivo* to improve our understanding of the cervical remodeling process on a biochemical scale and potentially enable *in vivo* human cervix monitoring.

2.6 *In vivo* Raman spectroscopy

Raman spectroscopy is an optical technique based on the Raman Effect, defined by an exchange of energy between incident photons and scattering molecules due to excitation to higher vibrational energy levels (Figure 2.7).

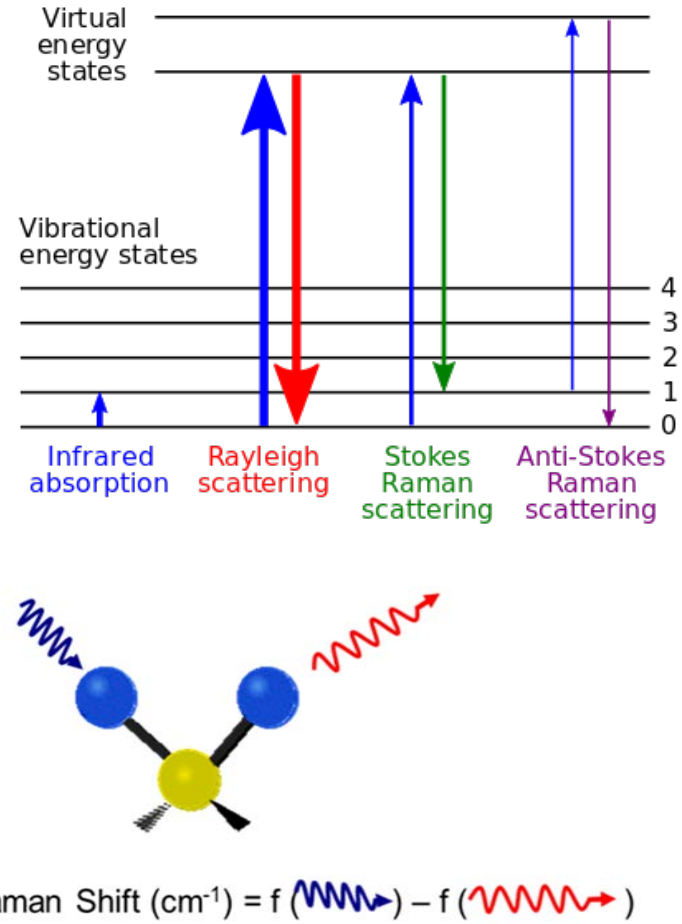

Figure 2.7. Top: Jablonski diagram depicting energy transitions for Rayleigh scattering and vibrational absorption and scattering phenomena. Bottom: Illustration of the Raman Effect: the excitation wavelength (blue, higher energy photon) interacts with the molecule and sets it into vibration, and scatters at a lower energy (red, lower energy photon). The difference in energy between the excitation and scattered photon is the Raman shift.

The Raman shift (ν (cm^{-1})) is calculated based on the simple equation:

$$\nu = \frac{1}{\lambda_{incident}} - \frac{1}{\lambda_{scattered}} \qquad \text{(Eqn. 2.1)}$$

which shows that the Raman shift is a *relative* change in energy based on the incident wavelength of light. This allows excitation with a variety of laser sources which will all produce the same relative Raman shift.

Not all molecules have the ability to Raman scatter; molecules must undergo a change in polarizability upon interaction with the incident light in order for a Raman event to occur. Infrared (IR) absorption, a complementary vibrational spectroscopy technique, requires molecules to change their dipole moment upon light interaction for IR absorption to occur. Thus, some molecules are Raman active, some are IR active, some can undergo both Raman and IR phenomena, and some molecules do not experience either.

Raman and IR spectroscopies yield sample-specific molecular fingerprints, from which the sample composition and, in some cases structure, can be ascertained. However, IR absorption is limited for biomedical applications because strong absorption of water molecules severely limits penetration depth. Thus, Raman spectroscopy has been much more widely used in biomedical applications.

A Raman spectrum consists of peaks which correspond to the different vibrational modes of molecules from which photons were inelastically scattered (Figure 2.8). In general, these peaks are spectrally narrow and correlate with defined molecules. The peaks of a Raman spectrum are associated with certain bonds in specific molecules and can be used to determine a sample's biochemical composition.

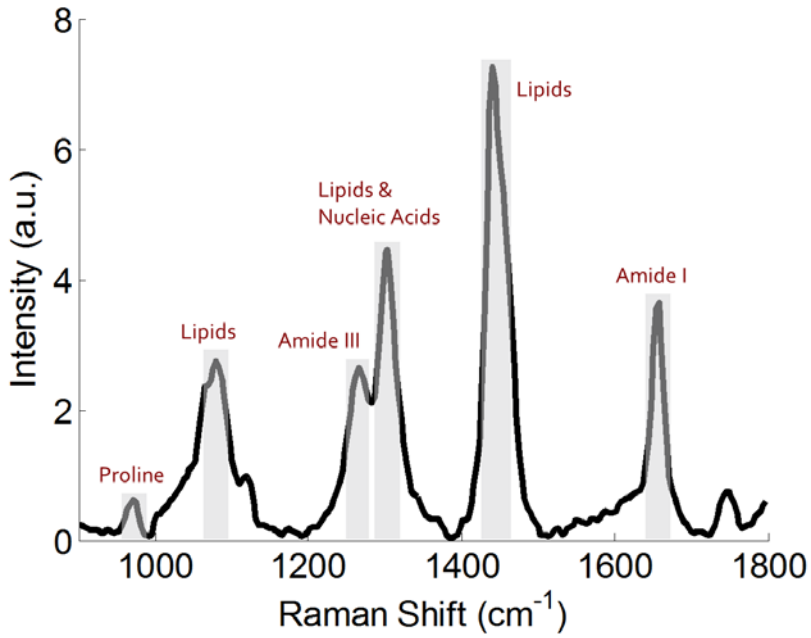

Figure 2.8. A Raman spectrum, generated by plotting all collected Raman scattered photons as a histogram with peaks representing molecular bonds within the sample.

To perform Raman spectroscopy, multiple pieces of equipment must be used. First, excitation upon the sample must be performed with a narrow band laser in order to calculate the shift between excited and scattered photons. After excitation, the scattered photons are collected by optical objectives or fiber optic probes and typically focused down to a small collimated beam. This beam is normally sent through a physical slit and then to a dispersion element such as a prism or grating. The slit minimizes the distance between photons of the same energy hitting the dispersion element. The closer in space the photons are when hitting the dispersion element, the higher the spectral resolution of the photons onto the detector. Therefore, small slit widths improve spectral resolution, but reduce light throughput. Dispersion elements spread out the scattered light onto the detector as a function of wavelength, such that each column of pixels on the detectors can be mapped to specific wavelengths of light. Detectors vary depending upon the excitation wavelength used. For biochemical applications with excitation at 660 or 785 nm,

silicon CCD detectors are most commonly used. For higher wavelengths, InGaAs detectors are used owing to their higher quantum efficiency in the infrared. Due to low signal intensity inherent to Raman scattering, all elements in a Raman spectroscopy system are designed to be highly efficient. Raman spectrographs minimizing the number of optical elements throughout which the light must pass and the detectors are typically cooled to -50 °C or lower to reduce thermal noise.

2.7 Prior work using *in vivo* Raman spectroscopy for detection of disease

Raman spectroscopy has been used for decades to detect disease and cancer-specific signals in various organs and soft tissues such as the cervix, bladder [80,81], oesophagus [82,83], skin [84,85], breast [86], gastrointestinal tract [87], and cervix [88], and *in vivo* human trials using Raman spectroscopy have recently been reviewed by Pence et al. [89]. Development of a fiber optic probe has enabled its use *in vivo* [88] with applications in many organ systems in animal models as well as humans.

Raman spectroscopy has been successfully applied to the *in vivo* cervix for the diagnosis of cervical dysplasia[88,90]. This technique displayed remarkable accuracy for detecting cervical abnormalities and was able to classify normal, and high-grade dysplasia with high accuracy [91]. However, low grade dysplasia demonstrated a poorer sensitivity. In an attempt to improve classification of low grade dysplasia, the effect of hormonal status on Raman spectra was evaluated [92]. Spectra from non-gravid patients with normal Pap testing results were classified based on hormonal status with 98% accuracy [92]. Accounting for hormonal status in dysplasia patients resulted in an increase in classification accuracy from 88% to 94% [93]. To further improve classification accuracy, four more patient variables were studied: body mass index

(BMI), obstetric history, ethnicity, and socioeconomic status, of which only obstetric history and BMI were found to have an impact on Raman spectra [94].

Raman spectroscopy has also been used to detect strains of HPV, an infection that is correlated with nearly all cases of cervical cancer [95,96]. Spectral analysis has been performed on cultured cells, such as primary human keratinocytes, CaSki, HeLa, SiHa and C33A cells, as well as *ex vivo* cervical cells from patients who were screened for HPV infection at Vanderbilt University. Classification accuracies from 89% to 100% for the cultured cells and 98.5% for the patient samples were found using discrimination algorithms, such as principal component analysis and sparse multinomial logistic regression [95,96].

2.8 Raman spectroscopy as a tool to investigate cervical remodeling during pregnancy

The cervix must transform from a stiff, rigid structure into a soft, distensible passageway for successful delivery of a fetus [43]. The mechanisms that lead to this transformation are not fully understood, particularly in patients who experience spontaneous preterm birth. Known biochemical constituents that undergo dramatic changes include an increase in cervical hydration, hydrophilic glycosaminoglycans, collagen solubility, prostaglandin release and inflammatory cells [97]. These changes, among others, result in reduced tensile strength and increased elasticity of the cervix, which lead to the successful passage of the fetus.

Raman spectroscopy is sensitive to tissue hydration, collagen content and structure, cell density, lipids, proteins and some individual amino acids [93,98-100]. To establish the feasibility of using this method for detecting biochemical changes in the cervix during pregnancy, a pilot study was conducted in mice [101]. *In vivo* Raman spectra were acquired from nongravid and pregnant wild type mice at multiple time points during pregnancy (full term = 19 days), as well

as post-partum one day after delivery. Measurements were made using a custom fiber optic probe that was gently inserted into the vagina and pressed against the cervix of anesthetised mice. Figure 2.9A illustrates the Raman spectra obtained from the *in vivo* mouse cervix over the 19-day mouse gestational cycle [101]. In nongravid mice, subtle spectral changes were found to differ between phases of the estrous cycle [101].

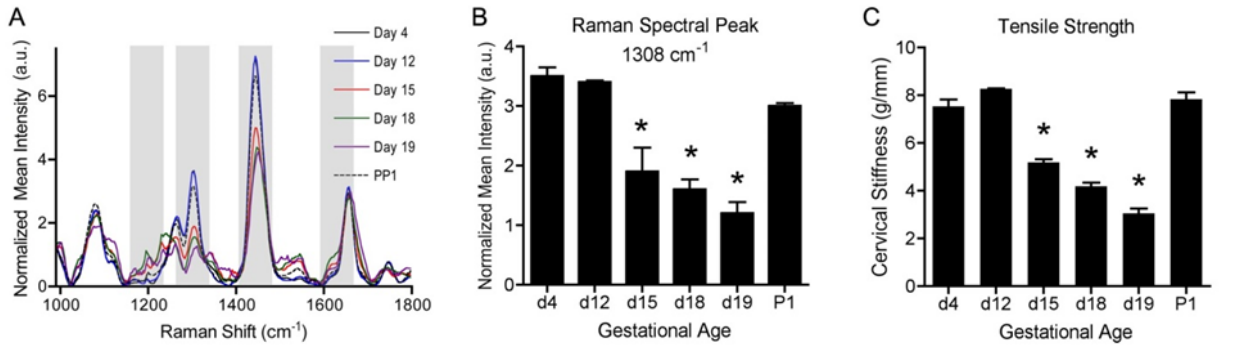

Figure 2.9. (A) Raman spectra of the *in vivo* mouse cervix over the course of gestation (gray regions $p<0.1$). (B) Change in Raman spectral intensity at 1308 cm^{-1} (n=5 per time point). (C) Cervical stiffness, measured from stress-strain curves (*$p<0.01$, n=5 per time point). Raman spectroscopy for this peak and cervical compliance are in strong agreement. Adapted with permission from ref. 95.

Biomechanical tests were performed on excised cervical tissues of the same mice at different gestational ages to determine whether any Raman peaks correlated with mechanical properties as a function of gestational age. One important trend observed was the decrease in intensity at 1308 cm^{-1}, a peak indicative of lipids (Figure 2.9B), that correlates well with decreasing tensile strength and increasing cervical distensibility (Figure 2.9C) as parturition nears [101]. In addition, as the cervix collagen matrix becomes solubilised with advancing gestational age (Figure 2.10B), the full-width at half maximum value at the 1650 cm^{-1} peak

increases [101]. These changes, as measured using the Raman spectroscopy, indicate that this technique can indirectly probe the mechanical properties of the *in vivo* pregnant cervix.

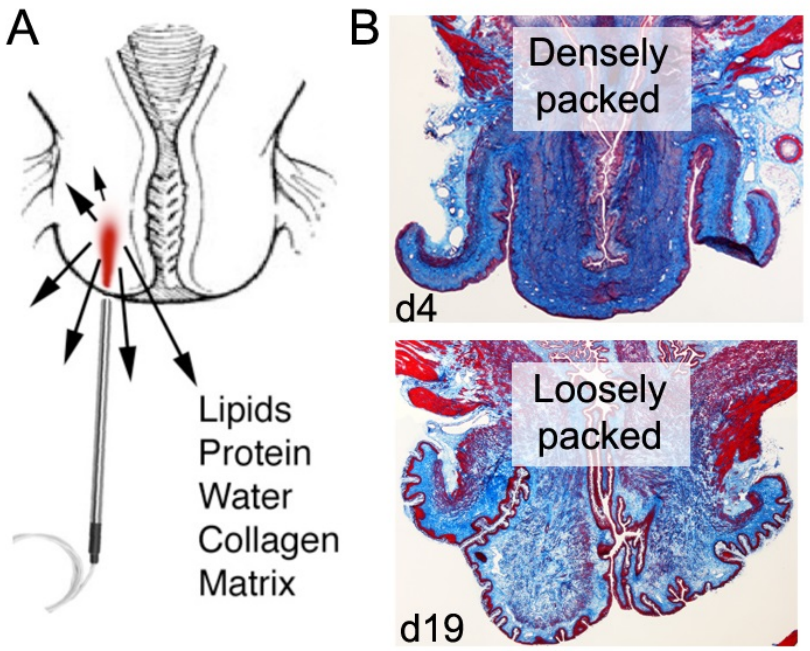

Figure 2.10. (A) *In vivo* Raman spectroscopy of the cervix. (B) Trichrome stains of the pregnant mouse cervix at early (d4) and late gestation (d19); collagen is densely packed at the beginning and reorganizes in preparation for delivery.

The late stages of cervical remodeling were characterised by acquisition of the Raman spectra from term gestation mice on day 19, starting approximately 12 hours before the time of expected delivery and then every two hours until delivery. As delivery approached, Raman spectra exhibited decreasing intensities in the 1300 cm^{-1} lipid peak depicted in Figure 2.11A, as well as the 1440 cm^{-1} lipid bond and Amide I and III bonds (1660 cm^{-1} and 1265 cm^{-1}, respectively) (not shown). Such changes did not occur at earlier time points during pregnancy, as can be observed in measurements taken from day 15 mice (Figure 2.11B). This shift illustrates the value of Raman spectroscopy for prediction of impending delivery.

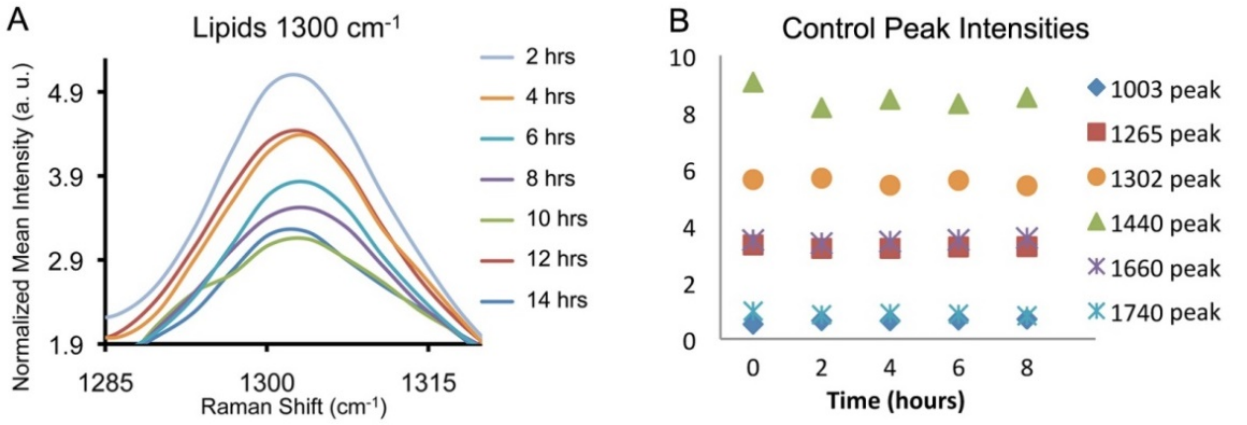

Figure 2.11. (A) Raman peak at 1300 cm^{-1} indicative of lipids from d19 mice (n=5) monitored every two hours, starting 12 hours prior to delivery. (B) Six Raman peaks plotted from d15 mice (n=5, representative plot) monitored every two hours for a total of eight hours; intensities are stable over time.

In summary, Raman spectroscopy is a powerful, non-invasive method that has the potential to quantitatively measure a number of biochemical components and properties, such as collagen cross-linking, tissue hydration and tissue elasticity that can be correlated with cervical remodeling that occurs with pregnancy. While employing multiple methods to evaluate the pregnant cervix is advisable, the preliminary results discussed here demonstrate that Raman spectroscopy is a technique that can offers many advantages of previous methods and has high potential to make an important clinical impact. The main advantage of this approach is the clinical applicability of Raman spectroscopy as has been demonstrated in cervical dysplasia. Using a clinical Raman system, we have initiated studies in human subjects to both monitor the dynamic biochemical changes that occur in the cervix throughout pregnancy and determine the predictive capability of this technique for translation into clinical use.

2.9 Acknowledgments

This work was presented in part by Dr. Reese at the biennial meeting of the International Perinatal Collegium, July 2013. The authors acknowledge the financial support of the National Institutes of Health (Grant No. R01-CA-095405, AMJ and HD 044741, BCP), a predoctoral fellowship (Grant No. T32-HL-7751-15) for EV, and a predoctoral fellowship (NSF Graduate Research Fellowship) for CO.

CHAPTER 3

IN VIVO RAMAN SPECTRAL ANALYSIS OF IMPAIRED CERVICAL REMODELING IN A MOUSE MODEL OF DELAYED PARTURITION

Text partially adapted from:

CM O'Brien, JL Herington, N Brown, IJ Pence, BC Paria, JC Slaughter, J Reese, and A Mahadevan-Jansen. "*In vivo* Raman spectral analysis of impaired cervical remodeling in a mouse model of delayed parturition." *Scientific Reports* 7 (2017).

3.1 Abstract

Monitoring cervical structure and composition during pregnancy has high potential for prediction of preterm birth (PTB), a problem affecting 15 million newborns annually. We use *in vivo* Raman spectroscopy, a label-free, light-based method that provides a molecular fingerprint to non-invasively investigate normal and impaired cervical remodeling. Prostaglandins stimulate uterine contractions and are clinically used for cervical ripening during pregnancy. Deletion of cyclooxygenase-1 (Cox-1), an enzyme involved in production of these prostaglandins, results in delayed parturition in mice. Contrary to expectation, Cox-1 null mice displayed normal uterine contractility; therefore, this study sought to determine whether cervical changes could explain the parturition differences in Cox-1 null mice and gestation-matched wild type (WT) controls. Raman spectral changes related to extracellular matrix proteins, lipids, and nucleic acids were tracked over pregnancy and found to be significantly delayed in Cox-1 null mice at term. A cervical basis for the parturition delay was confirmed by other *ex vivo* tests including decreased tissue distensibility, hydration, and elevated progesterone levels in the Cox-1 null mice at term.

In conclusion, *in vivo* Raman spectroscopy non-invasively detected abnormal remodeling in the Cox-1 null mouse, and clearly demonstrated that the cervix plays a key role in their delayed parturition.

3.2 Introduction

Pregnancy, labor, and the delivery of offspring (parturition) are highly regulated processes in all species. However, the mechanisms underlying the progression to term or preterm birth and onset of labor remain incompletely understood. Spontaneous preterm birth is considered a clinical syndrome that has multiple causes, including infection, cervical insufficiency, uterine over-distension, and others [24]. In all instances, cervical remodeling and dilation are required for successful expulsion of the fetus [65]. The cervix is endowed with important structural properties that ensure a tightly closed womb until the fetus is ready for delivery, and to act as a barrier against external infection. At the beginning of pregnancy, the cervix is a stiff, rigid cylinder with a highly cross-linked extracellular matrix that provides mechanical strength to maintain cervical closure [43,65]. Over the course of pregnancy, this collagen-dense matrix is transformed into a compliant structure that allows passage of a fetus. Normal cervical remodeling during pregnancy involves a significant transition in mature to immature collagen cross-links [32], a reduction in proteoglycans which control packing of collagen fibrils, a significant increase in the glycosaminoglycan hyaluronan [51], and a significant increase in tissue hydration [50,102]. Circulating as well as local hormone/endocrine levels are known to orchestrate these cervical changes [35,43,49,103,104], but a full understanding remains elusive.

Cyclooxygenase (Cox)-derived prostaglandins (PGs) serve as key signaling molecules during pregnancy [105-107]. PGF2α plays an important role in the involution of the ovarian corpus luteum (luteolysis) in mice and subsequent decline in progesterone signaling leading to uterine contractions [105,108,109]. However, there is conflicting evidence for PGs as mediators of cervical ripening. Topical prostaglandin E (PGE) application is a potent stimulus for the induction of cervical ripening in women and animal models [103,110-113], and PGs are required for cervical maturation during inflammation-induced preterm birth in mice [114]. Conversely, expression of Cox-1 and Cox-2 enzymes in the cervix is not increased at term in normal mouse models of pregnancy and neither are the concentrations of PGs or their receptors [114]. Furthermore, PG concentrations in cervical mucus do not increase prior to parturition in women [115-117]. In addition, seminal fluid has high levels of PGs but has not been shown to promote cervical ripening [118]. A greater understanding of PG-mediated changes in the cervix is needed to clearly understand normal remodeling physiology and reduce adverse pregnancy outcomes.

Classical research approaches for investigating physiology are too invasive to be used in pregnant women; therefore, animal models inform much of our current knowledge regarding hormone/endocrine factors in pregnancy and cervical maturation [119,120]. Two cyclooxygenase isoforms, Cox-1 and Cox-2, are responsible for catalyzing arachidonic acid to form prostaglandin H2 (PGH2), which is promptly converted by various synthases into specific PG species. Cox-1 is generally considered a constitutively expressed enzyme, whereas Cox-2 is induced in response to inflammation and other stimuli but is otherwise not active during pregnancy. Mice lacking the gene encoding Cox-1 (*Ptgs1*) exhibit delayed parturition [105,106,121,122]. Previous reports in mice suggest that the absence of prostaglandins normally produced by Cox-1 prevent luteolysis and therefore the fall in circulating progesterone, thereby explaining the delay in parturition [122].

However, recent work from our group has shown that the uterus contracts normally in Cox-1 null mice [123], leaving the reason for parturition delay unanswered. Herein, we hypothesized that abnormal cervical maturation, rather than impaired uterine contractility, plays a key role in the parturition delay of Cox-1 knockout (KO) mice.

To investigate cervical remodeling in Cox-1 KO mice throughout parturition, we employed a non-invasive method capable of probing the cervical microenvironment longitudinally *in vivo*. As previously discussed, numerous innovative cervical assessment tools that span optical, acoustic, electrical, and direct mechanical approaches have been developed [1,65,124]. These tools have already improved our understanding of cervical remodeling in term and preterm birth. A few of these techniques are directly sensitive to biochemical composition. Fluorescence spectroscopy has also been used to measure collagen concentration and solubility in women and animal models [73,125], which has consistently shown decreasing fluorescence intensity throughout pregnancy. Diffuse reflectance spectroscopy has measured significant increases in water and decreases in hemoglobin after application of prostaglandins for cervical ripening [126], as well as changes in optical properties based on hormonal status [127] and stage of pregnancy [79]. Second harmonic generation, an optical imaging method that probes fibrillar collagen, has confirmed increasing collagen dispersion throughout pregnancy in *ex vivo* human [77] and mouse studies [76,128]. More recently, optical coherence tomography was used to measure the three dimensional structure of collagen fibrils in the human uterine cervix, and found higher dispersion in excised pregnant tissues than non-pregnant samples [129]. These studies have yet to be performed *in vivo*, but contribute to increasing our understanding of collagen's role in cervical remodeling during pregnancy.

In this paper, we present the application of Raman spectroscopy, a real time light-based approach that probes biochemical information of tissues *in vivo,* to study the pregnant cervix. Raman spectroscopy measures inelastically scattered photons generated by light interaction with molecular bonds. Each molecule has specific vibrational frequencies, and Raman-scattered light can be analyzed to determine the type of molecules present in any target tissue. Raman spectroscopy is sensitive to proteins, water, nucleic acids, lipids, and carbohydrates, and measures these markers simultaneously with high specificity [130-133]. Raman spectroscopy was first applied to the *in vivo* cervix in the context of cervical dysplasia detection[134]. While conducting optimization of cervical dysplasia detection algorithms, it was discovered that Raman spectroscopy is sensitive to the effects of hormonal status on healthy cervical tissue [135-137]. These findings led to the investigation of longitudinal biochemical changes that can be measured by Raman spectroscopy in the cervix during pregnancy *in vivo*, both in mouse models and human subjects [1,138].

The goal of this study was to non-invasively test the hypothesis that cervical remodeling, rather than uterine contractility, is impaired in Cox-1 KO mice and contributes to their delayed parturition phenotype. *In vivo* Raman spectroscopy was used to determine whether biochemical differences exist in the cervix of Cox-1 KO mice during pregnancy compared to wild type (WT). Additionally, we examined whether Raman spectra could be correlated with changes in biomechanical properties of the cervix including stiffness and distensibility in WT and Cox-1 KO mice. Finally, *ex vivo* biochemical assays were performed to validate results obtained from *in vivo* Raman spectroscopy.

3.3 Methods

3.3.1 Animals

All experiments involving animals were conducted in accordance with the regulations described in the NIH Guide for the Care and Use of Laboratory Animals, using protocols approved by Vanderbilt University Medical Center's Institutional Animal Care and Use Committee (IACUC). Two groups of mice were investigated, CD-1 wild type (Jackson Laboratory) and Cox-1 null [121]. The Cox-1 null mouse was outbred to the CD-1 strain for 10 generations [105]. Animals were housed under a 12 hour dark-light cycle. Timed matings were conducted in the evenings and the presence of a post-copulatory plug the following morning defined gestation day 1. Wild type mice in this colony typically deliver on the evening of day 19 (designated d19.5). Six time points during pregnancy were investigated for each mouse genotype; WT mice were measured on days 4, 12, 15, 18, 19, and non-gravid, whereas Cox-1 KO mice were measured on days 4, 12, 15, 19, 20, and non-gravid. Non-gravid mice were measured in the diestrus phase of the estrous cycle as determined by vaginal lavage.

3.3.2 *In situ* hybridization

Eleven micrometer thin frozen uterine sections were obtained from WT and Cox-1 KO mice and mounted on the same glass slides and *in situ* hybridization was performed as previously described [139].

3.3.3 *Ex vivo* myometrial contractility

Uterine myometrial strips were collected post-mortem, and used in an *ex vivo* isometric contractility assay as previously described [140].

3.3.4 Raman spectroscopy

A portable, fiber optic probe-based Raman spectroscopy system was used (Fig. 3.2*E*) for all Raman measurements acquired. The system consisted of an imaging spectrograph (Holospec f/1.8i, Kaiser Optical Systems, Ann Arbor, MI) coupled to a thermoelectrically cooled CCD camera (PIXIS: 256BR, Princeton Instruments, Princeton, NJ). A 785 nm diode laser (Innovative Photonic Solutions, Monmouth Junction, NJ) delivered 80 mW of power through a custom made fiber optic probe (Fig. 3.2*D*) (EmVision, Loxahatchee, FL) to the cervix.

The system was wavelength calibrated using a neon-argon lamp, and naphthalene and acetaminophen standards were used to determine the exact excitation wavelength for subsequent Raman shift calculations. The system was corrected for spectral response using a tungsten lamp that was calibrated by the National Institute of Standards and Technology. Spectra were smoothed using a Savitzky-Golay filter, background subtracted, and fluorescence subtracted using a modified polynomial fit method previously described [141].

During measurements, all room lights were turned off. For *in vivo* experiments, animals were anesthetized using isoflurane, and the vaginal cavity and cervix were rinsed gently using saline. A small speculum tube was inserted to improve visualization of the mouse cervix and ensure contact of the fiber probe with the proper tissues during measurements (Fig. 3.3*A*-*C*). A range of 5-10 spectra were taken at multiple locations around the ectocervix of each mouse with

an integration time of 3 seconds per measurement. For *ex vivo* experiments, the cervix was excised and immediately measured using an integration time of 10 seconds.

3.3.5 Raman data analysis

Processed, non-normalized Raman spectra were used for data analysis. The signal to noise ratio (SNR) and adipose tissue signal from each Raman spectrum was calculated, and spectra with low signal (less than 100 counts at the 1440 cm^{-1} peak) as well as spectra with high adipose content (greater than 1800 counts at the 1440 cm^{-1} peak) were removed from analysis. Raman spectra were averaged by each mouse for display in Figures 3.2 & 3.3. Ratios from Raman peaks were calculated prior to averaging, and the results were subsequently averaged for each mouse. Peak ratios sensitive to ECM, lipids, and nucleic acids were plotted using the mean and standard error for each mouse model and gestation. Ratios were used as a way to normalize and make comparisons across many data sets that have varying levels of signal intensity and SNR. Student t-tests (two-sided) were performed to determine statistical significance (α=0.05) between WT and Cox-1 KO mice at each gestation measured.

Using the RMS package, Raman spectra were modeled using generalized linear models in the R software. The rate of change of various Raman peak ratios and NNLS coefficients over gestation were modeled and the WT and Cox-1 KO curves were compared. In this analysis, the Raman peak ratio or NNLS coefficient of interest was the dependent variable, whereas the gestation time and mouse model were independent variables. To account for signal intensity fluctuations, the spectral intensity (measured as the intensity of the 1440 cm^{-1} peak) was added as another independent variable which acts as a baseline offset. The time variable was modeled as a restricted cubic spline with three nodes to allow for non-linear behavior with respect to time. The

last time point for each model (WT=19, Cox-1 KO =20) was assigned an indicator variable that allowed for the capture of significant changes at the end of pregnancy. The mouse model was set as a factor variable. To account for heteroscedasticity, the robust covariance function created in the RMS package ('robcov') was used to adjust the standard errors. Finally, to evaluate interactions between the gestation time and mouse model, an ANOVA was performed on the generated curves from the developed regression model.

Non-negative least squares analysis was performed to determine the contributions of 3 different biochemical components as a function of gestation and mouse model [86,142,143]. This analysis follows the equation

$$Y = \beta * X + \varepsilon \quad \text{(Eqn. 3.1)}$$

where the design matrix X was filled with pure biochemical spectra (collagen type-I (Sigma), adipose tissue (collected from mouse abdomen post-mortem), and water), and the tissue spectrum being analyzed in Y. The optimum coefficients β that minimize the error ε were determined for each spectrum. For this analysis, NNLS regression was performed (MATLAB) such that components could not have a negative contribution on a spectral fit. For this study, the term "residual' was defined as the difference between the "observed spectrum" and the "fitted spectrum". A negative residual meant that in certain regions of the spectrum, the "fitted spectrum" was of greater intensity than the "observed spectrum." None of the NNLS coefficients were calculated to be negative. The residuals per spectrum were summed and all spectra with a summed residual higher than 0.3 were removed from further analysis. The average coefficients for each biochemical component were calculated as a function of mouse model and gestation. Spearman correlations were performed on four Raman peak ratios and the collagen NNLS coefficient which were compared with biomechanical measures.

3.3.6 *Ex vivo* biomechanical testing

Cervical tissue was excised post-mortem by cutting perpendicularly across the uterocervical junction where the uterine horns converge into the cervical canal. All vaginal tissue was removed and the dimensions of the cervical tissue were measured. The freshly excised cervical tissue was immediately placed in oxygenated Krebs Bicarbonate buffer at 37 °C for 10 minutes to equilibrate. Next, the tissue underwent stress-relaxation testing using a Radnoti Organ Bath System. This method allowed assessment of the viscoelastic behavior of each cervical tissue. The system was calibrated by recording force (measured in volts) with no added weight and with a 100 gram test weight, and the measured voltage was converted to force (mass x gravity). The tissue was then mounted on two stainless steel triangular hooks and attached to a force transducer with a mechanical drive. The hooks were slowly pulled apart until tension in the tissue was measured, after which the separation between the hooks was reduced to determine the "initial dilation" of the cervical tissue without strain-induced stress. This baseline distance (initial dilation) was recorded for each specimen, and then the stress-relaxation testing protocol was initiated as follows. The cervical tissue remained in an unloaded state for four minutes, and then experienced a strain of 0.1 mm/s for a total of ten seconds (one mm displacement), after which the strain was held constant for four minutes. This protocol was repeated until tissue failure, defined as the displacement at which sudden loss of stress is experienced by the tissue under tensile loading [144], as shown in Fig. 3.5*A*. This process was controlled using stepper motors (Applied Motion Products) that were programmed with an Arduino Uno board. Recorded data was converted into stress based on the cross-sectional area of the tissues. Total dilation was calculated as the initial dilation plus displacement during biomechanical testing prior to tissue failure. Equilibrium stiffness was calculated for each tissue by plotting the average stress from

the last 30 seconds of each stress cycle and generating a curve. The slope of the linear region of each curve was calculated as a simple measure of stiffness, as well as a model fit to the following exponential model described by Timmons et al [114]:

$$\text{Stress}=(A/B)*[\exp(\text{cervical opening}*B)-1] \quad \text{(Eqn. 3.2)}$$

where the parameters A and B measure the stiffness at small and large displacements, respectively. The impulse stiffness was calculated for each tissue by plotting the maximum stress achieved from each stress cycle and generating a curve, which was similarly evaluated by taking the slope in the linear region, and a fit to the exponential model. Statistical analysis was performed on initial dilation, total dilation, equilibrium stiffness A and B coefficients, and impulse stiffness A and B coefficients using t-tests (* indicates $p<0.05$).

3.3.7 *Ex vivo* biochemical assays

For all *ex vivo* biochemical assays, cervical tissues were excised post-mortem, immediately flash frozen with Super Friendly FREEZE'IT (Fisher Scientific) and then placed in -80 °C.

Progesterone concentrations were measured by the Endocrine Technologies Support Core (ETSC) at the Oregon National Primate Research Center (ONPRC, Beaverton, OR) using extraction-radioimmunoassay (RIA) [145]. Tissue samples were weighed and homogenized in 1 ml PBS, then extracted with 6 ml diethyl ether, dried under forced air stream and re-dissolved in assay buffer (0.1% gel-PBS). Progesterone values were corrected for extraction losses determined by radioactive trace recovery performed simultaneously with sample extraction, which ranged between 95.3-96.8% (n=3). The assay range for the P4-extraction RIA was 5-750 pg/tube. The intra-assay variation for the assays ranged from 5.8%-8.9% and inter-assay

variation was 7.3%. Overall inter-assay variation for extraction-RIAs in the ETSC is less than 15%.

For cervical hydration and collagen content assays, tissues were weighed, and then lyophilized overnight. After freeze-drying, the tissues were weighed again. Based on these measurements, water content was determined as (wet weight/(wet weight+dry weight)). Next, a standard collagen extraction procedure was performed as previously described [49]. To quantify collagen content, a hydroxyproline assay was performed per manufacturer's instructions (BioVision, Milpitas, CA).

3.4 Results

3.4.1 The uterus contracts normally during delayed parturition in Cox-1 KO mice

Examination of Cox-1 (*Ptgs1*) and Cox-2 (*Ptgs2*) messenger ribonucleic acid (mRNA) expression on the day of expected delivery (day 19) in WT mice (Fig. 3.1*A***)** revealed strong Cox-1 expression in the uterine luminal epithelium (LE) but low expression in the cervix; Cox-2 expression was low throughout the lower uterine segment. The timing of delivery was significantly delayed ($p = 0.0001$) in Cox-1 KO compared to WT mice (Fig. 3.1*B*). Despite strong Cox-1 expression in the uterus, representative tracings from *ex vivo* spontaneous uterine contractility experiments show that contraction patterns (Fig. 3.1*C*), and contractile activity (area under the curve of contractions per unit time) did not differ between WT and Cox-1 KO uteri on gestation day 15, 19, or comparison of WT day 19 versus Cox-1 KO day 20 (Fig. 3.1*D*). Thus, normal uterine function during delayed parturition suggests that the cervix may contribute to the delay, providing motivation for studying cervical remodeling in this model.

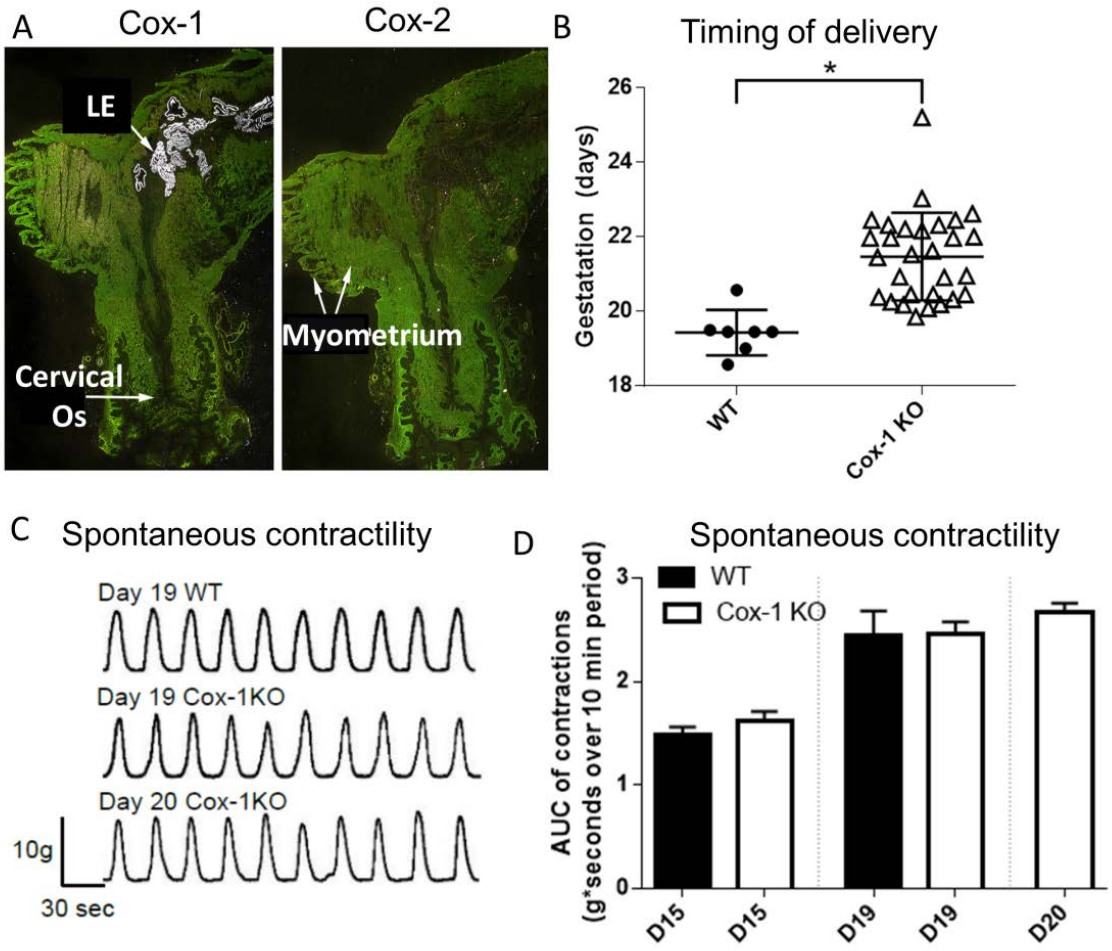

Figure 3.1**:** Cox-1 expression in the pregnant mouse uterus, and the effect of global Cox-1 deletion on parturition and uterine contractility. A) In situ hybridization of 35S-labeled Cox-1 and Cox-2 in WT day 19 mouse uterus. B) Timing of delivery was recorded from pregnant WT and Cox-1 KO mice (*p=0.0001). C) Representative *ex vivo* contractility tracings of myometrial strips from pregnant mice on the indicated days of pregnancy. D) Recordings of myometrial contractility (n=5-11 mice per group) were analyzed for area under the curve (AUC). Mean ± SEM.

3.4.2 Raman spectral signatures from wild type and Cox-1 KO cervices deviate at the time of parturition

An approach for using Raman spectroscopy to assess the biochemical status of the cervix over time in WT and Cox-1 KO mice was developed. Raman spectra were acquired *in vivo* from the cervix of non-gravid (NG) and pregnant WT and Cox-1 KO mice using a portable Raman

spectroscopy system (Fig. 3.2*A*-*E*). Measurements were taken from multiple sites on the ectocervix with the aid of a speculum (Fig. 3.2*B*-*C*) for visualizing the probe location. A custom-built fiber optic Raman probe was used for spectral acquisition and a 3 second integration time was used for each spectrum. Average peak-normalized spectra (normalized to 1440 cm^{-1} peak for spectral visualization purposes only, all subsequent statistical analysis was performed on non-normalized spectra) were plotted for each mouse model over the course of pregnancy (n=8-10 mice per group, per time point) (Fig. 3.2*F*-*G*). Regions of interest (gray bands, Fig. 3.2*F*-*G*) that showed maximum differences were identified for further analysis (Figs. 3.3-4).

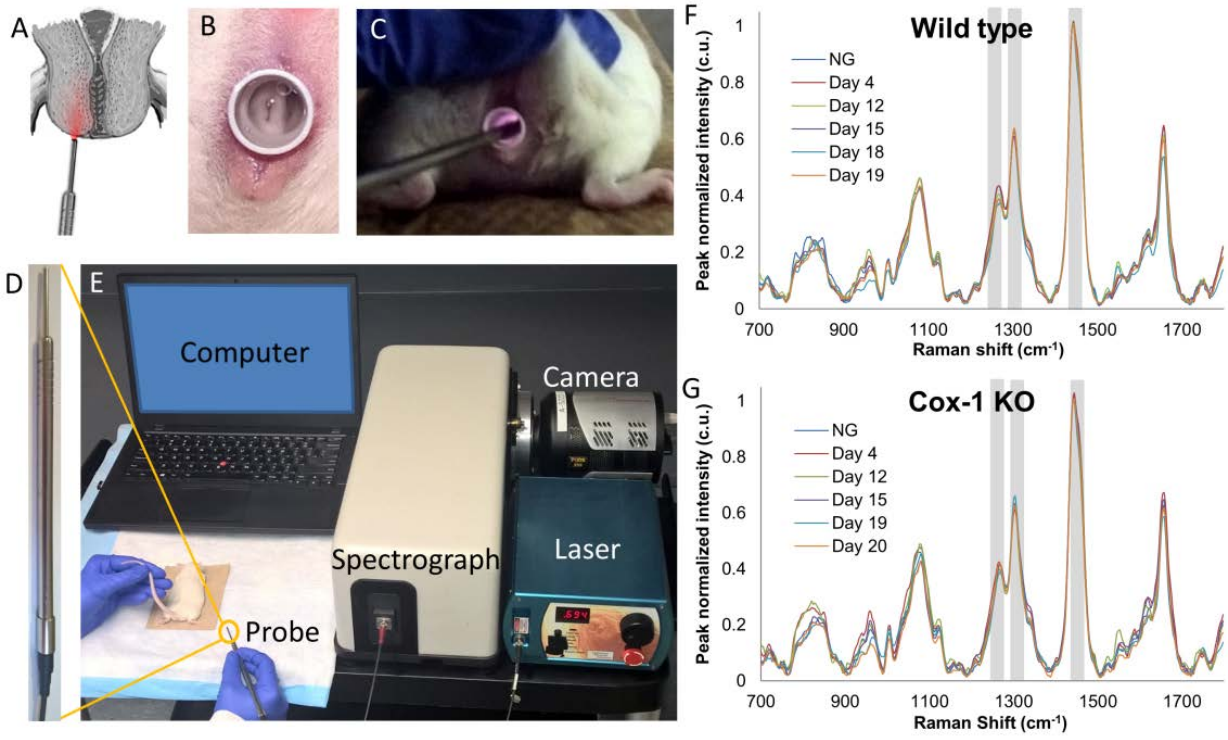

Figure 3.2: *In vivo* Raman spectroscopy system for cervical assessment during pregnancy. A) Illustration showing the placement of the Raman spectroscopy fiber optic probe against the ectocervix of the mouse. B) Mouse cervix visualized using a speculum. C) *In vivo* Raman spectroscopy during measurement of mouse cervix. D) Raman spectroscopy fiber optic probe. E) Image of *in vivo* Raman spectroscopy system. Average Raman spectra from different time points during pregnancy in WT (F) and Cox-1 KO (G) mice. Gray boxes indicate regions that were highlighted in Figures 3.3-4.

Ratios of multiple Raman peaks were calculated and plotted as a function of gestation day and mouse model to quantitatively evaluate spectral changes over time. Of the various peaks analyzed, the 1304 cm^{-1} peak increased while the 1265 cm^{-1} peak decreased throughout gestation (dashed lines in Fig. 3.3*A*-*B*). The 1304 cm^{-1} to 1265 cm^{-1} Raman peak ratio tentatively assigned to lipid/protein change [130,131] increased starting at day 12 in both mouse models, however, the rate of change was higher and reached a larger ratio in the WT compared to the Cox-1 KO (Fig. 3.3*C*) ($p<0.05$). Furthermore, a sharp decrease was observed in the WT on day 19 of pregnancy ($p<0.05$), but this decrease did not occur in the Cox-1 KO until day 20 (Fig. 3.3*C*). The trends seen in other Raman peaks at 1003 cm^{-1} (phenylalanine [130]), 1440 cm^{-1} (lipids [131]), and 1657 cm^{-1} (proteins [130]) are displayed in Figure 3.4. To test the generalizability of the Raman spectral changes measured over pregnancy, as well as provide curve analysis and interpolation between measured points, a generalized linear model was developed (Fig. 3.3*D*). The 1304/1265 cm^{-1} peak ratio model showed similar features to the data presented in Fig. 3.3*C*, and revealed highly significant changes as a function of gestational age ($p<0.0005$) and mouse model ($p<0.0005$).

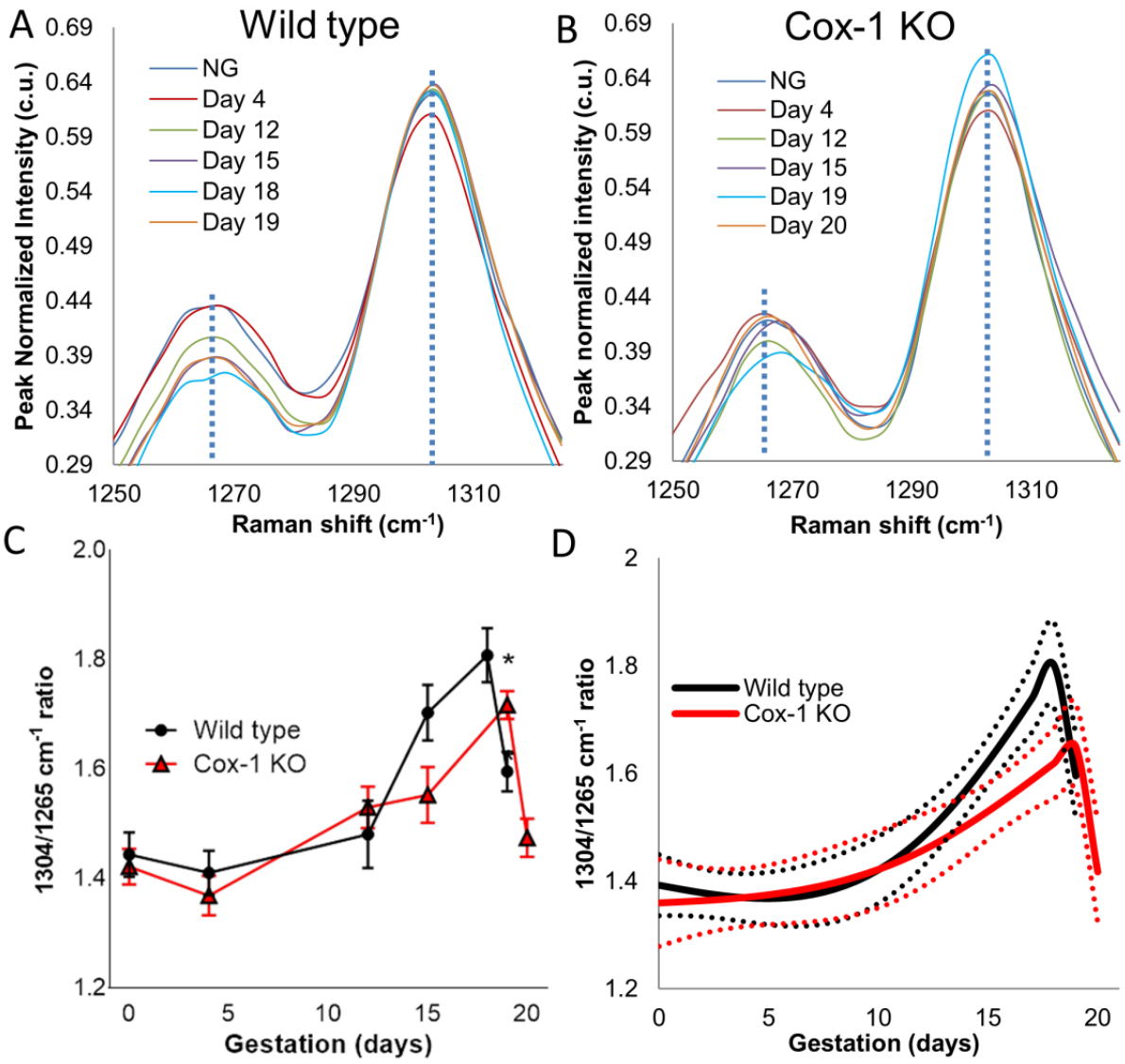

Figure 3.3: Raman spectral bands change with pregnancy and are delayed in the Cox-1 KO mouse compared to WT. Average Raman spectra from the 1265 cm^{-1} peak (blue dashed line) and 1304 cm^{-1} peak (blue dashed line) during different time points of pregnancy in WT (A) and Cox-1 KO (B) mice. C) Mean ± SEM of the 1304 cm^{-1} to 1265 cm^{-1} peak ratio as a function of gestation in WT and Cox-1 KO mice (p-<0.05). D) Modeled longitudinal trajectories of the 1304 cm^{-1} to 1265 cm^{-1} Raman peak ratio.

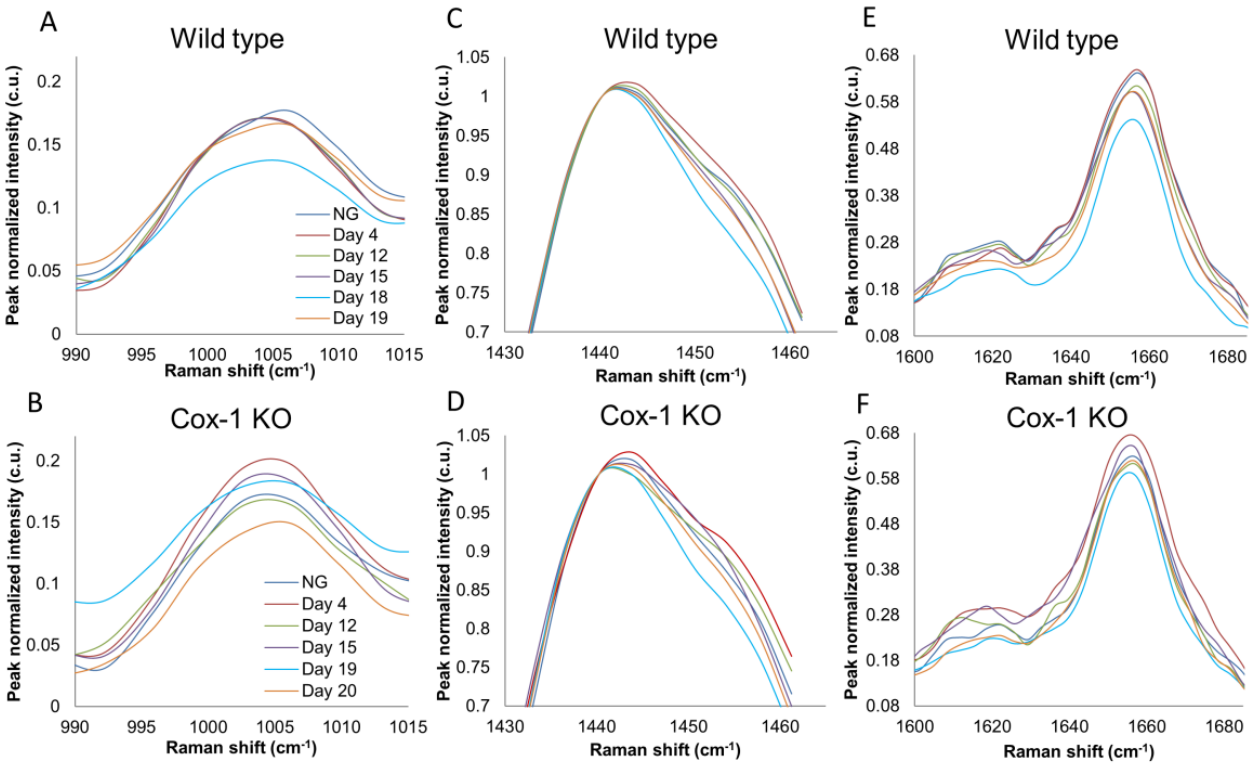

Figure 3.4: Average Raman spectra from the 1003 cm-1 peak (A & B), 1440 cm-1 peak (C & D), and 1657 cm-1 peak (E & F) during different pregnancy time points in WT and Cox-1 KO mice. Spectra were peak-normalized to the 1440 cm-1 peak for ease of visualization.

Besides 1304/1265 cm^{-1}, multiple peak ratios displayed significantly different trajectories over the course of pregnancy between WT and Cox-1 KO mice. Fig. 3.5*A* shows the trajectory of the 1265 cm^{-1}/1440 cm^{-1} ratio which gradually decreased until day 12 in both mouse models. The WT showed a steeper decrease from day 12 to day 18, but then sharply increased on day 19. The Cox-1 KO did not decrease as steeply and not until day 15 before sharply increasing on day 20. The three phases of spectral change may be analogous to the softening, ripening and dilation phases[43] in WT and Cox-1 mice but with a delay in the ripening to dilation transition in the Cox-1 KO mice. The 1265/1440 cm^{-1} ratio model showed significant changes over the course of

pregnancy ($p<0.0005$) and as a function of mouse model (($p<0.0005$), as well as in the interaction between gestation and mouse model ($p<0.05$) (Fig 3.5B).

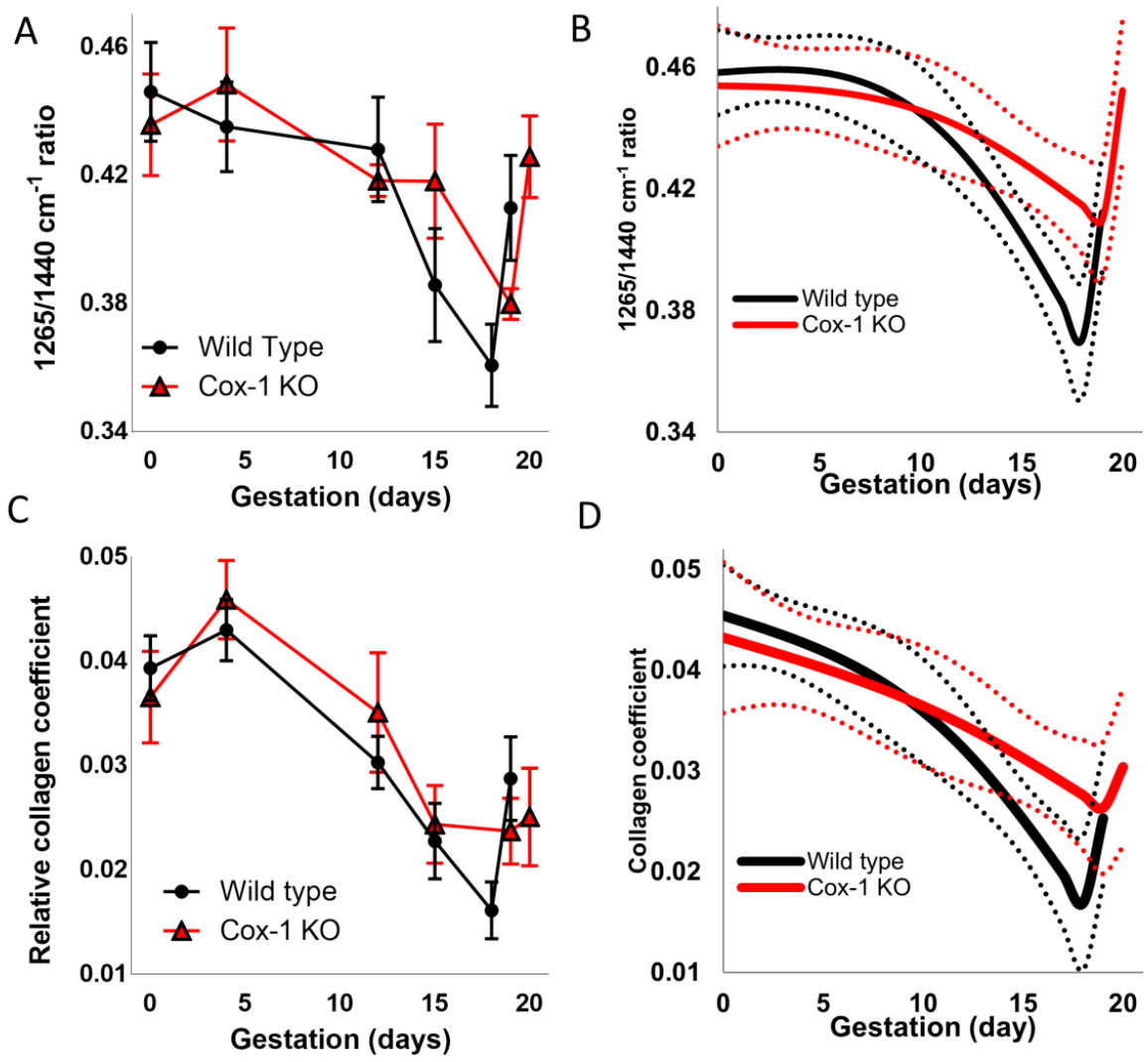

Figure 3.5: Raman spectra reveal delayed remodeling in the Cox-1 KO mouse at term. Mean ± SEM (A) and modeled longitudinal trajectories (B) of the 1657 cm^{-1} to 1440 cm^{-1} peak ratio. Mean ± SEM (C) and modeled longitudinal trajectory (D) of the non-negative least squares model collagen coefficient as a function of gestation in WT and Cox-1 KO mice.

A non-negative least squares (NNLS) analysis was performed to understand the biochemical basis of the *in vivo* Raman spectra. Pure spectra were collected from collagen I,

water, and adipose tissue which revealed characteristic fingerprints, demonstrating molecular specificity (Figure 3.6).

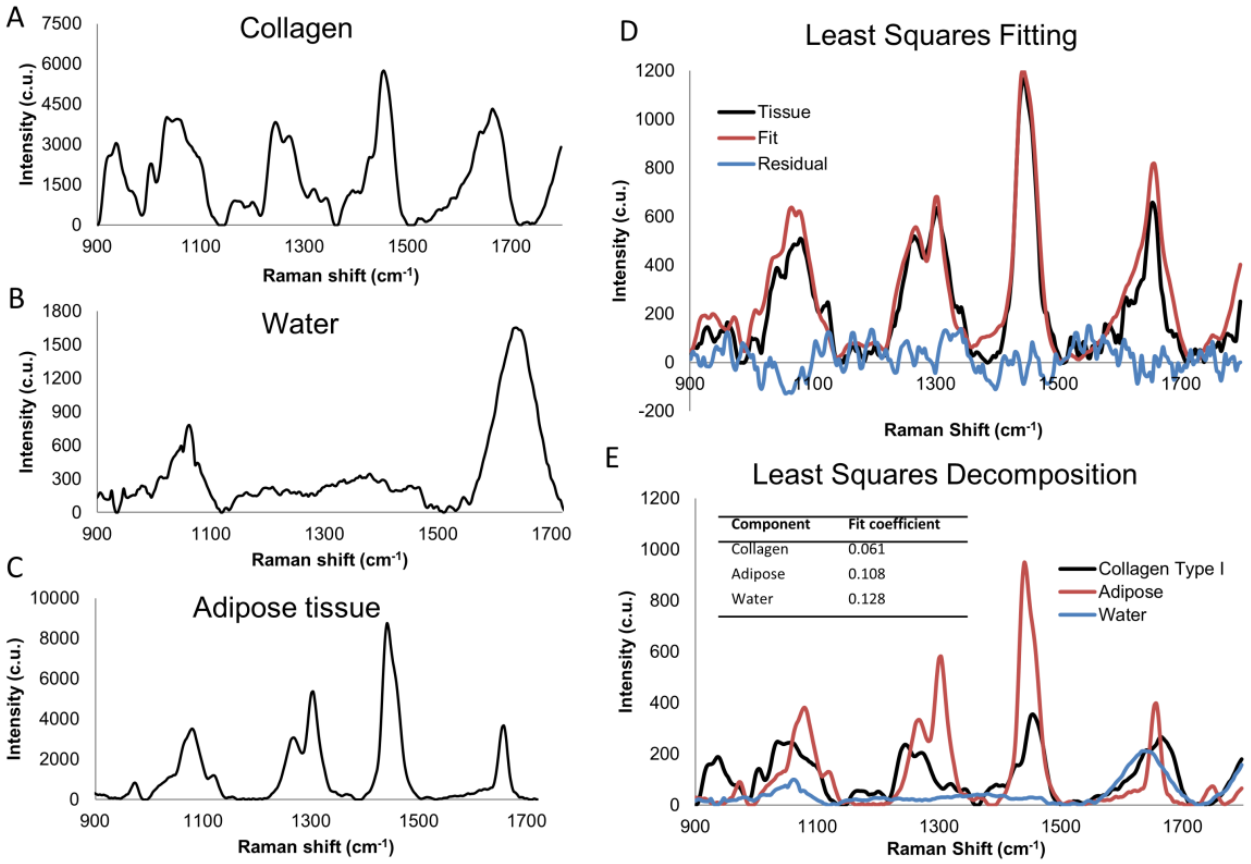

Figure 3.6: Non-negative least squares components and model fits. Raman spectra of A) collagen I, B) water, and C) mouse adipose tissue. D) Overlay of representative cervical tissue spectrum (black), least squares fit (red), and the residual (blue). E) Pure spectra multiplied by their fit coefficients from the tissue spectrum in D, with their fit coefficients inlaid in the plot.

Although adipose tissue is not known to be present within the cervix, it is likely that surrounding fat pads such as the inguinal, perigonadal, and lower pelvic fat pads were detected in some of the Raman spectra[146], and as such adipose was incorporated into the NNLS model. A representative cervical tissue spectrum (black) was fit using the NNLS model (red) developed using the pure component spectra, and then overlaid with the residual (blue) (Figure 3.6D). The

residual was small and fluctuated above and below zero. Furthermore, the least squares fit was decomposed such that the contribution from each component was easily seen (Figure 3.6E). The contribution of collagen in Raman signals decreased over the course of pregnancy starting on day 12 in WT and Cox-1 KO mice. WT levels steadily declined until day 18 and then spiked on day 19, but Cox-1 KO levels plateaued at day 15 and increased on day 19 and 20 (Fig. 3.5C). The collagen coefficient was also analyzed using the developed generalized linear model (Fig. 3.5D), and revealed significant changes over gestation ($p<0.0001$), but no significant differences were reported between mouse models. To verify this result without the influence of adipose tissue, the cervix was excised from non-gravid and day 19 WT mice and Raman spectra were obtained. The spectra were fit to the NNLS model which revealed that the collagen coefficient was lower on day 19 of pregnancy (Figure 3.7), similar to the *in vivo* results.

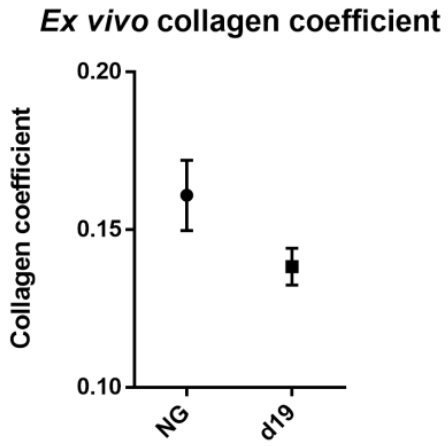

Figure 3.7: Non-negative least squares collagen coefficients obtained from excised non-gravid (n=8) and day 19 (n=4) WT cervix tissues. Plotted as mean ± SEM, (p=0.05).

3.4.3 Wild type and Cox-1 KO *ex vivo* cervical biomechanical properties deviate at the end of pregnancy

After performing *in vivo* Raman spectroscopy, the cervices of select mice (n=8-9 per group, per time point) were excised for paired *ex vivo* biomechanical testing to determine whether mechanical properties changed in response to altered tissue biochemistry with pregnancy. A defined tissue displacement protocol was followed for biomechanical testing (Fig. 3.8*A*). Representative data from a WT day 15 cervix that underwent stress-relaxation testing is shown in Fig. 3.8*B*; red circles indicate the impulse stress experienced by the tissue for each increase in displacement and provides information regarding the elastic nature of the tissue. Blue circles indicate the equilibrium stress that cervical tissues maintained after a strain, providing information on viscous properties.

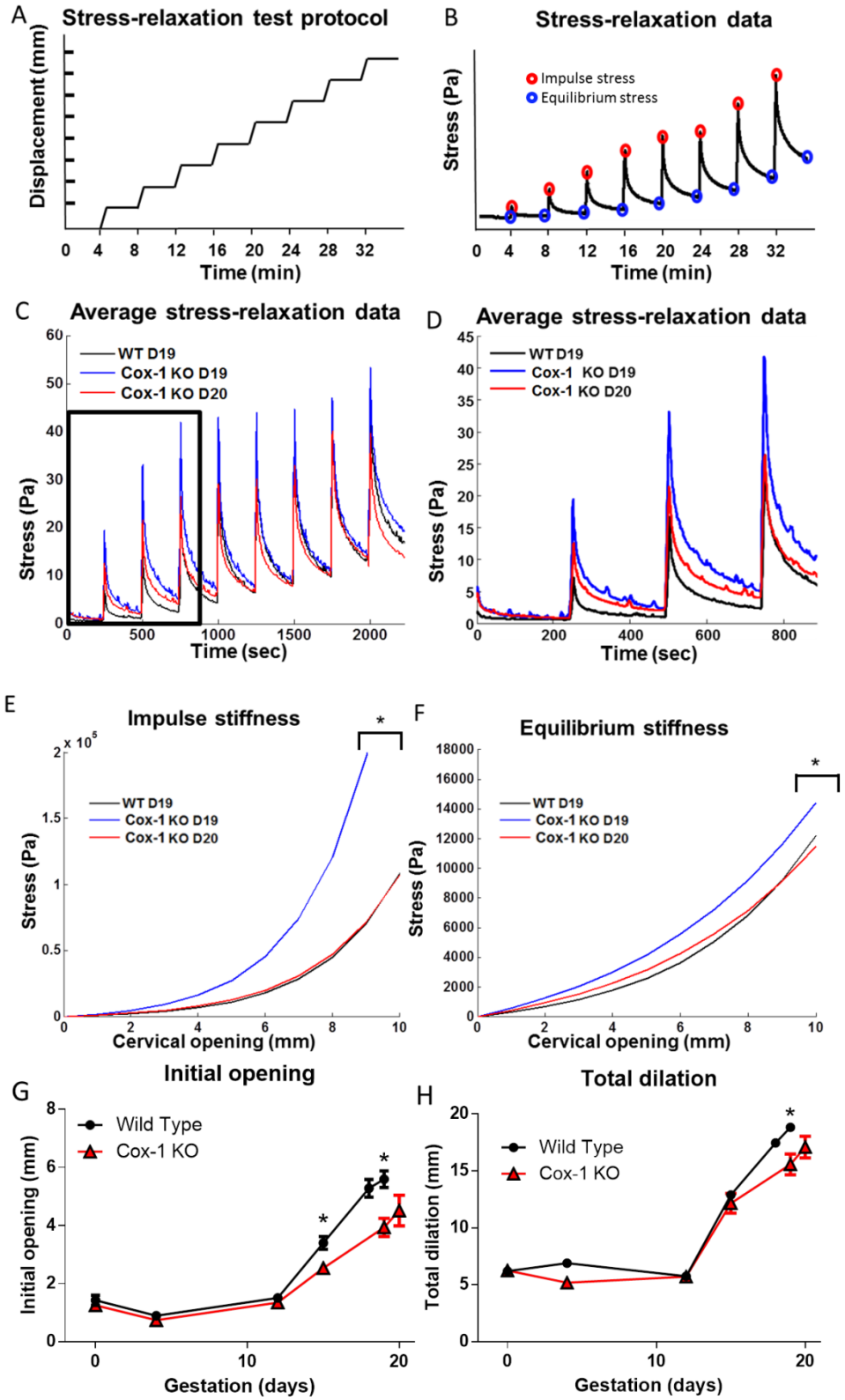

Figure 3.8: Cox-1 KO mice have less distensible cervices at term than WT. A) Displacement protocol used for biomechanical stress relaxation tests. B) Representative data from stress-

relaxation biomechanical tests. Red circles highlight the maximum impulse stress observed for each displacement; blue circles highlight the equilibrium stress observed four minutes post displacement. C) Average stress-relaxation recordings from WT day 19, Cox-1 KO day 19, and Cox-1 day 20 cervical tissues. D) Inset of the average stress-relaxation data from the first three displacements. E-F) Average exponential fits to the impulse stiffness and equilibrium stiffness results from WT day 19, Cox-1 KO day 19, and Cox-1 KO day 20 cervical tissues, *$p<0.05$ compared to day 19 WT. G) Unloaded dilation of *ex vivo* cervical tissues from WT and Cox-1 KO mice across gestation (n=8-10 per group, per time point). H) Total dilation of *ex vivo* cervical tissues prior to tissue failure.

Average raw data generated from WT day 19, Cox-1 KO day 19, and Cox-1 day 20 mice segregated into distinct groups (Fig. 3.8*C-D*). Over the first three displacements performed (Fig. 3.8*D*), Cox-1 day 19 tissues experienced the greatest amount of stress per millimeter of displacement, followed by the Cox-1 day 20 tissues, and then WT day 19 tissues, which exhibited a smaller degree of stress, particularly at the first two displacements.

The impulse and equilibrium stress were modeled using an exponential curve described by Timmons et al. [114] to compare the stiffness of the cervical tissues in WT and Cox-1 KO mice. The stresses were significantly greater in the gestation day 19 Cox-1 KO tissues compared to day 19 WT and day 20 Cox-1 KO (Fig. 3.8*E-F*). The A and B coefficients were significantly higher in Cox-1 KO day 19 tissues compared to WT day 19 and Cox-1 KO day 20 (Table 4.1, $p<0.05$), indicating that the Cox-1 KO tissues experienced greater stress at small and large displacements, respectively. Taken together, these data (Fig. 3.8*A-F*) indicate that the Cox-1 KO cervix is more rigid at term, but becomes more like the compliant WT cervix after one additional day of gestation.

Table 3.1: Coefficients of the cervix viscoelasticity model

Model:	Stress=(A/B)*[exp(cervical opening*B)-1]			
Equilibrium stiffness	**A**	**+/- SEM**	**B**	**+/- SEM**
d19 WT	253.49	78.85	0.26	0.02
d19 COX-1 KO	*520.62	153.41	0.18	0.03
d20 COX-1 KO	380.61	111.49	0.19	0.03
Impulse Stiffness	**A**	**+/- SEM**	**B**	**+/- SEM**
d19 WT	678.82	232.65	0.42	0.05
d19 COX-1 KO	*1512.47	491.83	0.45	0.12
d20 COX-1 KO	849.36	375.92	0.39	0.12

Significant differences were observed between the Cox-1 KO day 19 and WT day 19 tissues among the A parameters in both the equilibrium and impulse stiffness curves ($p<0.05$).

Initial dilation of the cervical os measured in excised, unloaded tissues was significantly different ($p<0.05$) between time-matched WT and Cox-1 KO mice on gestation day 15 and 19, as well as between day 18 WT and day 19 Cox-1 KO (Fig. 3.8*G*). However, day 19 WT compared to day 20 Cox-1 KO was not significantly different, indicating catch-up dilatability of the post-mature Cox-1 KO cervix under baseline conditions. Total cervical dilation (initial dilation + displacement at failure during stress-relaxation testing) was measured across gestation (Fig. 3.8*H*). On day 19 of pregnancy, the WT cervix was able to dilate to a greater extent than Cox-1 KO before tissue failure occurred ($p<0.05$). No difference was observed between the day 19 WT and day 20 Cox-1 KO cervices, suggesting eventual catch-up of KO tissues as the parturition delay continued.

3.4.4 *In vivo* Raman spectra correlate with *ex vivo* biomechanical measures

Multiple Spearman correlations were computed between Raman spectral features and mechanical measures (Fig. 3.9). The black box highlights correlations between Raman spectra and biomechanical properties of the cervix where strong positive correlations (bright red) and strong negative correlations (bright blue) were observed. Many of these comparisons were statistically significant, with the highest correlations coming from the Raman spectral collagen coefficient ($p<0.005$ for all biomechanical comparisons), followed by the 1304/1265 cm^{-1} lipid/protein ratio ($p<0.05$ for all biomechanical comparisons).

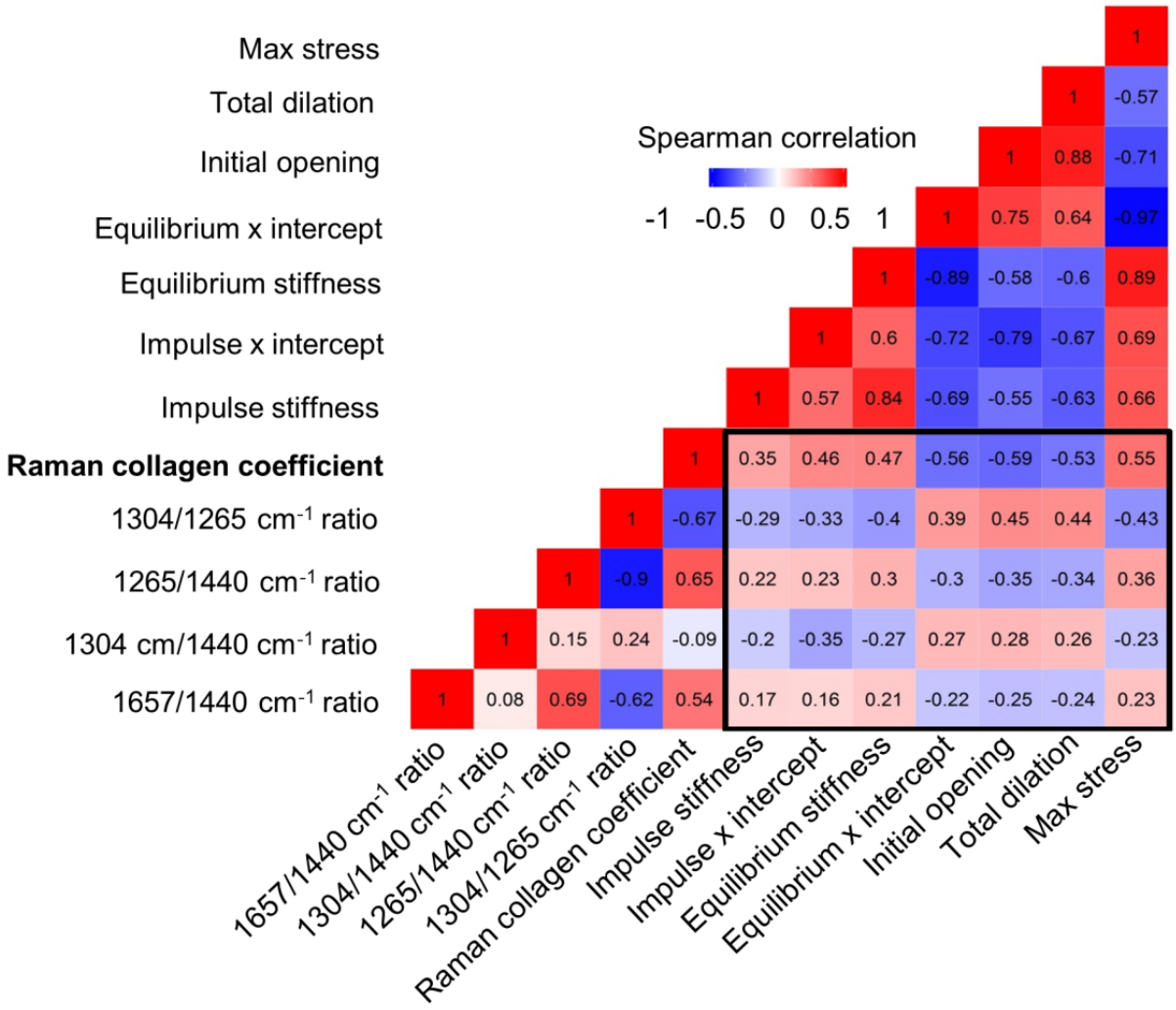

Figure 3.9: *In vivo* Raman data correlate with *ex vivo* biomechanical properties. Spearman correlation matrix containing four Raman peak ratios and a non-negative least squares component representative of collagen signatures for comparison to the impulse stiffness, impulse x intercept, equilibrium stiffness, equilibrium x intercept, initial opening, total dilation, and maximum stress measures obtained during biomechanical testing.

3.4.5 Cervix progesterone levels remain elevated in Cox-1 KO mice at the end of pregnancy

Progesterone levels are elevated during pregnancy to maintain a quiescent state in mice. Cervical tissue progesterone levels were measured using radioimmunoassay detection in WT mice on gestation day 17 to determine progesterone levels prior to the onset of labor, on gestation day 19 to measure pre-parturition levels, and on day 19.5 to measure levels at the time

of active labor. Similarly, Cox-1 KO cervical tissues were measured on gestation days 17, 19, and 19.5, as well as gestation day 20 due to delayed parturition (Fig. 3.10*A*). As expected, gestation day 17 progesterone values were the highest in both WT and Cox-1 KO pregnant mice since luteolysis had not yet occurred. On gestation day 19, progesterone levels declined in both WT and Cox-1 KO mice compared to day 17 ($p<0.001$) although Cox-1 KO levels remained significantly elevated compared to WT ($p<0.005$). On gestation day 19.5, progesterone levels were significantly lower ($p<0.05$) in the WT group compared to time-matched Cox-1 KO mice. While Cox-1 KO mice still had higher mean progesterone levels on gestation day 20 compared to WT mice on gestation day 19.5, the difference was not statistically significant ($p=0.13$).

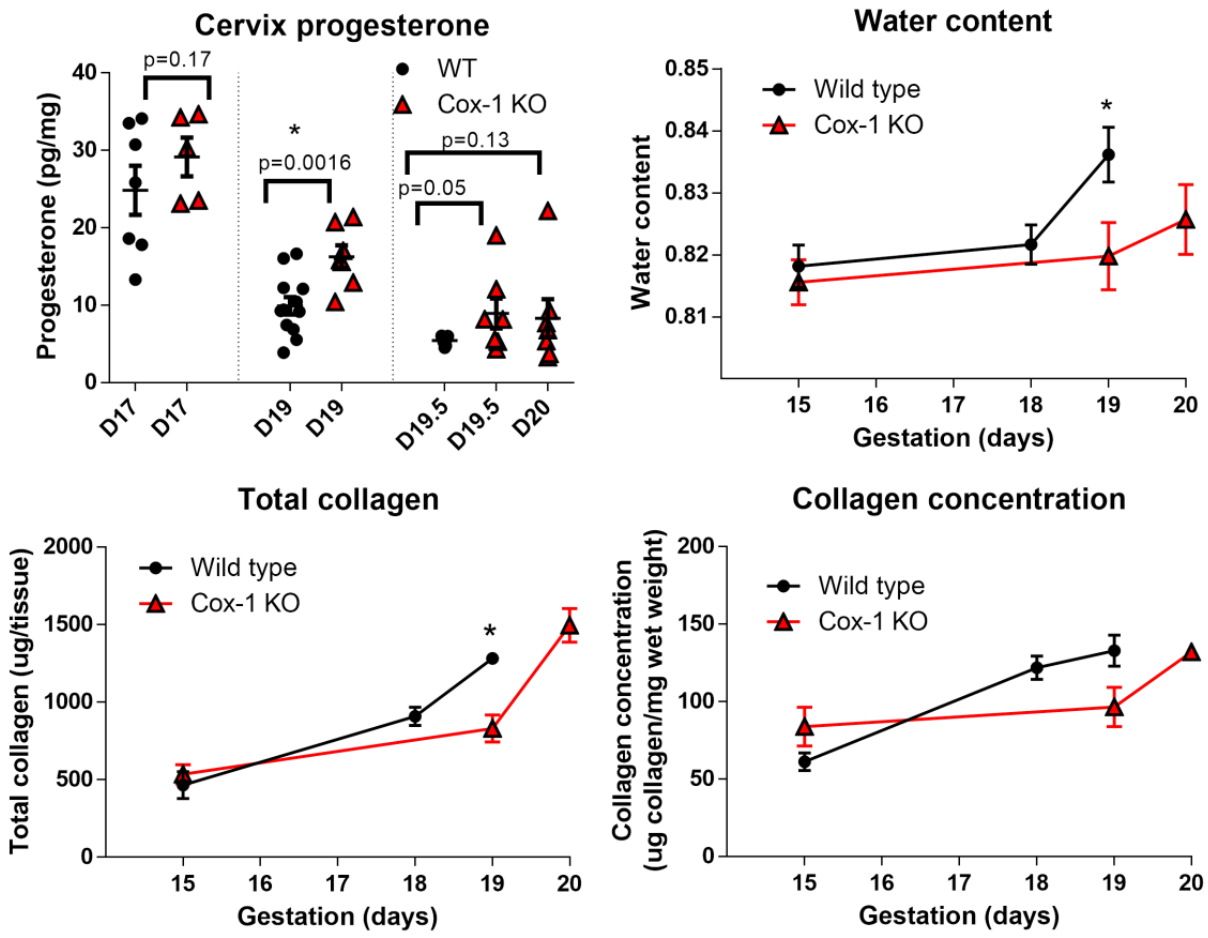

Figure 3.10: *Ex vivo* biochemical assays of cervix composition show delayed remodeling and Cox-1 KO mice. A) Cervix progesterone levels. B) Water content. C) Total collagen. D) Collagen concentration (μg/mg wet weight). Plotted as mean ± SEM, *p<0.05 compared to day 19 WT.

3.4.6 Tissue hydration and collagen content significantly differ at term gestation

In order to validate the results obtained from *in vivo* Raman spectroscopy, we performed *ex vivo* biochemical assays to measure tissue hydration and collagen content in cervix samples from WT and Cox-1 KO mice. Gestation day 19 WT mice had significantly greater water content than Cox-1 KO mice on day 19 ($p<0.05$) but not day 20 as indicated by these assays (Fig. 3.10*B*). An established collagen assay based on hydroxyproline content was used to determine

the total collagen content (micrograms of collagen per tissue) (Fig. 3.10*C*). Total collagen slowly increased from day 15 within both WT and Cox-1 KO mice. However, significantly higher ($p<0.01$) levels of collagen were detected in WT mice on day 19, which was eventually achieved in the Cox-1 KO mice on day 20 of gestation. No significant differences were observed between WT and Cox-1 KO cervical tissues in collagen concentration (Fig. 3.10*D*) for any time points examined.

3.5 Discussion

Prostaglandins are key regulators of multiple aspects of female reproduction, including uterine contractility, and cervical ripening in inflammation-induced preterm birth [114,147,148]. Impaired luteolysis and prevention of the expected progesterone decline in Cox-1 KO mice is currently considered the mechanism for delayed parturition in these mice [122] and similar models of prolonged gestation [108,122,149-153]. Despite speculation of suppressed uterine contractility of Cox-1 KO mice, we observed unhindered uterine contractility despite a 2-3 day delay in delivery of offspring, indicating that uterine contractility is not the basis for delayed parturition and suggests that impaired cervical remodeling may be responsible for preventing normal birth timing [123]. We used Raman spectroscopy to show for the first time that parturition-related changes in biochemical composition of the cervix are delayed in Cox-1 mice. This optical technique correlates to biomechanical measures of cervical rigidity and can be used to non-invasively stage maturation of the cervix over the course of pregnancy and in the pre-parturition period leading up to birth.

Although prostaglandins are widely regarded as essential molecules for cervical ripening, our data showing restricted Cox expression in the pregnant mouse cervix corroborate recent

unexpected findings by Timmons et al. [114] where low levels of Cox-1 and Cox-2 expression and low cervical prostaglandin levels were noted during normal pregnancy. Cervix prostaglandin levels were increased in the immediate post-partum period, likely related to heightened Cox expression or via prostaglandin synthesis in nearby uterine tissues (Fig. 3.1), which then bind and activate cervix prostaglandin receptors [154]. While upregulation of Cox-2 can partially compensate for the absence of Cox-1 in the uterus [155], we previously showed that prostaglandin levels were at the lower limits of detection in Cox-1 KO uteri [105]. Interestingly, our present study showed that deletion of Cox-1 did not impair uterine contractions (Fig. 3.1 *C-D*). It was previously thought that Cox-1-derived prostaglandins directly stimulate myometrial contractility or that PGF2α acts on the corpus luteum, leading to subsequent luteolysis, progesterone fall, and uterine activation for labor [156]. The compensatory mechanisms enabling normal uterine contractions in Cox-1 KO mice are not yet fully understood, but support an impaired cervical remodeling hypothesis that was tested in the current study.

In vivo Raman spectroscopy revealed significant changes in the biochemical makeup of the cervix over the course of pregnancy. Highly significant differences observed in Cox-1 KO compared to WT cervices near term provide the first evidence supporting impaired cervical remodeling as a novel factor responsible for the parturition delay in Cox-1 KO mice. In particular, Cox-1 KO mice show a gradual increase in the 1304 cm^{-1}/1265 cm^{-1} peak ratio compared to a non-linear increase in the WT peak ratio over pregnancy, with a sharp decrease at term in WT and one day after term in Cox-1 KO (Fig. 3.3). The peak at 1265 cm^{-1} decreased linearly over pregnancy, which is assigned to the Amide III vibration (C-N stretching and N-H in-plane bending from peptide backbone) present in various structural proteins, as well as in-plane cis double bond =C-H bending from lipid molecules such as adipose tissue and

phospholipids [131,157]. The 1304 cm^{-1} peak is assigned to scissoring and twisting vibrations of CH_3 groups in lipids [131], but also has overlap with spectral bands in actin, elastin, and nucleic acids [130,133,158,159]. Thus, this ratio is tentatively assigned as a lipid-to-protein ratio and may be indicative of an increase in collagen disorganization relative to cellular content in the softening and ripening stages of pregnancy.

A reduced rate of change in the 1265 cm^{-1}/ 1440 cm^{-1} ratio was observed in the ripening phase in Cox-1 KO mice compared to WT (Fig. 3.5*A*-*B*). The 1440 cm^{-1} peak is characteristic of CH_2/CH_3 scissoring in lipids [131]. Collagen and other extracellular matrix proteins break down over the course of pregnancy [32] and are likely responsible for the observed decrease in this ratio as pregnancy advanced. Significant changes over the course of pregnancy were also noted in the NNLS collagen coefficient (Fig. 3.5*C*-*D*), where both WT and Cox-1 KO levels significantly decreased starting on day 12 of pregnancy. The collagen concentration is known to decrease during pregnancy [49,160], which aligns with results from both the *in vivo* and *ex vivo* Raman spectra. In contrast to the peak ratios, the Cox-1 KO collagen coefficient did not sharply rise at term, nor were significant differences found between WT and Cox-1 KO mice at term, indicating that sharp changes observed prior to parturition in Figs. 3.3 and 3.5*A*-*B* may not be centered on collagen. It should be noted that although the pure components measured for the developed NNLS model account for a large amount of the variability observed in the collected data set, not all of the potential biochemical contributors to the measured Raman signal are incorporated. Additional cervical components include but are not limited to actin, elastin, glycosaminglycans, and nucleic acids [27,28,43], and likely contribute to the sharp changes observed prior to delivery in both WT and Cox-1 KO mice in the Raman peak ratios (Fig. 3.3*C* and 3.5*A*), and WT mice in the NNLS analysis (Fig. 3.5C).

Differences observed in Raman spectra were supported by *ex vivo* biomechanical tests (Fig. 3.8), which showed that the cervix of day 19 Cox-1 KO mice had significantly higher impulse stiffness and equilibrium stiffness compared to day 19 WT. Possible explanations for the impulse stiffness include higher levels of collagen crosslinks in the Cox-1 KO tissue at term [32], whereas less dispersion of collagen fibers and less hydrated cervical stroma could prevent viscous relaxation resulting in higher equilibrium stiffness [44,48]. Furthermore, Cox-1 KO day 19 tissues were less compliant in both unloaded states (initial dilation) as well as the maximum stretch-induced dilation state (total dilation or ultimate cervical compliance) compared to day 19 WT cervices. The latter two measures offer complementary information. Initial dilation reflects tissue compliance without application of any external force (other than gravity) similar to cervical dilation assessment in non-laboring women. For example, pregnant women with cervical dilation < 3 cm require additional force to produce dilation sufficient for parturition compared to women dilated to 8 cm (maximum of 10 cm for complete dilation), even if both patients have an equally softened cervix. Although the *in vivo* cervix is always under load [161], our experiments isolated the cervix from surrounding tissue forces and pressure from the fetus to provide information on inherent cervical distensibility. Total dilation, which yields the maximum stretch cervical tissue can withstand prior to tissue failure, is similar to the requirement for human cervical dilation to 10 cm. Regardless of cervical diameter at the onset of labor, delivery will not be successful until complete dilation is achieved, and is therefore an absolute, not relative requirement for parturition. Together, this information confirms that normal transition to the cervical dilation phase was delayed in Cox-1 KO mice, resulting in reduced capacity to reach the final dilation needed to successfully deliver at term.

Successful passage of a fetus depends on achievement of cervical remodeling and complete cervical dilation. Currently, physical and biomechanical assessments are the most commonly used measures of cervical remodeling. Here, we showed that Raman peak ratios and changes in biochemical composition of the cervix correlate with biomechanical properties and physical changes in cervical stiffness and compliance (Fig. 3.9). The highest correlation observed was between the Raman collagen coefficient and the initial dilation. Fibrillar collagens largely govern the mechanical properties of cervical tissue, supporting the feasibility of using Raman measurements to interrogate cervical maturation during the quiescent phase of pregnancy and with impending parturition. Biochemistry is known to play a key role in mechanical properties [44,47,48]; however, biochemistry alone cannot fully capture the structure and packing of all molecules that contribute to biomechanical properties. As such, pairing Raman spectroscopy with another structurally-focused modality could greatly improve the determination of mechanical properties *in vivo*. Engineering models of cervical biomechanics [162] and biochemical inputs determined via Raman spectroscopy could be valuable additions when applying such models towards non-invasive assessment of cervical tissue.

Ex vivo biochemical assays similarly revealed differences between WT and Cox-1 KO cervical tissues at the end of pregnancy. Significantly higher progesterone levels were noted in Cox-1 KO mice on day 19 compared to WT, however unlike previous reports [122], progesterone levels clearly fell in both groups, albeit not to the same extent. This suggests the possibility of a progesterone-mediated delay in cervical dilation, similar to two other mouse models of delayed parturition in which systemic progesterone levels remain elevated: Steroid 5a-reductase type-1 knockout mice and Tg/Tg mice with an insertion in chromosome 6 [149,152]. Water content rose significantly on the final day of pregnancy in WT mice, which was not observed in the Cox-1

KO day 19 tissues. Cervical hydration typically increases over the course of pregnancy, particularly in the ripening/dilation phase [49,50,102]. Similarly, total collagen per cervical tissue rose significantly on the final day of gestation in WT mice compared to Cox-1 KO, however collagen levels in the day 20 Cox-1 KO cervix eventually caught up to day 19 WT levels (Fig. 3.10*C*).

One limitation of this study is the contribution of adipose tissue to the *in vivo* Raman spectra collected from the cervix. Multiple steps were taken to minimize the influence of adipose tissue whilst maintaining information from the cervix, including an automated system for removing spectra that had high adipose content (spectra with the 1440 cm^{-1} peak >1800 counts). In addition, the generalized linear model incorporates the 1440 cm^{-1} signal intensity as a model variable so that the non-adipose content could be independently analyzed. This allowed for prediction of how the spectra would change over gestation given a constant adipose contribution. This method can be used for other applications where an additional signal is interfering with spectra from a desired location, including interference from adipose tissue and bone. Beyond quantitative data exclusion (by pre-determined criteria) and post-processing analysis, a variety of hardware solutions could be used to minimize the variability introduced by adipose. Use of a custom Raman fiber optic probe that is focused to superficial tissue depths could reduce contribution from deep adipose layers [163]. Furthermore, a spatially offset probe design could provide depth-resolved information with minimal signal from adipose tissue reaching the low source-detector distance fibers [164]. Finally, use of a lower wavelength such as 680 nm or 532 nm would inherently limit the penetration depth of the laser light, and therefore reduce contribution from adipose tissue located behind the cervix, however visible excitation sources are likely to lead to greater tissue heating and autofluorescence signal generation [165].

In summary, we identified delayed cervical remodeling in pregnant Cox-1 KO mice as an underlying mechanism for prolonged gestation. Specifically, *in vivo* Raman spectroscopy detected significant differences between WT and Cox-1 KO cervical tissues during pregnancy, particularly in peaks representative of proteins and lipids. Spectral analysis correlated with biochemical changes, biomechanical testing, and reduced cervical dilation in Cox-1 KO mice at term. This study underscores the importance of studying the cervix in the context of abnormal parturition, which remains a relatively under-investigated organ. Difficulty obtaining molecular information from cervical tissue without compromising pregnancy has driven new innovation, including *in vivo* Raman spectroscopy. As a non-invasive, real-time technique that can be performed longitudinally, biochemical differences that occur throughout pregnancy can be detected without tissue injury or potential harm. Our study demonstrates that this technique, which has been used in a variety of human studies [89], has clear potential for direct clinical translation.

3.6 Acknowledgments

The authors wish to thank Dr. Kelsey Mayo for the illustration of the cervix in Fig. 3.2, and the Endocrine Technologies Support Core (ETSC) at the Oregon National Primate Research Center (ONPRC) supported by NIH Grant P51 OD011092 awarded to ONPRC. We thank Stanley Poole, Becca Williams, Woodi Woodland, and Kevin Qin for help executing experiments and data processing. We acknowledge our funding sources including an NSF Graduate Research Fellowship awarded to CO, and NIH R01 HD081121 (J.R. and A.MJ).

CHAPTER 4

IN VIVO RAMAN SPECTROSCOPY FOR BIOCHEMICAL MONITORING OF THE HUMAN CERVIX THROUGHOUT PREGNANCY

Text partially adapted from:

CM O'Brien, E Vargis, A Rudin, JC Slaughter, G Thomas, JM Newton, J Reese, KA Bennett, and A Mahadevan-Jansen. "*In vivo* Raman spectroscopy for biochemical monitoring of the cervix throughout pregnancy," (AJOG, in press).

4.1 Abstract

The cervix must undergo significant biochemical remodeling to allow for successful parturition. This process is not fully understood, especially in instances of spontaneous preterm birth. *In vivo* Raman spectroscopy is an optical technique that can be used to investigate the biochemical composition of tissue longitudinally and non-invasively in humans, and has been utilized to measure physiology and disease states in a variety of medical applications. The purpose of this study is to measure *in vivo* Raman spectra of the cervix throughout pregnancy in women, and to identify biochemical markers that change with the preparation for delivery and post-partum repair. Sixty-eight healthy pregnant women were recruited. Raman spectra were measured from the cervix of each patient monthly in the first and second trimesters, weekly in the third trimester, and at the six week post-partum visit. Raman spectra were measured using an *in vivo* Raman system with an optical fiber probe to excite the tissue with 785 nm light. A spectral model was developed to highlight spectral regions that undergo the most changes throughout pregnancy, which were subsequently used for identifying Raman peaks for further

analysis. These peaks were analyzed longitudinally to determine if they underwent significant changes over the course of pregnancy ($p<0.05$). Finally, six individual components that comprise key biochemical constituents of the human cervix were measured to extract their contributions in spectral changes throughout pregnancy using a linear combination method. Patient factors including body mass index (BMI) and parity were included as variables in these analyses. Raman peaks indicative of extracellular matrix proteins (1248, 1254cm^{-1}) significantly decreased ($p<0.05$), while peaks corresponding to blood (1233 and 1563 cm^{-1}) significantly increased ($p<0.0005$) in a linear manner throughout pregnancy. In the post-partum cervix, significant increases in peaks corresponding to actin (1003, 1339, 1657 cm^{-1}) and cholesterol (1447 cm^{-1}) were observed when compared to late gestation, while signatures from blood significantly decreased. Post-partum actin signals were significantly higher than early pregnancy, whereas extracellular matrix (ECM) proteins and water signals were significantly lower than early weeks of gestation. Parity had a significant effect on blood and ECM protein signals, with nulliparous patients having significant increases in blood signals throughout pregnancy, and higher ECM protein signals in early pregnancy compared to patients with prior pregnancies. Body mass index (BMI) significantly affected actin signal contribution, with low BMI patients showing decreasing actin contribution throughout pregnancy and high BMI patients demonstrating increasing actin signals. Raman spectroscopy was successfully used to biochemically monitor cervical remodeling in pregnant women during prenatal visits. This foundational study has demonstrated sensitivity to known biochemical dynamics that occur during cervical remodeling, and identified patient variables that have significant effects on Raman spectra throughout pregnancy. Raman spectroscopy has the potential to improve our understanding of cervical maturation, and be used

as a non-invasive preterm birth risk assessment tool to reduce the incidence, morbidity, and mortality caused by preterm birth.

4.2 Introduction

Over half of all spontaneous preterm birth (sPTB) cases do not fall within any specific high-risk category, making the prediction and management of sPTB difficult [11]. While labor and parturition are coordinated processes involving many systems and organs for proper function, a full understanding of the cascade leading to labor and parturition has not been achieved, particularly in instances of sPTB. An arguably under-investigated but highly important organ for pregnancy maintenance and proper labor is the cervix, a dense extracellular matrix (ECM) that is infiltrated by cells, blood vessels, and smooth muscle [27,31]. The normal process of cervical remodeling that facilitates vaginal delivery occurs in four overlapping stages (softening, ripening, dilation, and repair) that have unique biochemical features and vary in duration among patients (Figure 2.4) [43]. Furthermore, these processes are affected by patient factors including parity [166-169], prior vaginal delivery [44], and body mass index (BMI) [170-174].

Biochemically, the most abundant component of the ECM is fibrillar collagen, accounting for over 70% of the cervix tissue dry weight [44]. Other important ECM components include elastin, hyaluronan, sulfated glycosaminoglycans, proteoglycans, and water. During the softening phase, hydration and vascularity increase, remodeling the collagen matrix [43]. The ripening phase involves an accumulation of hydrophilic molecules including glycosaminoglycans such as hyaluronic acid, further increasing cervical tissue hydration. Additionally, collagen becomes increasingly soluble. While the total amount of collagen remains the same, the collagen concentration decreases due to an influx of water and other matrix constituents [29]. Next, cervical dilation occurs as a rapidly so the cervix can expand and dilate for delivery. Finally, during

cervical repair, the collagen matrix of the cervix rebounds through an inflammatory process similar to wound healing [55,56], with an increase in macrophages and neutrophils that orchestrate ECM rebuilding [53]. Collagen remodeling occurs in all phases of cervical maturation, and has been identified as the most important component in the mechanical strength in the cervix [44,45]. A firm relationship has been established between the extent of collagen cross-linking and tensile strength in both the pregnant mouse [46] and human cervix tissues [37,47,48].

Researchers are working to develop new tools to quantitatively and non-invasively evaluate cervical remodeling *in vivo* to aid both basic understanding of the remodeling process and clinical decision-making. These methods include magnetic resonance, acoustic, mechanical, electrical, and optical techniques [1,65,124]. Light-based approaches can enable the study of tissue morphology and biochemistry depending on the light-tissue interaction process used. Two optical methods have been used *in vivo* to specifically monitor collagen. Fluorescence from collagen can be obtained by exciting tissue at ~340 nm. Previous studies have shown that fluorescence decreases over the course of pregnancy in mice and women [73-75]. Excitation at ~950 nm can produce an optical phenomenon termed second harmonic generation in collagen fibers, and can be used to create collagen-specific images that show well-defined collagen networks and ECM remodelling over the course of pregnancy [76,77].

Beyond collagen, near-infrared spectroscopy has been used to monitor optical absorbers including hydration and hemoglobin, and optical scatterers such as collagen and cellular organe lles by measuring diffuse light scattering [78,79]. Absorption by hemoglobin as well as optical scattering were shown to increase throughout pregnancy, and absorption by water significantly increased during cervical ripening after exposure to the prostaglandin misoprostol [78,79]. Ectocervix surface area determined by images from an endoscopic camera reveal increased

surface area in pregnant patients throughout pregnancy, and was attributed to increased hydration [175]. While fluorescence, second harmonic generation, near-infrared spectroscopy, and white light imaging have been applied *in vivo*, these methods provide only a partial measure of the biochemical micro-environment. A single method that can probe hydration, proteins, nuclear content as well as changes in vasculature could evaluate the role of each biomarker as well as the interplay between them during cervical remodeling.

Raman spectroscopy is an inelastic scattering technique that probes the vibrational energy levels of molecules. A Raman spectrum contains spectrally narrow peaks which provide specific molecular fingerprints that are related to biochemistry and structure. Raman signals corresponding to lipids, proteins, saccharides, nucleic acids, and water, offer direct information regarding the biochemical makeup of the tissue, and signal intensity is linearly related to molecule concentration. Care must be taken during the interpretation of spectra in instances of peak overlap, such as the overlap of protein and water at 1657 cm^{-1}. In such cases, all Raman features of a given molecule must be analyzed, and spectral unmixing methods may be employed. Using Raman spectroscopy for direct understanding of molecular processes is difficult *in vivo* due to the large number of biochemical constituents that contribute to Raman spectra. Thus, *in vivo* information mainly provides relative abundance of biochemical constituents and in some cases structure which may be used to inform biology. Due to its high sensitivity and specificity, Raman spectroscopy has been increasingly used in biomedical applications [89], including detecting dysplasia in the human cervix [88,133,176-180]. In recent years, sensitivity to the hormonal status of cervical tissue has been seen in Raman spectra[92,136,137], which was the first step in using Raman spectroscopy to study cervical remodeling in mouse models of pregnancy [2,101]. Although mouse models allow for observation of pregnancy in a

highly controlled manner, not all biology is conserved between mice and women, and clinical implementation introduces its own set of challenges.

The goal of this study is to test the feasibility of measuring Raman spectra of the *in vivo* cervix in pregnant women, and to characterize Raman signatures throughout pregnancy and post-partum. To this end, sixty-eight pregnant patients were enrolled in the study, and their cervices were measured throughout pregnancy and post-partum. Statistical analysis was performed longitudinally on the collected spectra, and highly significant changes in the spectra are observed as a function of gestation. In addition, patient factors including body mass index and obstetric history had significant effects on Raman spectra. To our knowledge, this is the first report using Raman spectroscopy to study cervical remodeling in pregnant women, demonstrating feasibility of the approach and identifying biochemical features associated with the phases of cervical remodeling.

4.3 Materials and methods

4.3.1 Patient recruitment

This study was approved by the Vanderbilt University Medical Center's Institutional Review Board (#100544) and followed the guidelines of the Declaration of Helsinki. Pregnant patients receiving prenatal care at the Vanderbilt Women's Health Center were recruited using informed, written consent. To be eligible for enrollment, patients had to be at least 18 years old and able to provide legally valid prospective informed consent. Relevant patient information such as obstetric history, medications, age, BMI, and estimated date of delivery were all included in each patient's research chart. At the end of the study, patient outcome, delivery date and time

were also recorded. Patient demographics are listed in Table 4.1. A total of 68 patients were enrolled in this study based.

Table 4.1: Patient demographics and outcome.

Variable	**Measure**
Total patients (n)	68
Obstetric History	
No prior pregnancies (n)	28
Prior pregnancies (n)	40
Prior vaginal deliveries (n)	30
Pre-pregnancy BMI[a]	
Mean (± SEM)	29.3 (7.6)
Underweight/normal (<25) (n)	19
Overweight (25-30) (n)	25
Obese (30-35) (n)	8
Severely obese (35-40) (n)	7
Morbidly obese (BMI>40) (n)	8
Obstetric outcome[b]	
Delivered vaginally at term (n)	32
Delivered vaginally preterm (n)	4
C-section at term (n)	25
C-section preterm (n)	5

[a]BMI was not available for one patient

[b]Outcome was not available for two patients

4.3.2 Experimental setup

A portable Raman spectroscopy system was used for data collection (Figure 4.1A). The system consists of a 785 nm diode laser (Innovative Photonics Solutions), an imaging spectrograph (Kaiser Holospec), a deep-depletion thermoelectrically cooled CCD camera (Princeton Instruments), a laptop computer, and a Raman spectroscopy fiber optic probe (EmVision LLC). The Raman probe (fiber optic probe approximately 2.1 mm in diameter, plus external stainless steel casing totaling 6.3 mm in outer diameter) consists of one optical fiber that transmits light from the laser to the tissue, surrounded by seven collection fibers that deliver the backscattered light to the spectrograph. The laser power at the sample was set to 80 mW.

4.3.3 Clinical protocol

After obtaining written, informed consent, the patient underwent a speculum exam performed by a certified Women's Health Nurse Practitioner. The cervix was exposed and cleaned with a cotton swab soaked in sterile saline before the Raman probe was gently placed in contact with the cervix to obtain a Raman spectrum (Figure 4.1B). The overhead room lights were turned off, and 3-5 measurements were taken from separate locations around the ectocervix, taking care to ensure that the probe was placed on the squamous epithelium. Each measurement used an integration time of 3 seconds, and the entire procedure took less than 10 minutes per visit. After each use, the Raman probe was disinfected after each patient in accordance with standard disinfection procedures. For each patient, spectra were acquired monthly in the first and second trimester, weekly in the third trimester, and at six week post-partum.

4.3.4 Data processing

Each day, the Raman spectroscopy system was wavelength calibrated using a Neon Argon lamp. The exact laser excitation wavelength and Raman shift were calculated using acetaminophen and naphthalene standards which have well characterized Raman shifts. The spectral response of the system was first determined using a NIST calibrated tungsten lamp, and then calibrated daily using a piece of green glass that has a similar broadband spectrum. The resultant calibration factor was applied to each spectrum based on the spectral throughput measured each day. Raman spectra were processed to remove ambient background light, smoothed using a Savitzky-Golay filter, and fluorescence subtracted using the modified polynomial method [141].

4.3.5 Data analysis

In order to determine how the average Raman spectrum changes over the course of pregnancy and post-partum, a restricted cubic spline function for Raman shift (cm^{-1}) with "k degrees of freedom" or "k-1 knots", where k was set to 65 was used. Sixty-five knots were used in order to fit high frequency changes in the spectrum as well as provide some spectral smoothing. Additional patient variables, including prior vaginal delivery and BMI were incorporated in this spectral model, resulting in a series of Raman spectra representative of various stages of pregnancy and post-partum.

Spectral regions that appeared to change throughout pregnancy based on observations from the spectral model were used for calculating changes in Raman peaks and Raman peak ratios over pregnancy. Peak ratio calculations provide data normalization and thus allow improved comparison across datasets with varying signal to noise ratios. Using this approach, the

following peaks were identified for further analysis: 1006, 1055, 1125, 1157, 1248, 1254, 1304, 1339, 1451, 1563, and 1657 cm^{-1}. To determine whether peak or peak ratio intensities changed as the cervix prepared for delivery, generalized estimating equations[181,182] (GEEs, a type of linear model that clusters data obtained from each patient over time in order to account for the inherent correlation between measurements from the same patient) were developed for longitudinal monitoring. The change in each peak or peak ratio over time was modeled and plotted with its mean and its 95% confidence interval based on the GEE output, and ANOVA was performed on the model output to determine statistical significance (* indicates $p<0.05$ over the course of pregnancy). GEE output plots enable the analysis of cervical remodeling as a continuous variable, such that the not only the spectral peak levels can be observed in each trimester, but also the rate of change within, between, and throughout all trimesters.

Next, major biochemical contributors to the Raman spectra were tracked throughout pregnancy and post-partum using a biochemical model termed non-negative least squares (NNLS) analysis. Pure components known to be present in the cervix were measured and the tissue spectrum was recreated using a linear combination of the pure components. The components used for the model were measured in their pure form and include actin, adenosine triphosphate, cholesterol, collagen type-I, deoxyribonucleic acid, glucose, glycogen, phosphatidylcholine, phosphatidylethanolamine, progesterone, and prostaglandin E_2 (Sigma, St. Louis, MO), glucose-6-phosphate (Roche Diagnostics GmbH, Mannheim, Germany), hyaluronic acid (Abcam, Cambridge, MA), blood (excess human blood from use in IRB-approved protocol #151532), and deionized water. All measurements were acquired using the same integration time and are displayed in Supplemental Figure 1.

Non-negative least squares analysis is most accurate when non-correlated spectral components are used in the model; therefore the correlation coefficient between each biochemical signal was calculated (Supplemental Figure 2). If any two biochemical components had a Spearman correlation coefficient higher than 0.75, one of the two components was chosen to be input for the model and the other was not included. The model was computed using MATLAB. The pure component spectra were loaded into a matrix with each column containing a pure component spectrum. Patient spectra were input to the model and the best fit coefficients from each component were calculated. In addition, the residual between the model fit and the tissue spectrum was calculated to ensure all regions of the Raman spectra were adequately represented.

To longitudinally monitor how each biochemical molecule changed throughout pregnancy, the biochemical coefficients were analyzed using GEEs as explained above. In addition, patient variables including obstetric history (parity) and BMI were incorporated into the model as continuous variables to determine their effects on Raman spectra throughout pregnancy. Studies have shown that BMI and parity have an influence on the ability of Raman Spectroscopy to correctly characterize cervical spectra [183], and are factors that contribute to the timing of parturition [170,171,174].

4.4 Results

4.4.1 Spectral changes throughout pregnancy

Raman spectra collected throughout pregnancy changed significantly as the cervix prepared for delivery. Representative spectra from one patient measured throughout her pregnancy and post-partum are shown in Figure 4.1C. Multiple regions show considerable

variation including 1030-1100 cm^{-1}, 1118-1200 cm^{-1}, 1230-1260 cm^{-1}, 1270-1330 cm^{-1}, 1440-1460 cm^{-1}, 1550-1600 cm^{-1}, and 1630-1670 cm^{-1}. The post-partum spectrum is particularly distinct from the prenatal measurements, and most closely resembles the earliest measurement obtained at the patient's 8 week prenatal visit. However significant increases in the 1118-1200, 1300-1350, and 1630-1670 cm^{-1} regions are observed, unique to the post-partum period.

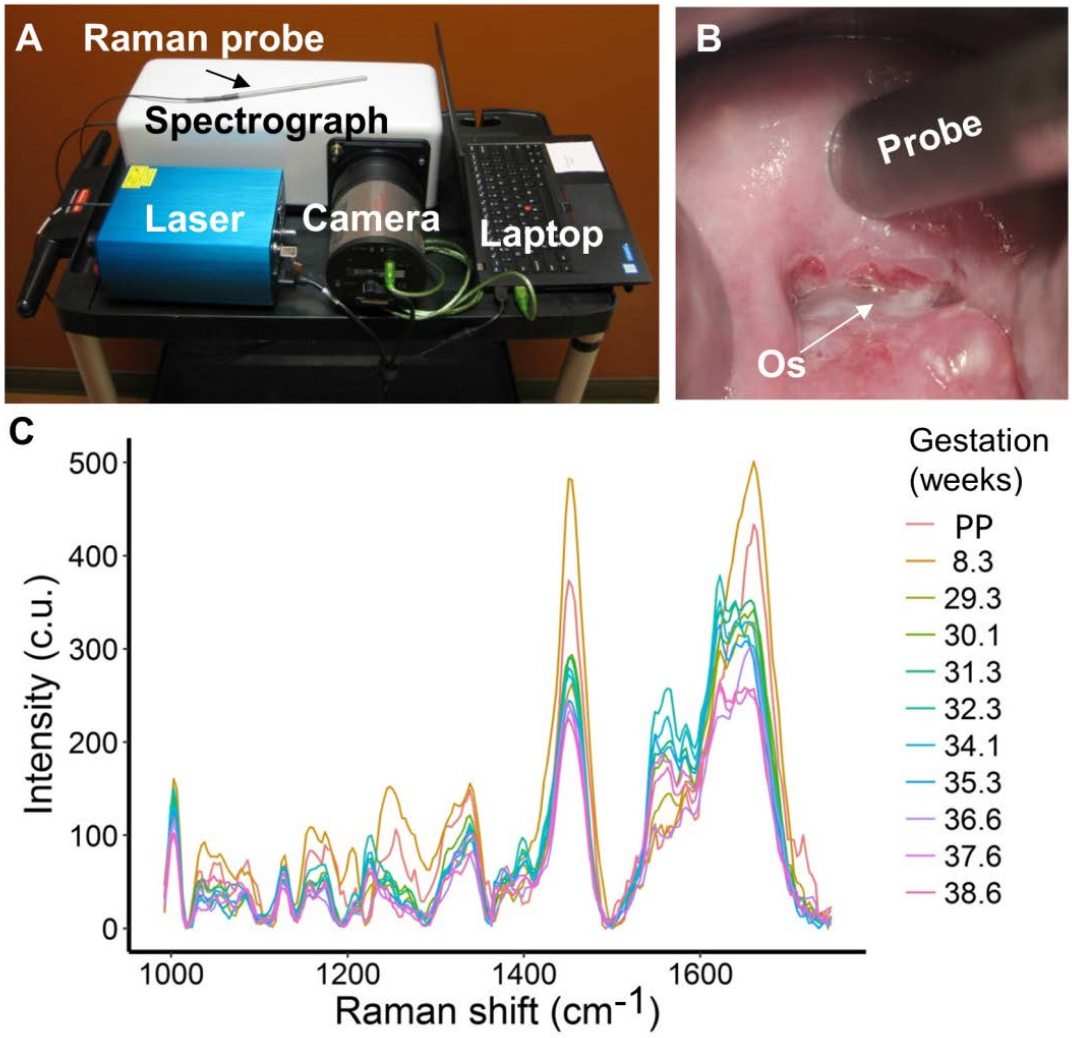

Figure 4.1. *In vivo* Raman spectroscopy of the cervix during pregnancy. A) Portable Raman spectroscopy system; B) Raman probe measurement from the cervix *in vivo*; C) Raman spectra from one patient over the course of her pregnancy and post-partum (PP).

The spectral model, which was developed to determine the average Raman spectra over the course of pregnancy for the entire patient population studied, is shown in Figure 4.2. Several significant changes were observed over pregnancy and post-partum, which are highlighted by the gray shaded regions in Figure 4.2 (* indicates significant change over the course of pregnancy with $p<0.05$). The 1530-1600 cm^{-1} region attributed to peaks observed in blood (as seen in Figure 4.5B) increases with advancing gestation, whereas bands characteristic of ECM proteins (as observed in the collagen spectrum in Figure 4.5C) (1030-1100 cm^{-1}, 1130-1200 cm^{-1}, 1230-1290 cm^{-1}, 1440-1460 cm^{-1}, and 1630-1670 cm^{-1}) and carotenoids (1130-1200 cm^{-1}) decrease throughout pregnancy. In addition, the left shoulder of the 1657 cm^{-1} peak appears to increase (Figure 4.2). Post-partum, bands observed in ECM proteins return to early pregnancy levels and there is significantly higher intensity in the 1270-1330 cm^{-1} range. Although Figure 4.2 depicts a computational representation of the data, the majority of the spectral changes that occurred throughout gestation are seen in the example patient spectra in Figure 4.1C, demonstrating the utility and accuracy of the model.

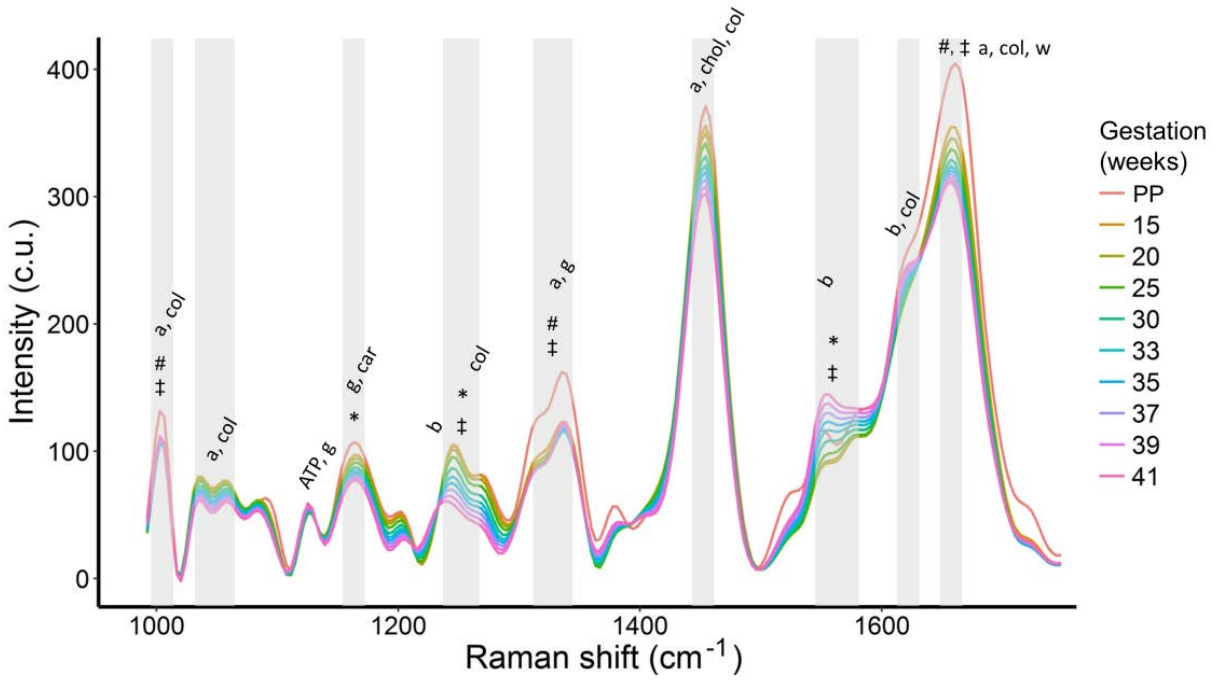

Figure 4.2. Computational model depicting how Raman spectra change over the course of pregnancy and post-partum. Shaded regions indicate spectral bands that exhibited significant changes throughout pregnancy (n=68): * indicates $p<0.05$ over the course of pregnancy, # indicates $p<0.05$ when comparing early pregnancy (<20 weeks) and post-partum (PP), and ‡ indicates $p<0.05$ when comparing late pregnancy (>37 weeks) to PP measurements. ($p<0.05$). Spectral regions associated with specific peaks are labeled as such: a- actin, ATP- adenosine triphosphate, b-blood, car-carotenoids, chol-cholesterol, col- collagen type-I, g-glucose, w-water.

Several peaks undergo significant changes over the course of pregnancy (* indicates $p<0.05$), including peaks at 1157, 1248, and 1254 cm^{-1} which significantly decrease throughout pregnancy, and the 1563 cm^{-1} peak which significantly increases as a function of gestation week (Figure 4.3). Post-partum measurements are significantly higher ($p<0.05$) in the 1304 and 1339 cm^{-1} peaks compared to early pregnancy (<22 weeks of gestation), and significantly lower in the 1006 and 1657 cm^{-1} peaks. A similar comparison of post-partum spectra to those taken at the end of gestation (>37 weeks) reveals significantly higher intensities post-partum at 1248, 1254, and 1339 cm^{-1}, and significantly lower intensities in the 1006, 1563, and 1657 cm^{-1}.

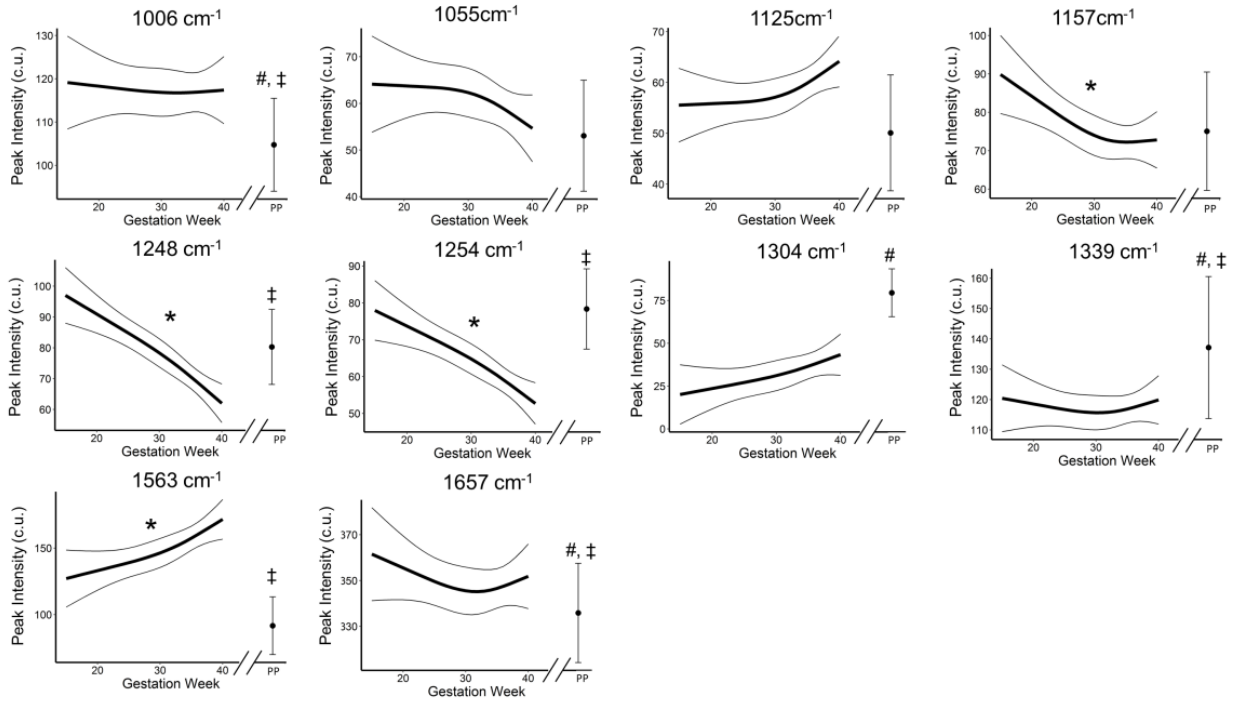

Figure 4.3. Raman spectral peak intensities over the progression of pregnancy. * indicates $p<0.005$ over the course of pregnancy, # indicates $p<0.05$ when comparing early pregnancy (<22 weeks) and post-partum, and ‡ indicates $p<0.05$ when comparing late pregnancy (>37 weeks) to post-partum measurements.

Raman peak ratio calculations reveal many features that change significantly throughout pregnancy and post-partum (Figure 4.4), including the 1254/1304 cm^{-1} ratio (ECM protein to actin & glycogen ratio) which decreases as term approaches ($p<0.0001$), and is significantly lower post-partum compared to early pregnancy (Figure 4.4A). In addition, the 1563/1248 cm^{-1} peak ratio (blood to ECM protein ratio) steadily increases over gestation ($p<0.0001$) (Figure 4.4B), and post-partum measurements are significantly lower than late pregnancy. The 1157/1339 cm^{-1} peak ratio (carotenoid to ECM protein ratio) significantly decreases throughout gestation until term ($p<0.005$), and post-partum measurements are significantly higher than early pregnancy (Figure 4.4C).

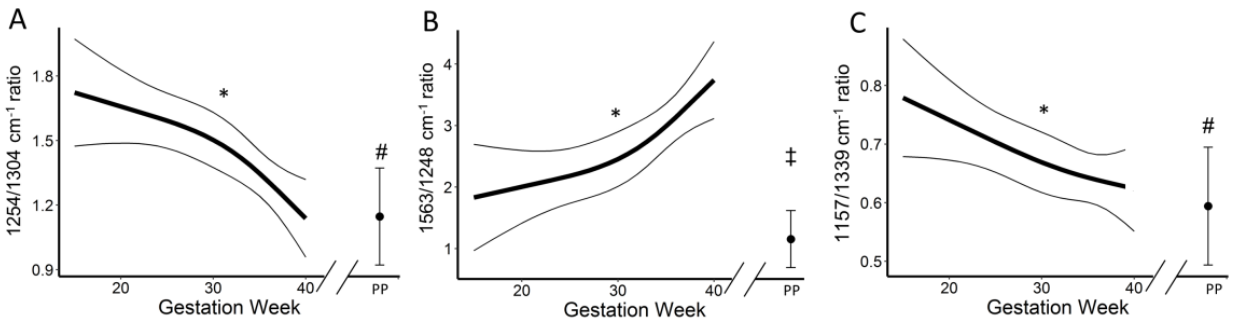

Figure 4.4. *In vivo* Raman peak ratios displayed in a general linear model over the course of pregnancy. * indicates $p<0.005$ over the course of pregnancy, # indicates $p<0.05$ when comparing early pregnancy (<20 weeks) and post-partum, and ‡ indicates $p<0.05$ when comparing late pregnancy (>37 weeks) to post-partum measurements.

4.4.2 Raman spectra of purified biochemical components

Six biochemical components were used to construct the least squares model (actin, blood, cholesterol, collagen I, glycogen, and water), and their Raman spectra are depicted in Figure 4.5A-F. These spectra showcase the specificity of Raman spectroscopy to different types of biomolecules. An example of an *in vivo* spectrum obtained from cervical tissue, overlaid with its least squares fit and resulting residual are displayed in Figure 4.5G. The residual is small and fluctuates above and below zero, with an R^2 value of 0.922, indicative of a good fit.

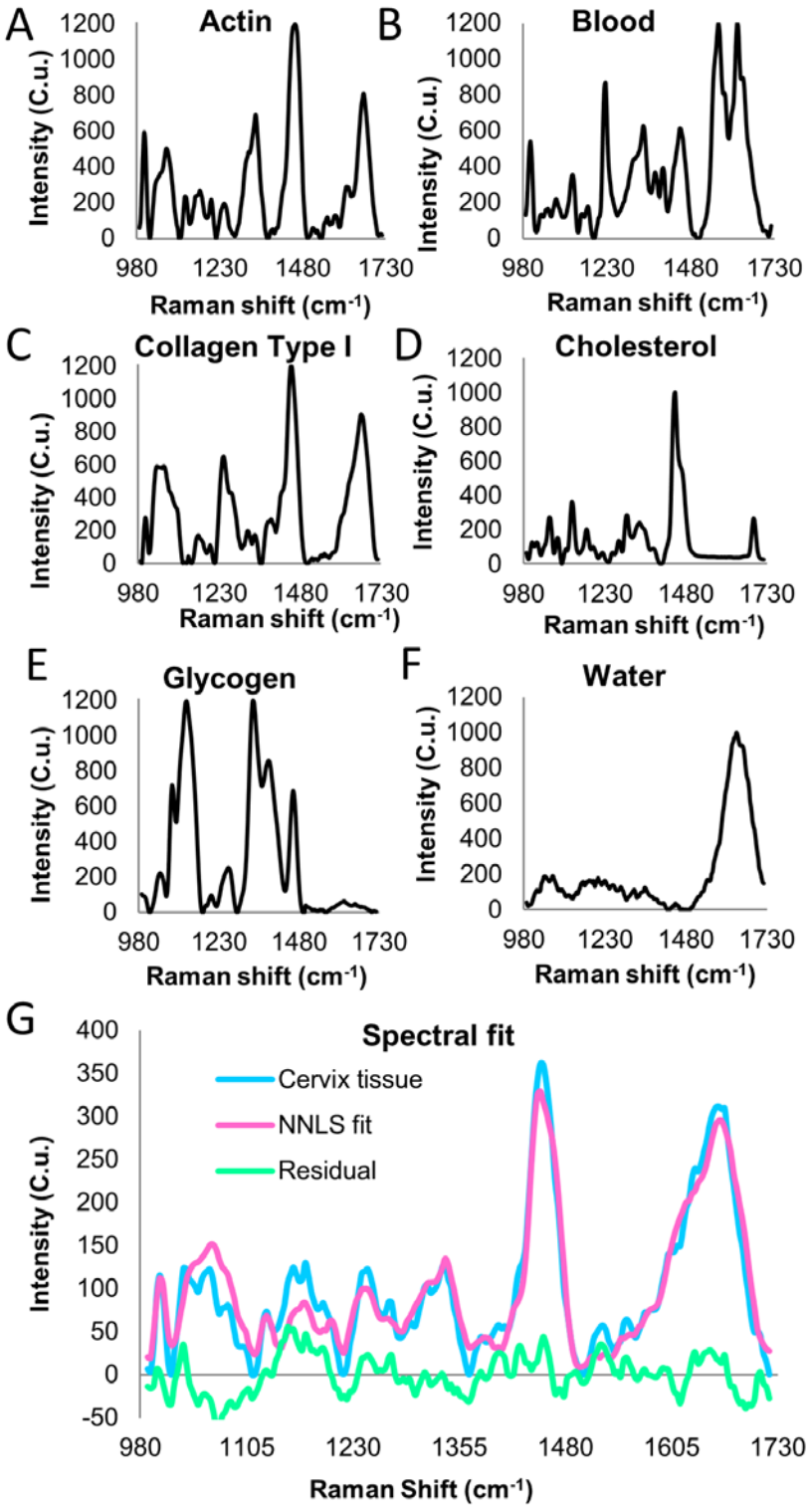

Figure 4.5. Non-negative least squares biochemical model of *in vivo* Raman spectra. A-F) Raman spectra from pure biochemicals (actin, blood, cholesterol, collagen type-I, glycogen, and water) and G) a representative cervix tissue spectrum (blue) with its model fit (pink) and residual (green).

The contributions of two biochemical components change significantly as a function of gestation (* indicated $p<0.05$), as shown in Figure 4.6. The contribution from blood significantly increases in a linear manner ($p<0.0005$), whereas the contribution from collagen decreases over the course of pregnancy ($p<0.0001$). Comparing post-partum measurements to early pregnancy (<22 weeks of gestation) reveal significantly higher ($p<0.05$) post-partum levels of actin, and a significantly lower contributions from collagen type-I and water. Additionally, comparison of post-partum to the end of gestation (>37 weeks of gestation) reveals significantly higher actin and cholesterol contribution, and significantly lower blood contribution in the post-partum fits.

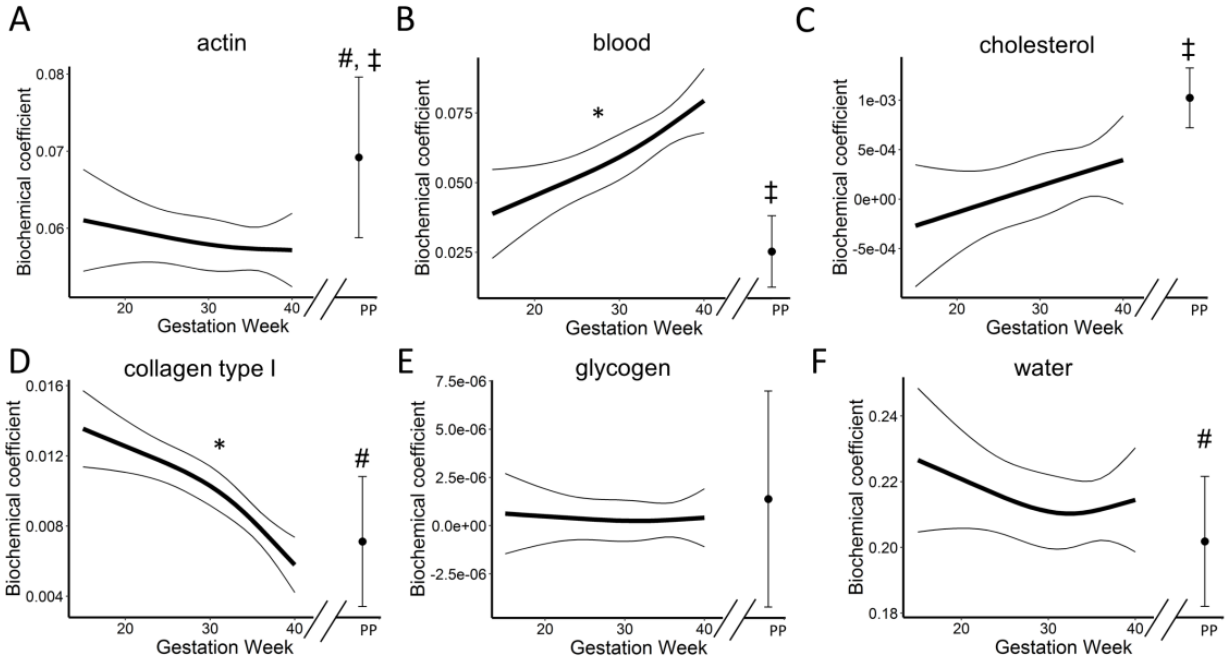

Figure 4.6. Biochemical contributions over the course of pregnancy. The fitted component coefficient for actin (A), blood (B), cholesterol (C), collagen type 1 (D), glycogen (E), and water (F), plotted against gestation week (mean +/- SEM). * indicates $p<0.005$ over the course of pregnancy, # indicates $p<0.05$ when comparing early pregnancy (<20 weeks) and post-partum, and ‡ indicates $p<0.05$ when comparing late pregnancy (>37 weeks) to post-partum measurements.

4.4.3 Effects of patient variables

While several patient variables were considered, two in particular were found to have an effect on Raman spectra during pregnancy and post-partum (Figure 4.7). From NNLS analysis, blood/vascularity signals have an inverse relationship with parity, with nulliparous patients showing significant increases in blood/vascularity signals as the cervix remodels, compared with a relatively stable blood contribution in parous patients (Figure 4.7A) ($p<0.05$). Individual peak analysis reveals that the 1125 cm^{-1} peak increases steadily in nulliparous patients, but does not increase until about 30 weeks of gestation in multiparous patients. Additionally, the 1254 cm^{-1} peak is significantly higher at the beginning of pregnancy and significantly lower near term in nulliparous patients, although parous patients do show decreases in this peak throughout pregnancy. Post-partum, parous patients had significantly higher contributions from cholesterol, while nulliparous patients had significantly higher intensities at 1006 and 1055 cm^{-1} (possibly caused by ECM proteins or actin) than parous patients.

Evaluation of the effects of BMI shows that low BMI patients (demonstrated by spectral model with BMI=25) have decreasing actin contributions as the cervix prepares for delivery ($p<0.05$) which levels outs as BMI increases. In addition, low BMI patients start with higher signal from 1248 cm^{-1}, a peak characteristic of ECM proteins, but decreases to a greater extent than high BMI patients as term. Post-partum spectra from low BMI patients have higher actin contribution and higher 1003 cm^{-1} peak intensity compared to high BMI patients (demonstrated by model with BMI=40). In addition, high BMI patients have higher contribution from collagen than low BMI patients in the post-partum period.

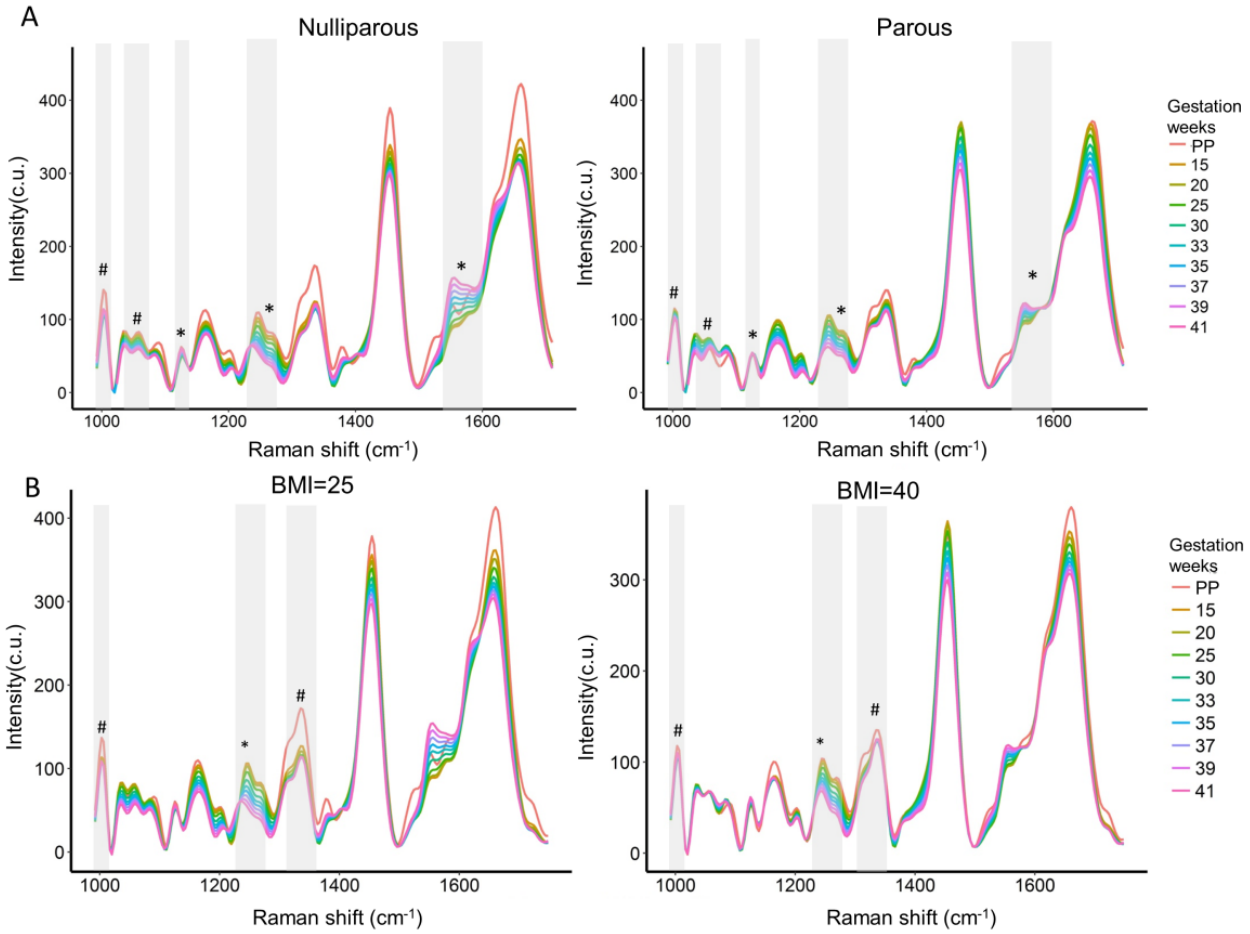

Figure 4.7. Computational model comparing Raman spectral changes as a function of gestation week and post-partum in A) nulliparous (n=29) vs. parous patients (n=37), B) patients with normal-overweight (≤35, n=51) and high (>35, n=15) body mass index. Gray bars highlight areas that underwent significant change over pregnancy or post-partum, * and # indicate that patient variable had significant effect on spectral region over the course of pregnancy and post-partum repair, respectively.

4.5 Discussion

Monitoring the cervix during pregnancy has many purposes; these include improved understanding of normal and abnormal physiology of cervical remodeling, estimating delivery time, and determining patient readiness for labor. The latter clinical task is currently conducted using the Bishop Score and in some cases ultrasound; however these methods provide limited information, mainly pertaining to cervical structure. In this study, Raman spectroscopy was

employed to non-invasively measure the biochemistry of the cervix over the course of pregnancy *in vivo* in women for the first time. This approach successfully measured known biochemical changes observed in multiple stages of pregnancy and post-partum repair, and established patient variables that affect the remodeling process, demonstrating the utility of Raman spectroscopy for cervical evaluation during pregnancy.

In vivo Raman measurements of the cervix acquired over the course of pregnancy revealed characteristic biochemical changes that occur in preparation for delivery. Decreases in peaks indicative of extracellular matrix proteins such as collagen (1055, 1248, and 1657 cm^{-1}) and increases in peaks corresponding to blood (1233 and 1563 cm^{-1}) are observed in the example patient spectra (Figure 4.1C), the spectral model determined from 68 patients (Figure 4.2), and the non-negative least squares analysis (Figure 4.6). An increase in blood signatures is attributed to the increase in vascularization that occurs as the cervix prepares for delivery [43] (Figure 4.6), a phenomenon which has also been observed in pregnant women using near infrared spectroscopy[79]. Decreases in ECM peaks are explained by the process of ECM remodeling where collagen becomes increasingly soluble due to reduced cross-links and dispersed at a lower concentration [29,43]. Trivalent collagen cross-links have been observed at 1660 cm^{-1}, and reductions in these cross-links (which have been previously reported in women[73] and mice[32,73]) likely contribute to the observed decrease in this peak during pregnancy[184]. Furthermore, the 1657 cm^{-1} peak (also known as the amide I region) broadened in preparation for delivery, a phenomenon that is known to be caused by structural disorder such as collagen fiber dispersion [185]. This broadening may also be attributed to increased blood signals which have a peak at 1619 cm^{-1}. In pregnant women, collagen solubility has been measured *in vivo* using laser-induced fluorescence where fluorescent intensity corresponding to collagen cross-links was shown to

decrease throughout pregnancy[74]. Fiber dispersion has been measured during pregnancy *ex vivo* in mice and women using second harmonic generation[128] and optical coherence tomography[129]. An increase in collagen fiber dispersion was seen using both techniques.

In the post-partum cervix, Raman spectral signatures were significantly different from measurements obtained during pregnancy, with increases in spectral features corresponding to actin and cholesterol, and decreases in features corresponding to blood, collagen type I, and water as observed in Figure 4.6. There are few studies focused on understanding post-partum repair, however multiple studies suggest that the repair process is governed by immune cells which infiltrate the cervix and create a proinflammatory environment that resembles wound healing [52-54]. Microarray studies have found that in addition to inflammatory genes, matrix synthesis and collagen strengthening genes are upregulated in the post-partum cervix [55,56]. Based on this evidence, it is possible that the spectral increases of actin and cholesterol are caused by an influx of immune cells and fibroblasts. Although post-partum contributions from glycogen did not reach statistical significance, a possible explanation for the observed heightened glycogen levels is intensive anabolic activity driving the repair process. Furthermore, the peak at 1160 cm^{-1} is found in many carotenoid antioxidants [157,186,187] which could be elevated post-partum to combat high levels of reactive oxygen species related to macrophages and neutrophil infiltration.

Two patient variables, parity and body mass index, affected spectral changes that were observed throughout pregnancy and post-partum (Figure 4.7). Nulliparous patients started pregnancy with higher spectral contributions from collagen (based on the NNLS model) compared to parous (Figure 4.7A). In fact, this observation is supported by an *ex vivo* study in which collagen concentration (determined via hydroxyproline assay) was measured from cervical biopsies taken from parous and nulliparous women, and revealed decreasing collagen levels as

parity increased [169]. These findings were corroborated with *ex vivo* biomechanical tests of non-pregnant tissues from patients with and without prior vaginal deliveries which revealed stiffer, less compliant tissue in patients without prior vaginal deliveries [44], and confirmed decreased collagen extractability, as well as increased sulfated glycosaminoglycans and hydration in patients with a history of prior vaginal delivery. It is likely that a permanent vascular network is established during the first pregnancy similar to permanent changes in mechanical properties[44], which would explain why patients with prior pregnancies had significantly higher baseline blood/vascularity levels compared to nulliparous patients. Taken together, these results are unsurprising, as multiparous patients generally have faster labors [166-168], indicating that some level of permanent cervical remodeling occurs after completing all four phases of cervical remodeling during a prior pregnancy.

Patients with low BMI have higher spectral signals corresponding to ECM proteins (1248 cm^{-1} peak) at the beginning of pregnancy (Figure 4.7B), but this intensity decreases significantly more than high BMI patients by term, indicating that high BMI patients experience a lesser level of ECM remodeling. One possible explanation for this observation is an increase in leptin, an adipokine that is elevated in pregnant patients with high BMI, which has been shown to disrupt MMP action on collagen in myometrial tissues and synthesizes myometrial collagen in late pregnancy [174,188,189]. It is possible that this phenomenon also occurs in the cervix, reducing the extent of cervical remodeling achieved, and contributing to extended labor times and increased C-section rates observed in high BMI (>30) patients[170-174]. In addition, actin signals decreased throughout pregnancy in low BMI patients, possibly caused by cervical cell apopotosis which occurs prior to labor [56]. However, actin signals did not decrease in high BMI patients, which may

also be attributed to high leptin levels which have been shown to prevent cell apoptosis *in vitro* [174,190].

Nine of the patients enrolled in the present study underwent preterm birth, ranging from 35 + 3/7 weeks to 36 +6/7 weeks gestation when they delivered. Analysis was performed to determine if any differences were observed in this data set compared to patients who delivered at term, but none reached statistical significance. This result is not surprising, as these patients had different obstetric histories, body mass indexes, and all delivered relatively close to term. For a powered analysis comparing patients with and without PTB, additional studies that specifically enroll a large number of high risk patients will be required.

Although not yet ready for the launch of a clinical tool, it is important to think about how such a tool would be used and incorporated into the current workflow. The long term goals include the ability to measure premature cervical change at the patient bedside, as well as determine the etiology of the changes measured. The authors envision that Raman measurements could be made from the cervix early in pregnancy such as at the first appointment to obtain a baseline measurement. The frequency with which measurements would need to be made has not yet been established, and will likely require studies that evaluate the cost-benefit analysis of a variety of frequencies. Short term, Raman measurements could be introduced as an additional test for assessment of premature cervical change and ideally provide clues pointing towards the etiology. It is also unclear whether data will need to be normalized to a previous measurement taken from the patient, or whether a single measurement could provide enough information to determine premature cervical change. Advanced predictive algorithms will need to be developed, first indicating abnormal spectral profiles, and then hopefully indicating abnormal changes with information regarding etiology. Based on results in this study, variables including parity and

body mass index will need to be incorporated into the algorithms. In addition to use as a PTB risk assessment tool, Raman spectroscopy could be used to aid our biological understanding of problems such as cervical insufficiency, ascending infection, and monitoring efficacy of new treatment strategies for preterm labor.

Limitations of this study include the need for validation of the Raman spectral findings. Investigation in mouse pregnancy is underway[2,138] which has the ability to validate *in vivo* findings from Raman spectra, and future study of patients undergoing hysterectomy will provide additional opportunity to compare *in vivo* Raman spectra to *ex vivo* biochemical assays. In addition, interpretation of Raman spectra can be difficult due to the overlap of many spectral features in biological samples and changes in structure rather than concentration. Although Raman spectral intensity and vibrational mode concentration are linear, multiple biochemical components may include the same vibrational mode such as C-H stretch found in organic molecules. Observing the full spectrum can aid in these cases as distinguishing features likely exist between different biomolecules. When using Raman spectroscopy as a biological tool, it is important to remember that Raman spectra yield a relative concentration of biochemical species comprising tissue at the time of measurement. This information can help in understanding of the current microenvironment, but its use for determining molecular function or understanding mechanisms of molecular processes is challenging *in vivo* due to the nature of high overlap from thousands of biomolecules. Lastly, in this study, the Raman spectra are not depth-resolved, and therefore comment cannot be made regarding whether the biochemical signals originated from the cervical epithelium or stroma. For example, it is currently not possible to determine whether actin signals originated from epithelial cells or fibroblasts and smooth muscle cells deep in the

cervical stroma. Raman probes can be developed that allow this capability and may be employed in future studies.

The main strength of this study lies in the ability to monitor multiple dynamic biochemical changes in the cervix as it remodels to deliver the fetus. Although other optical modalities are sensitive to certain biochemical components such as collagen or blood, Raman spectroscopy provides simultaneous monitoring of ECM proteins, lipids, blood, saccharides, antioxidants, and metabolic enzymes without the addition of exogenous labels or removal of tissue. This technique has high potential for better understanding the etiologies and progression of spontaneous preterm birth, and may also help to unveil the healing process that occurs during post-partum repair. Translation of Raman spectroscopy to clinical settings is becoming more realistic each year; real-time data processing has already been achieved [191,192], and fully characterized disease and/or physiology profiles allow for automation of data analysis and tissue classification at the bedside. Hardware advances are consistently moving forward, which promise to reduce complexity of the system [89]. These studies also bring us closer to identifying a spectral signature that defines cervical changes in normal pregnancy, increasing the potential to utilize Raman spectroscopy for predicting the timing of delivery and therefore early risk assessment for preterm birth.

In summary, this study highlights Raman spectroscopy as a tool to track meaningful chemical signals in cervical tissue throughout pregnancy and during post-partum repair. This is the first study to demonstrate the utility of Raman spectroscopy as a basic research tool in Obstetrics via its sensitivity to known dynamic biochemical changes that occur during cervical remodeling, and marking an important step towards development of a clinical tool. With continued advancement, Raman spectroscopy has the potential to improve patient care by arming

providers with information on the biochemical state of the cervix, close gaps in our understanding of cervical maturation, and identify women at risk for preterm birth.

4.6 Acknowledgments

The authors wish to acknowledge the Vanderbilt Biophotonics Center, Dr. Jennifer L. Herington, and Dr. Isaac J. Pence for helpful discussion, Dr. Bruce Beyer for aid in recruiting patients, Tamara Keown for helpful discussions and recruiting patients, Dr. Jennifer Thompson for clinical feedback and discussion, and the doctors, nurses, staff, and patients at the Vanderbilt One Hundred Oaks Women's Health Center for helping with all facets of patient recruitment and execution of the study.

CHAPTER 5

DEVELOPMENT OF A SPECULUM-FREE OPTICAL PROBE FOR CERVICAL ASSESSMENT

Text partially adapted from:

CM O'Brien, KJ Cochran, LE Masson, M Goldberg, E Marple, KA Bennett, J Reese, JC Slaughter, JM Newton, and A Mahadevan-Jansen, "Development of a speculum-free optical probe for cervical assessment," (in preparation for submission to the Journal of Biophotonics).

5.1 Abstract

Preterm birth (PTB) affects 15 million babies each year, and is the leading cause of neonatal death. Half of the cases of PTB have unknown cause, and there are no accurate methods for predicting PTB. Treatments are available to delay delivery and expedite development of the baby, but treatments require at least two days to take effect. Therefore early detection of PTB risk is needed. Detection of early changes in the cervix, an organ that must biochemically remodel to allow for passage of a fetus, could be a useful predictor for PTB risk. Researchers have been investigating the use of light-based methods to monitor biochemical changes in the cervix during pregnancy. However, all optical approaches presented thus far require patients to undergo a speculum exam, which patients find uncomfortable and/or painful, and which is not standard practice during prenatal care. Use of this exam reduces patient enrollment rates and provider willingness to participate in research, and remains a barrier for subsequent clinical translation of optical technologies. Herein, a speculum-free optical tool is presented that measures the cervix via introduction by bimanual exam, a procedure that is commonly performed during prenatal visits and labor for tactile monitoring of the cervix. The device incorporates a

Raman spectroscopy probe for biochemical monitoring, as well as a camera for visualizing measurement locations to ensure they are void of cervical mucus and/or blood. This device was tested in female lower reproductive tract mannequins, and a pilot group of patients receiving Obstetrics and Gynecological care. Results between measurements taken with and without the use of a speculum revealed similar spectra, demonstrating that Raman spectral information is conserved when using the speculum-free device. Additionally, the majority of patients stated that the new device reduced discomfort compared to measurements using a speculum. This device was successfully implemented in patients for biochemical measurement of the cervix, integrating with standard prenatal care, and has reduced a barrier in clinical translation of optical devices for future clinical monitoring of the cervix during pregnancy.

5.2 Introduction

Assessment of the uterine cervix is performed routinely during women's health visits for screening of cervical dysplasia using a Papanicolaou test as well as other cervical abnormalities such as cysts. The cervix and vaginal canal may also be evaluated in instances of pain or suspected infection. Additionally, the cervix is often checked during pregnancy to estimate the cervical consistency (soft or stiff) and to determine whether the patient's cervix has dilated.

Development of novel methods for non-invasive, quantitative measurement of the structural and biochemical state of the cervix is under way [1,65,124,193,194]. Optical techniques can provide information on structure and important biochemical components with known roles in cervical dysplasia and cervical remodeling during pregnancy. Optical methods applied for *in vivo* detection of cervical dysplasia include laser-induced autofluorescence, diffuse reflectance spectroscopy, optical coherence tomography, polarimetry, high-resolution microendoscopy,

confocal microscopy, and Raman spectroscopy [193,194]. In the realm of pregnancy, laser induced fluorescence [73], near infrared spectroscopy [79,126], and Raman spectroscopy have been employed in the human cervix *in vivo*. One significant limitation of the aforementioned research methods is that they currently require the cervix to be visualized with a speculum. This allows placement of the optical probes and cameras near or in contact with cleaned cervical tissue without contamination from cervicovaginal fluids. For many patients, the speculum examination is uncomfortable and painful [195,196], and is a significant barrier for many women who require medical care but do not wish to undergo this examination.

To improve patient comfort and recruitment, a number of investigators have designed alternative devices for cervical visualization [197,198]. The Pocket Colposcope [199] paired with a silicone vaginal inserter [198] guides a small imaging camera to the end of the vaginal canal and pushes vaginal tissue aside so that the cervix can be visualized without the use of a speculum. These devices were primarily designed for use in cervical dysplasia screening, where full visualization of the cervix at high magnification is desired. Additionally, speculum exams are not always standard practice, for instance during pregnancy. In such cases, the introduction of a speculum interrupts normal workflow and requires extra time and resources from medical providers. Therefore, alternative approaches to visualizing the cervix are of great interest, particularly for cervical evaluation during pregnancy which will be the focus of this study.

Practitioners in the field of Obstetrics & Gynecology use a variety of endoscopy-based tools to visualize the vaginal canal, cervix, endocervix, and uterus. Vaginoscopy is used to view the vaginal canal without the use of a speculum (a metal or plastic instrument that is inserted into the vaginal canal and spread open so that the cervix may be directly visualized) and typically irrigates the canal to allow for expansion of the vaginal walls for improved visualization.

Hysteroscopy is a minimally invasive procedure which introduces an endoscope through the vaginal and cervical canal for visualization of the uterus. This procedure can be performed with or without introduction of a distending medium, and both rigid and flexible instruments have been developed. The colposcope is used to obtain high magnification images of the cervix and is most frequently used for identifying precancerous lesions. This technique requires the use of a speculum for cervical visualization where the colposcope is brought near the entrance of the vagina and pointed towards the cervix for image capture through the vaginal canal. These clinical instruments have limitations, including the requirement of a speculum for colposcopy, or distension media during vaginoscopy or hysteroscopy.

Full visualization of the cervix is not typically necessary throughout prenatal care, during which the cervical structure and body (length, consistency, and stiffness) are most relevant as measured using a bimanual exam (practitioner inserts two gloved fingers into the vaginal canal for tactile assessment of the cervix) rather than a speculum exam. For example, the current study aims to develop a tool for use during pregnancy. The optical methods currently being investigated to better understand cervical remodeling take point measurements from cervical tissue, and thus also do not require full cervical visualization. In addition to patient aversion to the procedure, providers caring for pregnant patients have limited enthusiasm for new methods involving a speculum exam due to the increased time and effort required, especially when standard prenatal appointments last only 15-20 minutes. Therefore, the use of a speculum for optical cervical assessment significantly hinders research progress and clinical translation/adoption. Finally, methods that use distension media to expand the vaginal canal cannot be used during pregnancy because of increased risk for ascending infection. Therefore, a new approach that 1) does not require the use of a speculum, 2) does not use distension media, 3)

maintains optical data quality, and 4) fits easily into current clinical workflow, would catalyze research progress in the field of cervical remodeling during pregnancy and overcome a large barrier to clinical translation.

The goal of this study is to develop a speculum-free optical tool that can be used for monitoring of the cervix, and validate data quality between speculum-based and speculum-free data. For this proof of principle design, the optical method of choice was Raman spectroscopy. To this end, a camera-guided fiber optic probe was designed for insertion via bimanual examination, a procedure routinely performed during pregnancy and labor to monitor the cervix. Locations for ectocervical measurement were first visualized using the camera to ensure contaminants were cleaned prior to optical measurements. The optical probe was characterized, and measurements obtained with and without a speculum were compared. Finally, patients' perspectives on measurements taken with and without a speculum exam are presented.

5.3 Materials and methods

5.3.1 Probe design

The visual-guidance probe was developed in partnership with EmVision LLC (Loxahatchee, FL) and combined a filtered Raman spectroscopy probe with a small camera and illumination fibers (Figure 1). The Raman spectroscopy probe consists of seven 300 μm fused silica fibers for Raman scatter collection which surrounded one 300 μm low OH fiber for laser excitation, all contained in a 2.1 mm stainless steel tube. A micro lens is located at the distal end of the probe which has a 3 mm radius sapphire plano convex lens coupled to a MgF_2 window that facilitates excitation and collection cone overlap deep within the sample (Figure 1B). Although a lensed Raman probe was used in this study, any optical modality including diffuse

reflectance and fluorescence could be used. An adjacent stainless steel tube contains a 1 x 1 x 1.7 mm CMOS camera (NanEye2D, Awaiba, Austria), which has 120° field of view and a silica window placed in front of it to prevent autofluorescence and Raman scattering from the camera chip. The Raman probe and camera are enclosed together in a 4.6 mm stainless steel tube, and the gaps between the two compartments were hermetically sealed with medical grade epoxy. Surrounding this tube, four sets of four 500 μm diameter Eska fibers illuminate the camera (Figure 1). Eska fibers which have a polymethyl-methacrylate core core and a fluorine polymer sheath (Edmund Optics, Barrington, NJ) were chosen for their high numerical aperture (NA=0.51), which allow full illumination of the camera's field of view. These fibers are contained in another stainless steel tube, and the fibers are held in place using medical grade epoxy, with a 500 μm thick layer covering the fibers. The outer diameter of the distal end of the probe is approximately 7.1 mm, with metal casing extending 4 cm from the tip for ease of holding during measurements. The remainder of the fiber optic probe is covered in medical grade heat shrink tubing. The resolution of the camera was measured using an Air Force resolution test target, and the illumination area was determined by translating a pin hole and power meter across the probe tip, measuring transmitted light to determine the beam profile.

5.3.2 System setup

The laser excitation fiber of the probe was connected to a 785 nm diode laser (Innovative Photonics Solutions) and set to 80 mW of power at the distal end of the probe. The seven Raman collection fibers were connected to an imaging spectrograph (Kaiser Holospec) where the light was dispersed by a holographic grating onto a thermoelectrically cooled CCD camera (Princeton Instruments). Light from a tungsten halogen source (Ocean Optics) was sent through a low pass

filter so that only visible wavelengths were coupled to the Eska illumination fibers. A laptop computer controlled Raman data acquisition through a Labview interface, and Awaiba software was used to visualize probe placement during *in vivo* Raman measurements.

5.3.3 Testing in lower reproductive tract mannequins

Mannequins are commonly used in medical education to practice obstetrics & gynecology procedures and methods prior to experiences with patients [200]. To test the speculum-free probe prior to patients, a female lower reproductive tract mannequin was obtained from the Vanderbilt Center for Experiential Learning and Assessment Laboratory. The mannequin provided the female external genitalia, and a silicone rubber vaginal canal was constructed and inserted into the vaginal opening of the mannequin. A research scientist then curled their index finger and placed it at the end of the vaginal canal phantom to mimic the cervix. Synthetic cervical mucus was made using mucin and water to mimic the Raman spectral profile and consistency of cervical mucus found in the vaginal canal of pregnant women. Two obstetricians then practiced obtaining Raman spectra from the cervix of the mannequin using the visual guidance probe. To determine if the visual guidance probe could aid in identifying areas that needed to be cleaned prior to measurement, the cervix phantom was coated in synthetic mucus and the physicians were tasked with identifying the cervix, wiping away the synthetic mucus, and then obtaining a Raman measurement. These measurements were compared to a clean cervix phantom that had not been previously coated in synthetic mucus.

5.3.4 Clinical protocol

Ten premenopausal women obtaining prenatal or gynecologic care at Vanderbilt's One Hundred Oaks Women's Health Center were recruited using informed, written consent under Institutional Review Board #100544 and #010245, and following the guidelines of the Declaration of Helsinki. Inclusion criteria required patients to be at least 18 years old, able to provide legally valid consent, and speak English. Patient factors such as age, obstetric and gynecologic history, medications, and body mass index were recorded in each patient's research file.

In order to determine the data quality from the speculum and speculum-free approaches, a direct comparison was made by collecting Raman spectra with the visual guidance probe and with a standard speculum-based measurement. Specifically, the patient's provider performed a bimanual exam with the newly designed probe placed between their fingers. The provider located the cervix with their fingers and gently guided the probe to the 12, 3, 6, and 9 o'clock positions of the ectocervix. At each location, the camera with white light illumination was used to determine if the site was clean of mucus and/or blood. When needed, the provider would either wipe the area with their gloved finger or insert a small cotton swab to clean the area. Once the area was clean the probe was placed in contact with the tissue. The white light source was turned off and the 785 nm laser was turned on for Raman measurements. The overhead lights were also extinguished to prevent interference with Raman spectra. Three to five Raman measurements were taken in each location for 0.5 second integration and 6 accumulations.

After the bimanual exam, a speculum was inserted to directly visualize the cervix, and a cotton swab was used to clean the cervix of blood and mucus. Without the use of the camera guidance, the probe was gently placed at approximately the same locations that were measured

during the bimanual exam and the 785 nm laser source was turned on. Similarly, 3-5 measurements were taken at each location with the same integration time and number of accumulations. Once measurements were completed, the Raman probe and speculum were removed, and the entire procedure was complete. Between patients, the probe was disinfected according to standard protocols. Upon completion of the measurements, the patients were surveyed as to whether the speculum-free probe reduced discomfort during light measurements.

5.3.5 Data processing and analysis

Each day, the system was wavelength calibrated using a Neon Argon lamp, and the laser wavelength determined using acetaminophen and naphthalene standards. Spectral response was calibrated using a NIST calibrated standard reference material, 2241, and a correction factor was applied to each Raman spectrum. Ambient background light was removed from each spectrum, followed by noise smoothing with a Savitzky-Golay filter, and fluorescent background subtraction [141].

In the mannequin studies, a least squares analysis was performed based on the pure Raman spectra of the synthetic mucus and cervix phantom (skin from the finger). Each spectrum obtained by the providers during mannequin testing was fit, and the coefficients of the mucus and cervix phantom were compared between groups of measurements taken with and without mucus.

In the patient studies, mean and standard deviation spectra obtained with and without a speculum were plotted to determine areas of overlap and separation. Mean and standard deviation based on ectocervix location were similarly plotted as positions on a clock face. A Bland-Altman plot was used to compare the level of agreement between scores from the first

principle component of paired Raman measurements acquired with a speculum (gold standard) and with the speculum-free approach [201]. Finally, the source of variability within the dataset was evaluated using regression of the first principle component scores. Three variables were analyzed (patient, location, approach (speculum or speculum-free)) in a linear model individually and with interactions, and the coefficient of determination from each model was reported.

5.4 Results

5.4.1 Characterization of visually-guided Raman spectroscopy probe

A Raman spectroscopy probe with a camera and illumination was designed and fabricated (Figure 5.1). First, the quality of Raman spectra was determined by measuring multiple biochemical standards (cholesterol, glycogen, and vegetable oil) with the new probe as well as with a Raman probe used previously to measure spectra from the cervix of pregnant women. The spectra from the new speculum-free probe and the old probe were compared and appear nearly identical, confirming that the data quality was not compromised by the addition of the camera, epoxy, and illumination fibers in the new design (Figure 5.2A-C). The resolution of the camera at 4 mm for the sample was measured to be 356 μm using an Air Force resolution test target (Thorlabs, Newton, NJ), and the white light power at the sample was 0.5mW. The illumination cross-section was calculated based on the full-width at half maximum of the profile, and was 14 mm at 4 mm away from the pinhole, and 16 mm at a distance of 1 cm from the pinhole (Figure 5.2D-E). At 4 mm distance from the sample, a bimodal light profile was observed due to the separation of fibers around the Raman probe and camera. However at a distance of 1 cm, the light had diverged and the profile had changed to a Gaussian distribution, providing even lighting throughout the field of view.

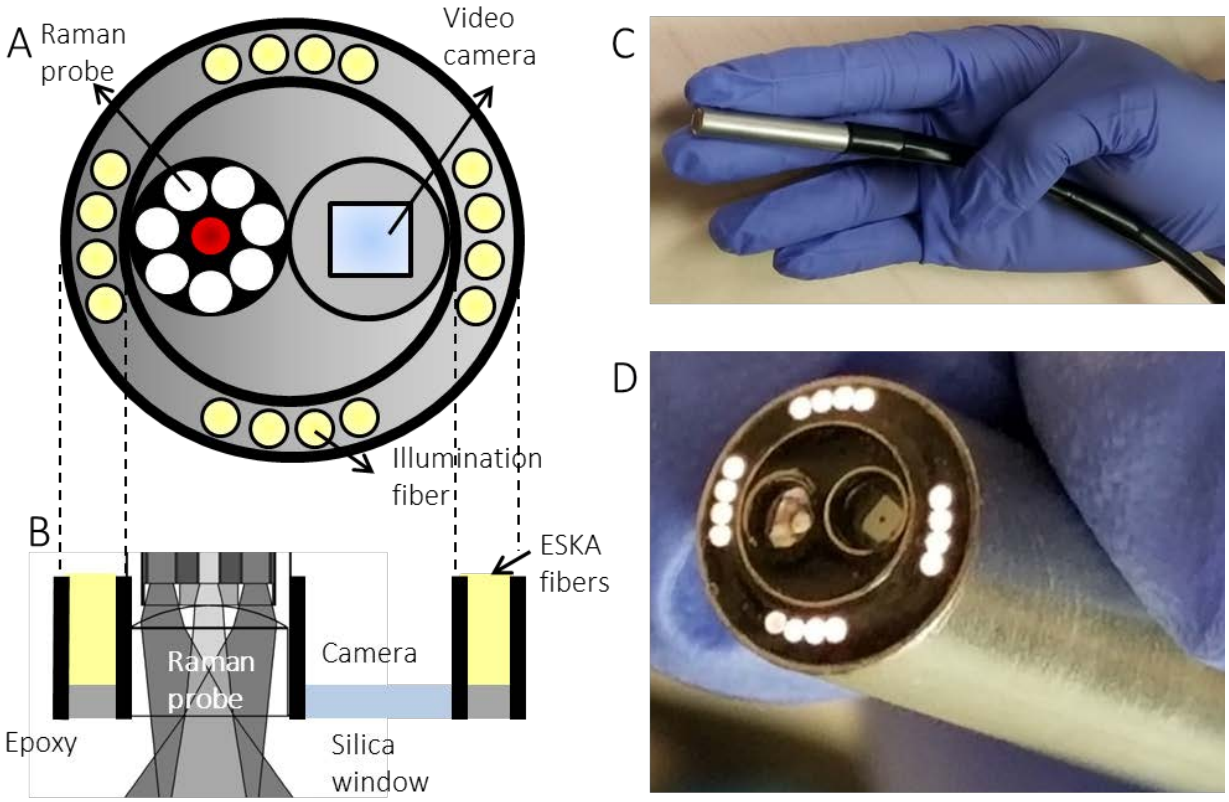

Figure 5.1: Speculum-free Raman spectroscopy probe. A) Schematic of probe design including Raman probe, camera, and illumination fibers; B) Speculum-free probe top-down cross-section, C-D) Speculum-free probe in gloved hand.

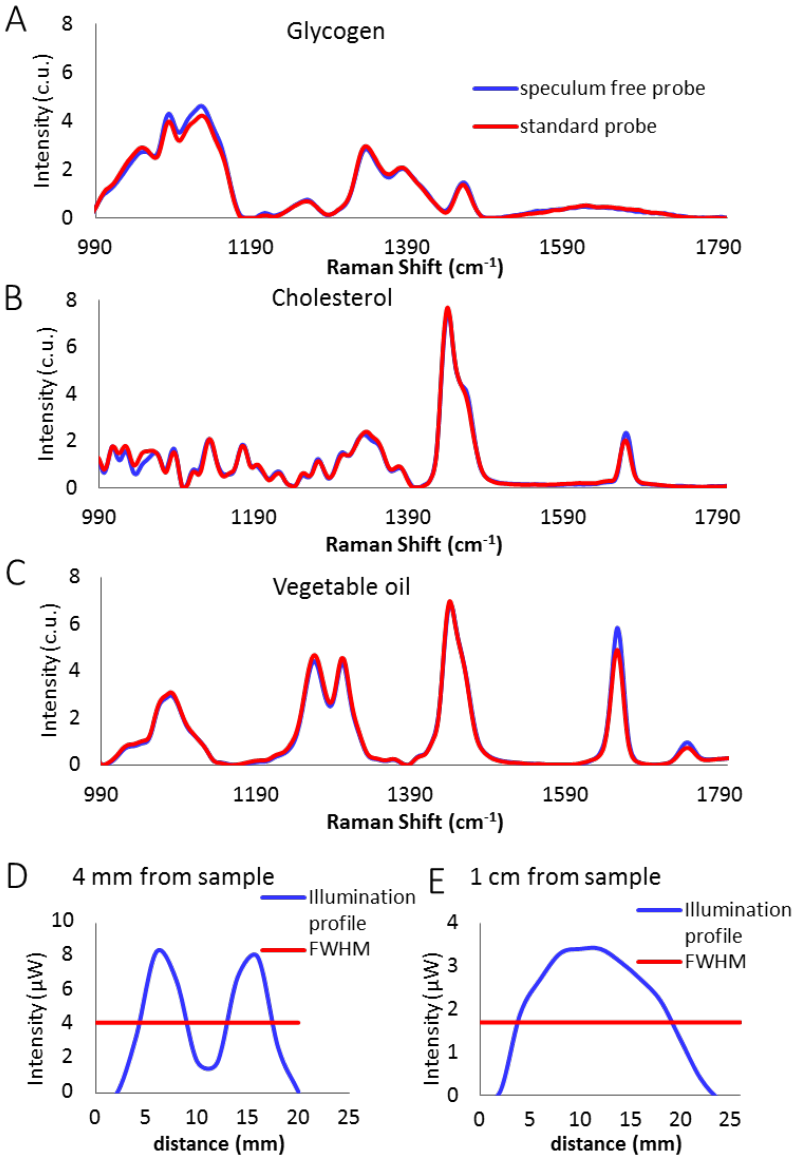

Figure 5.2: Raman probe characterization. Raman spectral comparison of A) glycogen, B) cholesterol, and C) vegetable oil obtained from the speculum-free probe and a standard forward looking probe. Illumination profiles at D) 4 mm and E) 1 cm distance from the sample.

5.4.2 Testing in obstetric lower reproductive tract simulators

A simulation for measuring Raman spectra from the cervix of female patients was conducted using a female lower reproductive tract mannequin (Figure 5.3A). Comparison of the Raman spectra measured from a clean cervix phantom to Raman spectra acquired from a cervix

phantom that was coated in synthetic mucus and then wiped clean using the visually guided Raman probe reveal nearly identical spectra (Figure 5.3B). In the spectra from the cervix samples wiped clean, minimal contamination from the synthetic mucus is seen. To measure the contribution of mucus in measurements that had synthetic mucus coated on the cervix phantom with subsequent cleaning with cotton swabs, a least squares fit based on pure synthetic mucus and pure cervix phantom (skin from index finger) Raman spectra was applied to each measurement acquired during mannequin testing. The resulting fit coefficients were analyzed using a t-test between measurements taken with and without synthetic mucus applied to the cervix. There was no significant difference between spectra that were acquired with and without synthetic mucus applied for the mucus coefficient ($p=0.36$) or the cervix phantom coefficient ($p=0.46$). The mucus coefficient was non-zero in cervix phantoms that had no synthetic mucus applied, which was a similar amount to measurements made with synthetic mucus wiped off, indicating that the contribution of synthetic mucus in those measurements was within the noise floor of the Raman spectra and did not contaminate spectral signals.

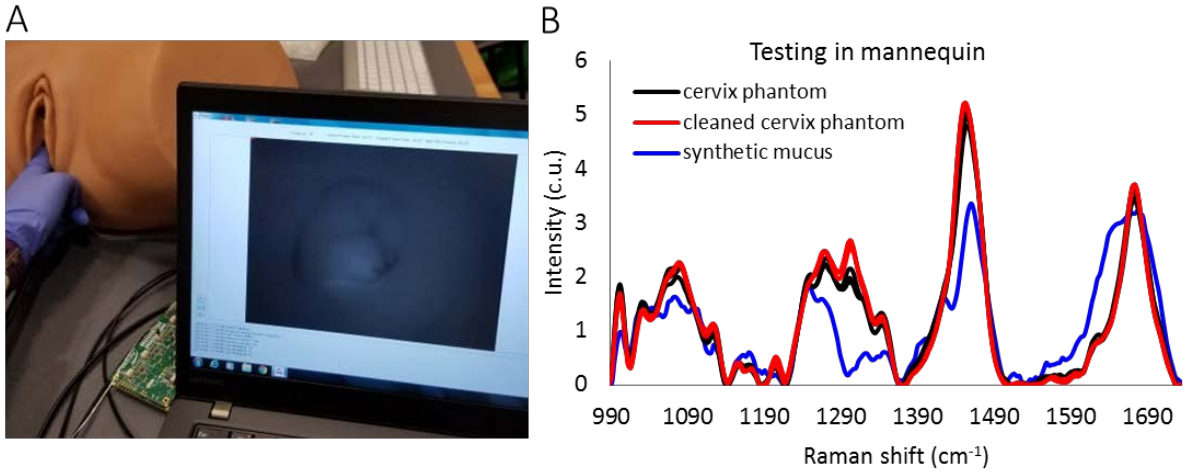

Figure 5.3: Testing of speculum-free probe in mannequins. A) Mannequin testing setup; B) Raman spectral comparison of cervix phantom without mucus (black), cervix phantom with mucus wiped off (red), and mucus phantom (blue).

5.4.3 Validation in patients receiving prenatal or gynecologic care

Spectra obtained from the cervix of one patient in the same location with and without the use of a speculum look very similar (Figure 5.4A), with the majority of differences between the spectra being due to high frequency noise rather than differences in Raman signal. Mean and standard deviation spectra are plotted of measurements obtained with and without a speculum from all patients (Figure 5.4B), where the standard deviations overlap in most areas. Spectral variability based on ectocervix location is plotted in Figure 5.4C, which reveals slight variability in Raman spectra based on location, similar to the levels seen in the comparison in Figure 5.4B.

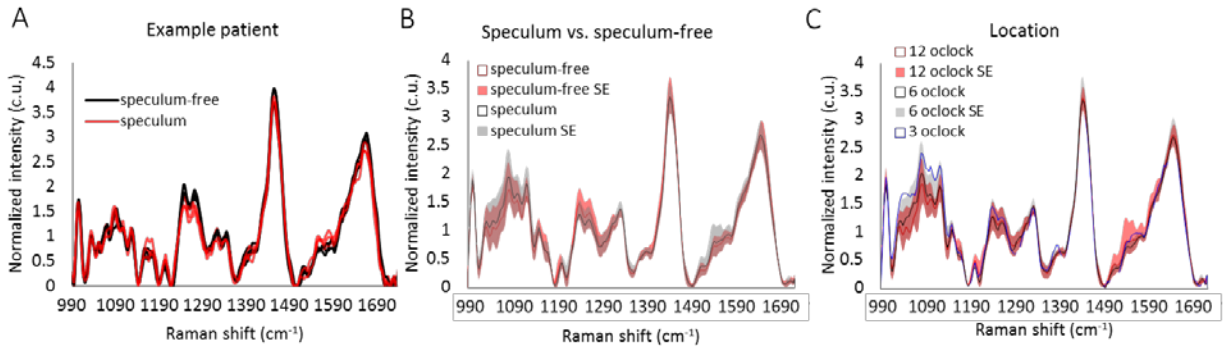

Figure 5.4: A) Raman spectral comparison of measurements taken from a patient using the speculum-free probe with (red) and without (black) the use of a speculum; B) mean and standard deviation spectra from speculum-free (black) and speculum based (red) measurements; C) mean and standard deviation spectra from four locations on the ectocervix.

A Bland Altman plot provided direct comparison of paired Raman measurements obtained with and without a speculum (Figure 5.5A) and revealed an average difference centered around zero and very little spread of the means of the two measures, both indicative of a high degree of similarity. Further, the majority of the paired measures fell within a single standard deviation of the difference between the two approaches. The small amount of variability

observed was analyzed using regression in R (Figure 5.5B). The highest variability was accounted for by including all three variables with interactions as is expected (94.2%). Interestingly, the interaction between patient and approach had the second highest coefficient of determination (55.5%), followed by the interaction of location and patient (44.5%). Individually, the patient variable explained the largest amount of variability (35.9%), followed by location (12%), and then the approach (4.2%). Although approach did not appear to account for a large amount of variability on its own, the interaction of approach and patients did explain nearly half of the observed variability. This may be due to certain patients having a "high" cervix that was difficult for the provider to reach using the speculum-free approach. In addition, the patient variable inherently includes location variability due to the difficulty of the provider measuring the exact cervical location with the speculum and speculum-free approaches, likely explaining the increased variability observed by this interaction.

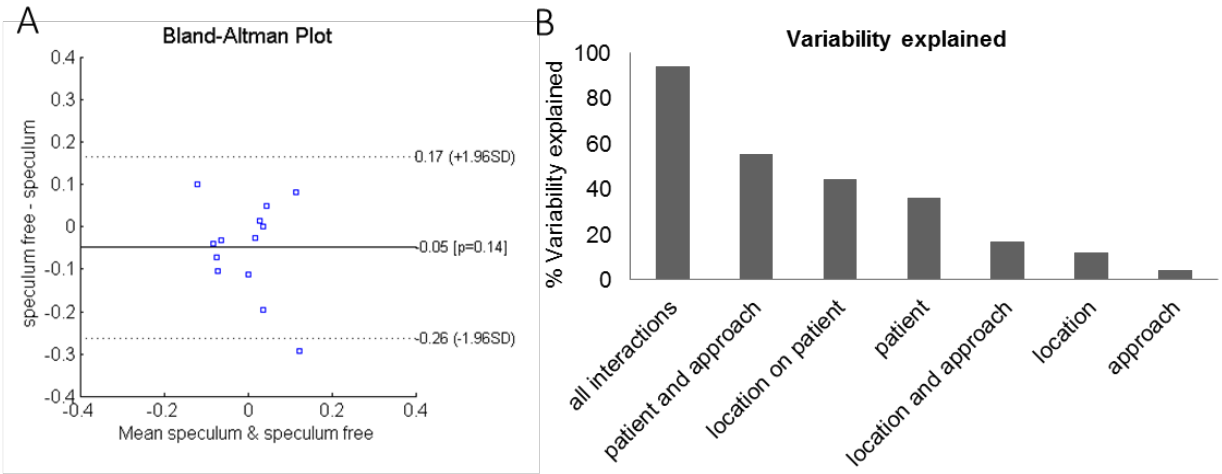

Figure5: A) Bland-Altman plot of the first principle component score of the Raman spectra from paired measures using the speculum-free and speculum-based approach; B) analysis of the contributions from patient, location, and approach variables on the variability observed in the first principle component score of the Raman spectra.

5.4.4 Patient experience using speculum-free Raman probe

Of the ten patients measured, 60% stated that the speculum-free probe reduced discomfort during Raman spectral data collection compared to Raman spectra acquired with a speculum. The remaining 40% of patients stated that the speculum-free probe was comparable to the speculum-based measurements. These patients additionally stated that they did not find speculum exams uncomfortable, possibly explaining why there was no improvement with the speculum-free probe.

5.5 Discussion

Developing tools for improved understanding of the structural and biochemical state of the cervix at the patient bedside has become a high scientific priority in recent years. The burden of cervical cancer is highest in low resource settings where medical providers are pushing for see-and-treat strategies to prevent loss to follow-up, requiring diagnostic tools that can accurately identify disease in minutes rather than days [202]. Researchers and clinicians have increased appreciation for the functional roles the cervix serves during pregnancy and labor, and recognize that spontaneous preterm birth cannot occur without premature cervical remodeling.[43] Optical approaches are sensitive to tissue biochemistry and structure, and therefore have very appealing qualities for non-invasive assessment of the cervix. However, these methods require contact or close placement to the cervix tissue, and have thus far been paired with a speculum examination for direct cervical visualization and probe placement. Patients must willingly enroll in research studies, and patient aversion to speculum examinations is well documented [195,196].

Investigation of the cervix during pregnancy poses additional challenges. Although there is great need and opportunity for advancement in this area, enrollment of pregnant patients into

scientific studies is inherently challenging [203] and many investigative strategies that have been classically used for biomedical investigation (such as assessment of cervical biopsies) are unethical in this context. Thus, researchers are constrained to using nondestructive tools such as ultrasound and optical techniques. Pairing optical techniques with speculum exams increases prenatal visit appointment times as they are not standard of care during pregnancy, and reduce the number of patients willing to participate in research. Finally, when patients do enroll, medical providers are burdened by the added complexity and time required to perform the speculum examinations and subsequent optical measurements, adding another set of barriers to the successful completion of research studies and translation of optical measurements into clinical obstetric care. To overcome these barriers, researchers must determine not only which noninvasive techniques can be used for cervical investigation, but how they should be incorporated to minimize patient discomfort, provider and patient time required, and complexity in order to maximize participation and clinical uptake.

In this study, we developed an optical probe designed to be inserted and guided to the cervix via bimanual exam. This exam is commonly performed during pregnancy and labor to assess the dilation, thinning, and consistency of the cervix, allowing easy integration with existing clinical workflow. This method reduces overall measurement time and eliminates need for additional examination. Furthermore, providers expressed willingness to incorporate these measurements into the bimanual exams as this method mimics common obstetrics procedures such as placement of Foley bulbs through the cervix for labor induction, and insertion of intrauterine pressure catheters through the cervix and uterus for contraction monitoring. The preservation of Raman spectral data quality was demonstrated by comparison to another Raman probe previously used to measure the cervix during prenatal visits. When testing the new

speculum-free probe in lower reproductive tract mannequins and women, the visual guidance of the speculum free probe sufficiently informed the provider whether the location for each measurement was clean prior to Raman measurement, ensuring the acquisition of reliable, uncontaminated spectra. Finally, the majority of patients stated that the speculum-free device reduced discomfort over measurements using a speculum, reducing a large barrier for the optical study of cervical remodeling during pregnancy and translation of such technologies into obstetric care.

A variety of improvements to the speculum-free probe design are likely to further increase patient and provider preference and research participant enrollment rates. The outer diameter of the probe is currently 7.1 mm which could be easily reduced to below 5 mm, minimizing discomfort. The distal end of the tip could be angled and smoothed to remove the harsh edges. In addition, added flexibility to the tip of the probe would improve access to the face of the cervix in cases where it is pointed down or to the side, which are currently challenging to measure. Furthermore, incorporation of an insertion device such as a tampon applicator or the silicone inserter designed by Asiedu et al. [198] could allow for the possibility of self-insertion and measurement, further reducing patient anxiety and provider examination time.

Although this device was specifically designed for use in pregnant patients, there are a variety of other clinical situations where a speculum-free cervical visualization and optical measurement tool could be of use. The speculum-free device could be tailored to provide dual testing of colposcopy and an additional specific technique without the use of a speculum during the same visit. This would be particularly useful for patients that have trouble tolerating a speculum exam including those with ongoing infection and open sores or wounds. In addition,

simple visualization of the cervix and/or vaginal canal for assessment of intrauterine device strings, investigation of pain symptoms, and trauma are other potential uses for this device.

In summary, an optical tool has been developed to assess cervix tissue biochemistry noninvasively during pregnancy without insertion of a speculum. This tool reduced patient discomfort and was preferred by patients without sacrificing data quality. This approach reduces significant barriers to allow higher throughput of clinical investigations of cervical remodeling during pregnancy, and enables translation of optical technologies into standard obstetric care. These advancements will accelerate data acquisition and ultimately expedite improved understanding of cervical remodeling physiology towards diagnostic and therapeutic interventions for preterm birth.

5.6 Acknowledgments

The authors wish to acknowledge the Vanderbilt Biophotonics Center, the Vanderbilt Center for Experiential Learning and Assessment (CELA), Jeremy Ford for useful discussions and experimental expertise with the probe development and testing, Jordan Halasz for assistance using the lower reproductive mannequins, Tamara Keown for helpful discussions and recruiting patients, and the doctors, nurses, staff, and patients at the Vanderbilt One Hundred Oaks Women's Health Center for helping with all facets of patient recruitment and execution of the study. This work was funded in part by NIH R01 HD081121.

CHAPTER 6

LONGITUDINAL BIOCHEMICAL MONITORING OF CERVICAL REMODELING IN LABORING WOMEN USING *IN VIVO* RAMAN SPECTROSCOPY

6.1 Abstract

In instances of spontaneous preterm birth, the cervix must transform from a rigid structure to a distensible channel that allows passage of a fetus. Vast biochemical changes must occur for this to happen, but our understanding of cervical remodeling during pregnancy and labor is incomplete, partly due to the lack of *in vivo* studies focused on tracking these changes over the course of pregnancy, labor, and post-partum. This study uses Raman spectroscopy, a light scattering technique capable of measuring biochemical fingerprints of tissues *in vivo*, to measure the cervix over the course of labor. Raman spectroscopy is sensitive to changes in extracellular matrix (ECM) proteins, lipids, nucleic acids, and tissue hydration. These constituents are known to change in the cervical remodeling process, and this technique can longitudinally monitor these changes in order to identify high risk "fingerprints" associated with impending labor and delivery. Sixteen pregnant patients undergoing induction of labor at Vanderbilt University Medical Center were recruited. Raman spectra were measured using an *in vivo* Raman system with a fiber optic probe throughout labor in four hour intervals until rupture of membranes. Spectral changes in preparation for delivery were plotted using a generalized linear model, revealing significant change over the course of labor. These findings demonstrate that *in vivo* Raman spectroscopy is sensitive to biochemical changes remodeling the cervix during labor, and may be a valuable clinical tool for PTB risk assessment.

6.2 Introduction

Preterm birth is the leading cause of death in neonates (<28 days of age) across the world [3]. Direct complications of preterm birth are responsible for one million deaths a year and are a risk factor in over 50% of all neonatal deaths [3]. Preterm births fall into two categories: spontaneous and indicated preterm delivery. Medically indicated preterm delivery occurs in the case of preeclampsia, infection, preterm premature rupture of membranes, and other conditions that complicate pregnancy [204]. In contrast, little is known about the process leading to spontaneous preterm birth, but it is always preceded by the incompletely understood cervical ripening and dilation process.

Discussion of the cervical remodeling process usually centers on collagen, as 90% of the cervix dry weight is composed of collagen. The other 10% of the cervix is made up of biological constituents such as glycosaminoglycans (GAGs), proteoglycans, and stromal and epithelial cells [39]. These constituents undergo dynamic changes during the cervical remodeling process that facilitate successful vaginal delivery [39]. The cervix can remodel in multiple ways, and the cervical ripening process that occurs during preterm delivery is not identical to the ripening process observed in term labor [57].

Quantitative analysis of biochemical changes in the laboring cervix will lead to better understanding of the cervical ripening and dilation process at term. Early markers of cervical ripening and dilation could be recognized, aid in the development of targeted therapies to delay labor. Multiple noninvasive tools are under investigation for providing quantitative evaluation of the cervix during pregnancy and labor [1,65]. Light-based methods offer many advantages, including ability to collect and analyze data in real time, non-invasive measurement, and biochemical sensitivity. Raman spectroscopy is a light scattering method that probes vibrational

modes of molecules within a sample, measuring biomolecular "fingerprints" of tissue. Herein, *in vivo* Raman spectroscopy was used to measure the cervix of laboring women and compared with outcome and time until delivery. The goal of the study was to identify biochemical changes that occur in the cervix in preparation for delivery.

6.3 Materials and Methods

6.3.1 Clinical protocol

Sixteen pregnant patients scheduled for labor induction and expected to have uncomplicated labors were recruited from Vanderbilt's Center for Women's Health under IRB #100544. The patient's provider determined if a patient was eligible to participate in the study based on strict inclusion/exclusion criteria, as well as their medical assessment. Informed written consent was obtained from each patient enrolled prior to performing any measurements. Patient demographics, methods and timing of labor augmentation were recorded (Table 1). For each patient, the following measurement protocol was used: the medical provider performed a speculum exam to visualize the cervix and clean off any blood or mucus. Next, the Raman probe was placed in gentle contact with the cervix and Raman spectra were measured from 4 sites on the ectocervix at 12, 3, 6 and 9 o'clock positions using an integration time of 3 seconds per measurement. No tissue was removed as part of this study. Raman measurements were taken at the same time points that standard bimanual cervical exams were performed. Current practice at Vanderbilt is to perform cervical exams every four hours when the cervix is < 6 cm dilated, and every two hours after the cervix is > 6 cm dilated. Once the membranes ruptured, Raman measurements were no longer acquired in order to avoid risk of infection.

Table 6.1 Patient characteristics and outcome

Patient	Age	Gestational Age	Race	Gravida	BMI (PP)	BMI (T)	Induction Method	Outcome
1002	28	41 weeks	W	2	29.9	39.0	misoprostol	C/S
1003	36	39 weeks	B	8	51.6	55.9	misoprostol	C/S
1004	23	39 weeks, 1 day	W	3	28.5	35.5	misoprostol, pitocin, AROM	SVD
1005	23	39 weeks	W	2	23.0	NA	pitocin	SVD
1006	29	40 weeks, 6 days	W	1	24.6	32.3	pitocin, foley bulb	SVD
1007	25	41 weeks	W	1	37.3	45.4	pitocin	SVD
1009	18	41 weeks	H	1	27.5	29.2	misoprostol, pitocin, AROM	SVD
1010	28	41 weeks	W	1	29.3	22.7	membranes stripped, pitocin, AROM	SVD
1011	25	37 weeks, 3 days	W	6	21.8	24.9	pitocin	SVD
1012	30	40 weeks	W	6	31.8	33.6	Pitocin, AROM	SVD
1013	32	39 weeks, 1 day	W	2	22.0	28.5	pitocin, AROM	SVD
1014	27	41 weeks	W	2	23.6	28.8	pitocin, foley bulb	SVD
1016	23	41 weeks	W	1	25.6	29.5	misoprostol, foley bulb, AROM, pitocin	C/S
1017	36	39 weeks, 3 days	W	4	38.0	40.1	pitocin, AROM	SVD
1018	31	39 weeks, 1 day	B	1	26.6	28.5	misoprostol, foley bulb, pitocin	SVD
1020	19	40 weeks, 6 days	B	1	32.8	39.0	misoprostol, foley bulb, pitocin	C/S

Abbreviations: W (white), B (black), H (Hispanic), C/S (cesarean section), SVD (spontaneous vaginal delivery)

Two clinical measures were used along with the Raman measurements to assess obstetric status: cervical length measured using transvaginal ultrasound and Bishop score obtained during bimanual exam. These clinical metrics were compared with Raman spectra, gestation length, and patient outcome.

6.3.2 Raman system setup

A portable fiber optic probe-based RS system was used to acquire Raman spectra from patients during labor. The system consists of a diode laser (785 nm) coupled to a fiber optic probe. An imaging spectrograph coupled to an air-cooled back-illuminated, deep-depletion charge coupled device (CCD) camera, controlled by a computer collects the Raman. A custom fiber optic probe incorporates inline filtering within the tip of the probe to minimize interference from signal generated in the components used in the probe. Spectra were calibrated using standard protocols and processed for fluorescence subtraction and noise smoothing [141].

6.3.3 Data processing and analysis

The longitudinal progression of cervical change was visualized using generalized linear models (GLM) with a restricted cubic spline that had 65 degrees of freedom. Spectra were modeled as a function of hours until delivery, starting 20 hours away in four hour increments. A Spearman correlation was performed for cervical length and Bishop score due to the continuous nature of these variables.

6.4 Results

Raman spectra were successfully measured from the cervix of laboring patients throughout the course of labor (Figure 6.1).

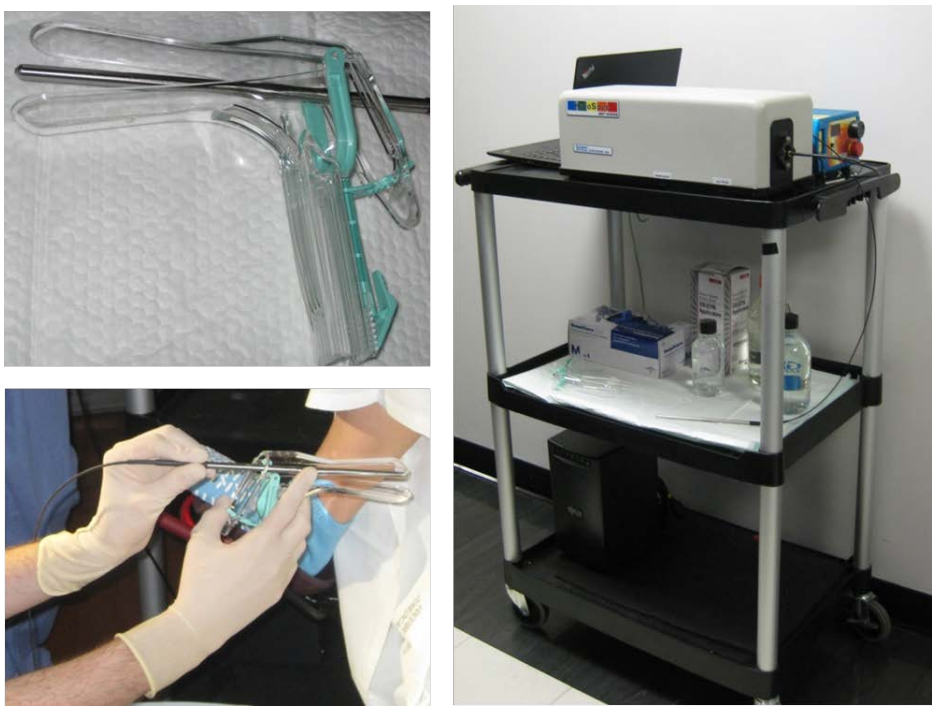

Figure 6.1. *In vivo* Raman spectroscopy for cervical monitoring during labor.

In order to aid visualization, a spectral model based on generalized linear models was developed, and plots of the spectra according to hours until delivery were generated (Figure 6.2). Many spectra changes are observed, including a large increase in the 1265, 1304, 1440, and 1657 cm^{-1} peak intensities within 8 hours of delivery. These tall, narrow peaks are classic features of triglyceride containing tissues like adipose tissue [131], however their appearance during labor is surprising and not well understood at this time. Decreases are observed in the 1003 and 1339 cm^{-1} peaks which are attributed to proteins, and are likely caused by collagen matrix degradation.

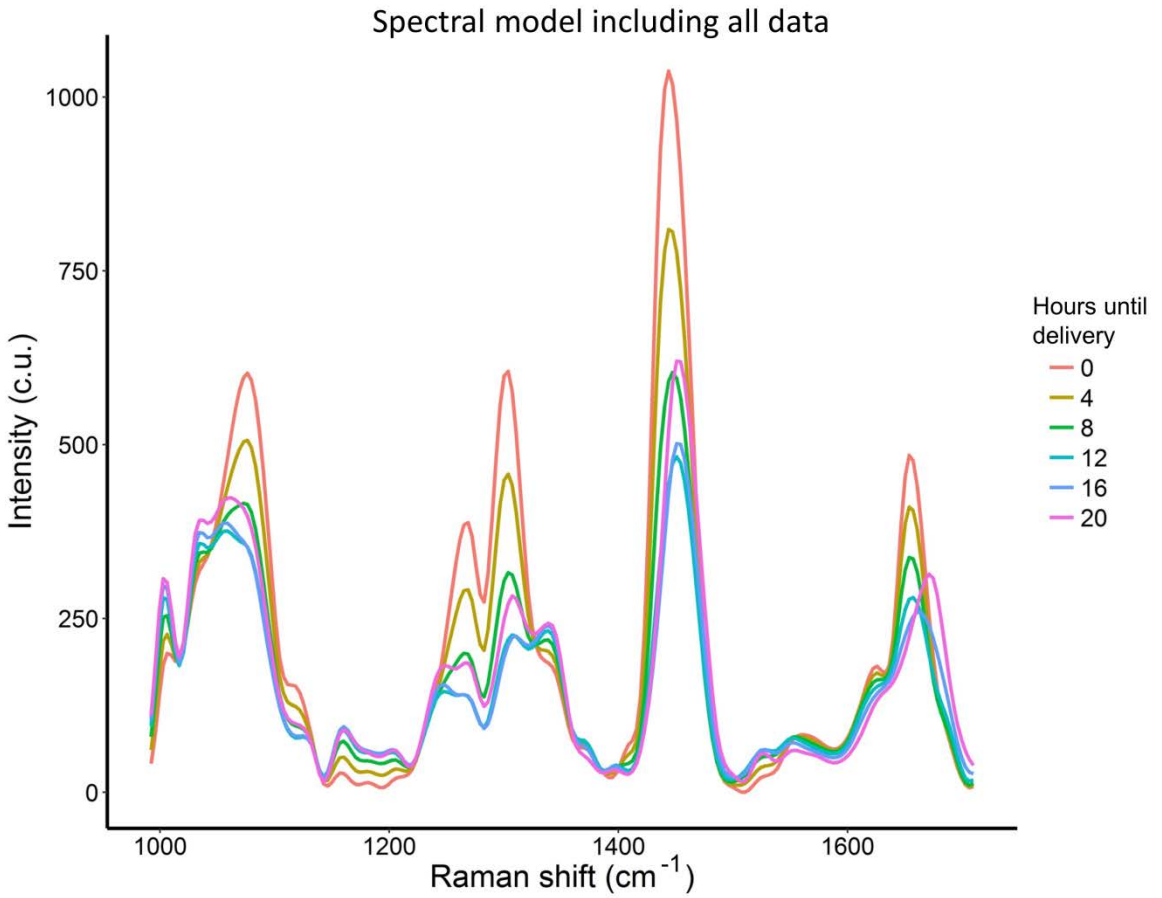

Figure 6.2. Computational model depicting Raman spectral changes as the cervix prepares for delivery (model computed from n=16 patients).

In a preliminary analysis from four patients, the correlation between Raman features, obstetric outcome measured as hours until delivery, and cervical length were compared (Figure 6.3). Four Raman peaks were chosen for comparison, including the 1003, 1265, 1335, and 1451 cm^{-1} peaks. Upon comparison to time until delivery, the 1451 cm^{-1} peak intensity had the highest correlation coefficient of -0.79 (Figure 6.3), followed by the 1265 cm^{-1} peak intensity with a coefficient of -0.7, and the cervical length measure yielding a correlation coefficient of -0.58. The highly correlated Raman peaks are both attributed to triglyceride molecules, and show a similar increase prior to delivery as that observed in the 16 patient dataset in Figure 6.2. No

correlation was observed between any of the Raman spectral features and time since start of induction. This result is expected as patients begin induction in cervical states ranging from no dilation and full thickness to 6 cm dilation and 80% effaced, and thus the time since start of induction may have little relation to the biochemical state of the cervix.

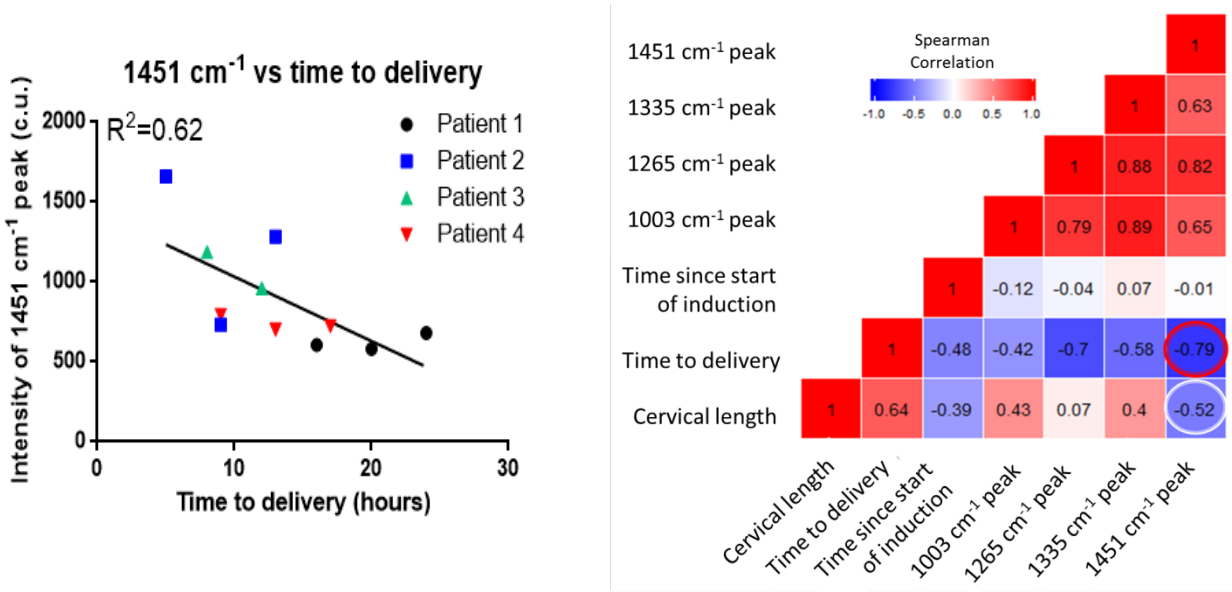

Figure 6.3 Preliminary analyses from four patients investigating the 1440 cm^{-1} peak intensity as a function of hour until delivery (Left), and comparison of Raman spectral features and cervical length to outcome (Right).

The contribution from adipose signal is unexpected, and may be occurring from adipose pockets located at the internal os [205]. As the cervix effaces, the depth through which light must travel to reach such adipose pockets would decrease, and may explain why lipid signals are observed prior to delivery. A separate spectral model was developed in which lipid-rich spectra were excluded (Figure 6.4). In the new model, significant decreases in the 1003, 1248, 1339, and 1451 cm^{-1} protein peaks are observed. This result is in accordance with published literature describing reduced extracellular matrix concentration during the ripening and dilation phase [43].

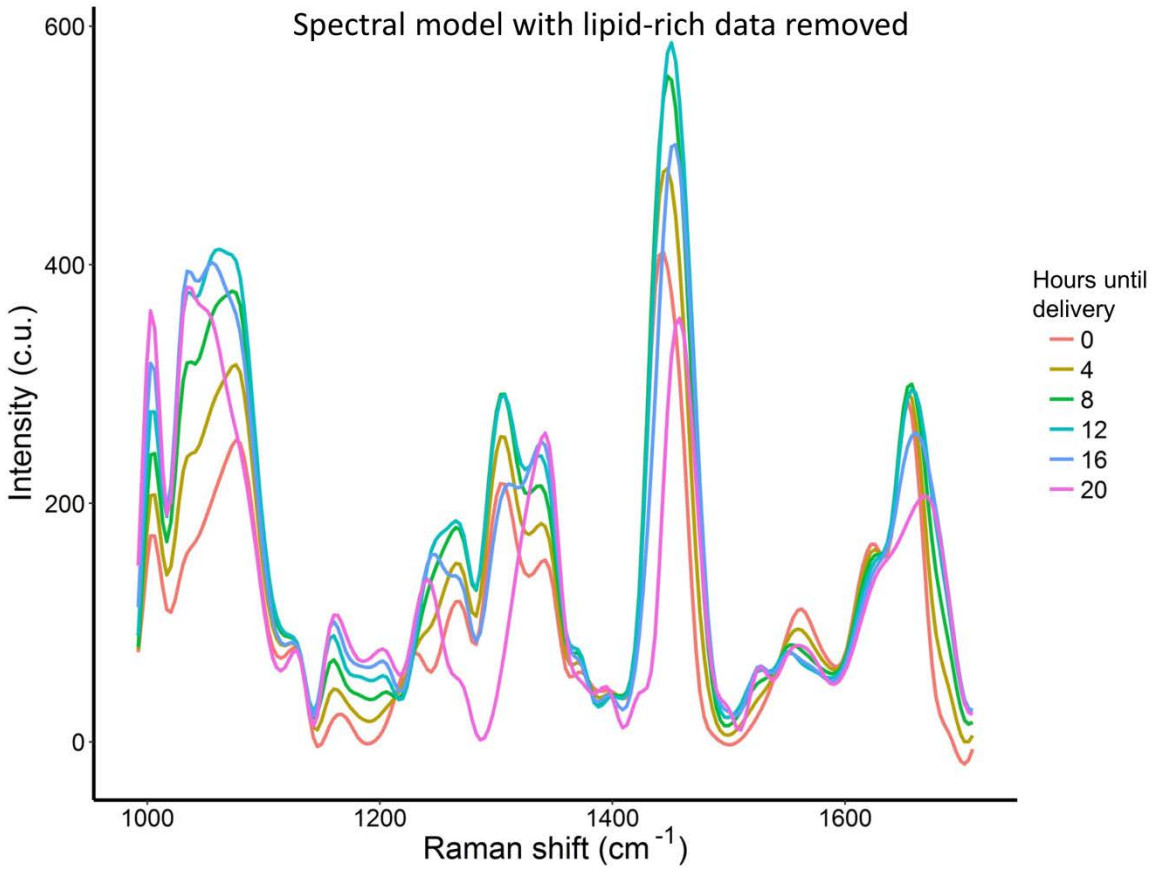

Figure 6.4 Computational model developed without contribution from lipid rich spectra (computation model developed from n=16 patients).

6.5 Discussion

Although data analysis is still under way, interesting results have already been observed, including the presence of high triglyceride signals prior to delivery, and significant decreases in Raman peaks attributed to extracellular matrix. Additional analysis is needed to quantify the significance of the differences observed over the course of pregnancy. Raman bands that underwent the most changes throughout labor will be analyzed using generalized estimating equations (GEE), an extension of GLM that clusters measurements obtained from the same

patient [181,182]. Patient factors including body mass index, parity, and labor augmentation method will be incorporated into the GEE to assess the impact of these variables on cervical remodeling trajectories during labor.

In vivo Raman spectroscopy has high potential to elucidate dynamic biochemical processes that scientists have not previously been able to probe, and may ultimately improve patient care by providing a biochemical means to detect premature changes in cervical remodeling for identifying patients at high risk of preterm birth.

6.6 Acknowledgments

This work was funded in part by NIH R01 HD081121, NIH R01 CA095405, the NSF Graduate Research Fellowship (CO), and CTSA award no. UL1TR000445 from the National Center for Advancing Translational Sciences (NCATS). Its contents are solely the responsibility of the authors and do not necessarily represent the official views of the NCATS or the NIH.

The authors wish to acknowledge the Vanderbilt Biophotonics Center, Dr. Isaac J. Pence, Dr. Heather Maune for aid in recruiting patients, Dr. Jennifer Thompson for clinical feedback and discussion, and the doctors, nurses, staff, and patients in the Vanderbilt University Labor and Delivery Department helping with all facets of patient recruitment and execution of the study.

CHAPTER 7

CONCLUSIONS

7.1 Summary and integration

Maternal health providers all over the world are in need of accurate methods to recognize patients at risk of preterm birth. Current understanding of the physiologic changes leading to labor and parturition is incomplete, limiting development of both diagnostic and therapeutic strategies to combat preterm birth. Until recently, *in vivo* research methods were too invasive to be used as tools for discovery, particularly during preterm labor. In this dissertation, *in vivo* Raman Spectroscopy was used to simultaneously resolve collagen content, hydration, lipids, saccharides, and other biomolecules to investigate dynamic changes in biochemistry of the mouse and human cervix throughout pregnancy in order to gain a more detailed understanding of cervical remodeling in healthy and high-risk pregnancies.

In Aim 1, Raman spectra from 68 pregnant women were characterized over the course of pregnancy by measuring women monthly in the first and second trimester, weekly in the third trimester, and at the six week post-partum visit. An additional study measured 16 laboring women throughout the course of their labor. These are the first studies to measure the cervix of pregnant women using Raman spectroscopy, demonstrating feasibility of the approach, and providing a statistically powered study of the four phases of cervical remodeling in pregnant women. Results from this study found that indeed Raman spectral signals attributed to collagen decrease in preparation for delivery, whereas blood/vascular signals increase[43]. This is in agreement with literature. In the post-partum cervix, signals attributed to actin, glycogen, and

cholesterol were elevated, whereas blood, collagen, and water contributions were low. This spectral profile fits with the wound healing environment characteristic of the post-partum repair phase, in which inflammatory cells infiltrate the cervix. Increased cellular density may explain the increased actin and cholesterol contributions, whereas increased glycogen may be due to heightened anabolic activity during repair. In addition, two patient variables were demonstrated to impact Raman spectra over the course of pregnancy. Parity had effects on collagen and blood signals, with higher collagen signals observed in nulliparous patients at the beginning of pregnancy compared with patients who had prior pregnancies. This phenomenon has been demonstrated in excised human tissue sample where collagen content and tissue stiffness were higher in nulliparous patients [44,169]. In parous patients, higher blood signals were observed early in pregnancy compared to nulliparous, however they did not significantly increase as was observed in nulliparous patients, possibly indicating that sufficient vascular supply is established during prior pregnancies but must be developed in nulliparous patients. Patients with high body mass index (BMI) had less significant decreases in collagen signal compared to normal and low BMI. Interestingly, high BMI patients have higher probability of delivering after their due date, longer labors, and increased risk of stalled labor resulting in cesarean section [170-174]. Higher collagen signals observed in term high BMI patients may indicate that the cervix extracellular matrix has not remodeled to the same extent as low BMI patients, explaining the delay in labor onset and duration.

The statistical analysis performed on the pregnant patient dataset was accomplished through completion of Aim 2, in which a longitudinal biochemical model based on non-negative least squares was developed. For the model, fifteen biochemical contributors were measured and considered for inclusion, however only 6 were finally used (actin, blood, cholesterol, collagen I,

glycogen, and water) for analysis in the human dataset. This model performed data reduction of the high dimensional dataset in a way that allowed for interpretation of results, compared with other data reduction techniques. The least squares approach was also used for Aim 3, in which mouse models of pregnancy were measured over the course of gestation. For analysis in mice, only three components (adipose tissue, collagen I, and water) were used due to the large contribution of adipose tissue that limited detection of other biochemical constituents.

In Aim 3, a mouse model of delayed parturition (Cox-1 knock out (KO)) was evaluated to determine whether impaired cervical remodeling could be contributing to the phenotype. Results from Raman spectra over the course of pregnancy in wild type and Cox-1 KO mice revealed that the collagen coefficient determined from least squares fitting decreased in both models beginning on day 12, in accordance with cervical remodeling literature which observed decreased tissue stiffness, and increased collagen solubility and distensibility by day 12 of pregnancy[49], however there were no significant differences observed between the two models. In contrast, Raman peak ratios representing relative contributions from proteins and lipids decreased in both models beginning on day 12 of pregnancy, but increased in wild type mice at term. An increase was not observed in the Cox-1 KO mice until 1 day post term when the mice typically deliver their pups, demonstrating a delay in cervical remodeling. These results were compared to *ex vivo* biochemical tests which revealed increased distensibility and reduced tissue stiffness in wild type mice at term, whereas such levels were not reached in Cox-1 KO mice until one day post-term, similar to the *in vivo* Raman results. Finally, a relationship between *in vivo* Raman spectra and *ex vivo* biomechanical properties was established by performing a Spearman correlation between paired Raman spectra and biomechanics results from each mouse. The collagen coefficient had the highest correlation to biomechanical properties of stiffness, distensibility, and maximum

stress. Collagen is documented as having the most influence on the mechanical properties of the cervix [44,45], in agreement with results from this study.

An additional project was added to the originally proposed aims with the goal of developing a speculum-free approach to measuring the cervix in pregnant women. During studies in Aim 1, significant barriers to research progress and future clinical translation were discovered. Patients were reluctant to participate in research because of the use of the speculum examination to acquire measurements. In addition, speculum exams are not standard practice during prenatal care, which increased burden on Obstetrics providers when conducting the exam due to increased time and resources required. To this end, a Raman spectroscopy probe was constructed with the addition of a video camera and white light illumination fibers. The new probe was designed to be inserted into the vaginal canal via bimanual exam, rather than speculum exam, a procedure frequently performed during prenatal care and labor by Obstetrics providers. The cervix was located by the provider's fingers, and the speculum-free probe was guided along the fingers to the ectocervix. The camera is used to determine if the ectocervix location is clean of mucus and/or blood prior to Raman spectral measurement. Testing in mannequins and women revealed that Raman spectra acquired with and without a speculum were not significantly different, and the majority of patients stated that the speculum-free approach reduced discomfort.

Together, these studies form the foundation for the utility of *in vivo* Raman spectroscopy as a biomedical tool for investigation of cervical remodeling during all phases of pregnancy, and demonstrate feasibility towards a clinical cervical monitoring device. The data analysis methods and instrumentation improvements developed herein have helped to overcome significant hurdles

in data reduction, longitudinal analysis, and clinical translation specific to pregnancy, and will expedite progress in future work.

7.2 Recommendations

Throughout this work a number of hurdles were recognized, some of which still remain after completion of this dissertation. In addition, a number of opportunities for future work and exploration were identified, and offer opportunities for advancement.

1) Incorporation of additional optical information into Raman spectral measurements

Diffuse reflectance: Raman scattering is affected by the optical properties of the sample. Researchers have determined that the optical properties of the cervix are not constant throughout pregnancy [78,79], and are therefore impacting the Raman spectra collected in this dissertation. Adding a diffuse reflectance modality to the current optical probes would minimize uncertainty in Raman spectra interpretation, and provide better biochemical concentration approximations from least squares models. Furthermore, this approach will provide additional information about the cervical remodeling process that has not yet been investigated using diffuse reflectance.

Polarization: Polarization sensitive molecules yield unique Raman profiles based on the polarization of the light used. In the current system, polarization is not accounted for, even though some of the linear polarization from the diode laser is conserved at the tip of the fiber optic probe. Collagen is a birefringent material which produces distinct Raman spectra based on its alignment [206]. Furthermore, the cervix has been demonstrated to have axes of preferential collagen alignment [129], particularly in early pregnancy when the collagen fibers are tightly packed. As the cervix prepares for delivery, the collagen fibers decrease in concentration and

become dispersed [43], as has been seen using second harmonic generation imaging [76,77]. Polarization-sensitive Raman spectroscopy could provide additional information about the structure of the cervical extracellular matrix throughout pregnancy and post-partum repair, and will likely account for variability seen in some of the polarization-sensitive Raman peaks.

High wavenumber Raman spectroscopy: A dual fingerprint and high wavenumber Raman spectroscopy system has been developed and tested in gelatin phantoms, chicken breast, and *in vivo* mouse cervix tissue. A strong water peak is located in the high wavenumber region at 3500 cm^{-1}, and also contains information regarding the type of bonding that occurs within the sample. Applying this technique to monitoring cervical change during pregnancy will offer a higher accuracy hydration measurement and provide insight into the types of molecules the water interacts with as the cervix remodels. I recommend that this technique be extended to both the human and mouse projects, especially for measurements in preterm birth mouse models LPS and RU48. Both groups of mice deliver preterm, however the cervical tissue wet weight of RU486 treated mice significantly increases whereas LPS treated cervix tissue wet weight remains constant [57]. The water peak in the high wavenumber region of the spectrum should be very sensitive to the distinct cervical remodeling pathways of each treatment group, and may aid understanding of the cervical remodeling process in instances of preterm birth.

2) <u>Design of a deep tissue signal rejecting Raman probe</u>

Large contributions of adipose signal originating from fat pads behind and around the cervix overwhelm Raman spectra acquired from the cervix of mice. Fat has a significantly higher Raman cross-section compared to collagen, cellular components, and other extracellular biomolecules, so although less light is reaching the fat pads, more Raman photons are generated

by interacting with fat tissue. A shallow-focused Raman probe with very sharp excitation and collection cone overlap will minimize signal collection from deep layers and reduce contribution of adipose tissue in mouse cervical spectra. Designs for such a probe could include the addition of a ball lens [207], or by beveling the collection fibers.

3) Further development of speculum-free Raman spectroscopy probe for measurements in women

Multiple improvements should be made to the speculum-free fiber optic probe. First, the camera should be color sensitive, as opposed to the camera included in the current device. In addition, eska fibers should also be placed in the center of the probe to illuminate the center of the camera field of view when in close proximity to a sample. The current design has right angles at the probe tip and has a larger diameter than is necessary, both factors potentially causing discomfort for patients. The probe tip should be smoothed and the diameter of the probe decreased by more strategic placement of the illumination fibers near the center of the probe.

4) New patient populations for investigation

Expanding existing studies to include a number of new patient populations may help understand physiology behind risks factors for preterm birth and other obstetric outcomes. Patients with extremely low body mass index have increased risk for preterm birth [208], whereas patients with high body mass index have increased rates of post-dates, stalled labor, and unplanned cesarean section [170-174]. Results from our study in 68 pregnant women throughout pregnancy indicate that high body mass index affects Raman spectral changes as the cervix remodels. This observation should be investigated further by actively recruiting patients with

extremely low or high BMI to more deeply characterize the effects body mass index has on the cervix during pregnancy.

Additional cohorts of high risk patients should be recruited, including Hispanic and non-Hispanic black patients which have increased risk for preterm birth that is not understood at this time [209]. Additionally, patients diagnosed with cervical incompetence and patients with prior history of preterm birth. Although these groups of patients do have increased risk, no causal relationship has yet been presented, indicating that multiple factors likely contribute to cause preterm birth.

5) Increased recruitment of laboring patients

With the development of the speculum-free probe, efforts should be made to significantly increase enrollment of patients during active labor. This is an important part of the cervical remodeling process that lacks a great deal of physiological understanding. In addition, patients should be grouped based on the augmentation they received during labor, and they type of augmentation may change how the cervix remodels.

6) Development of predictive models

Increasing enrollment of patients into this study offers opportunities to validate the findings of this dissertation as well as develop and evaluate predictive models estimating the probability of delivery within a given time frame. Logistic regression models that include the gestation week of the measurement can be easily implemented once the most consistent and robust features that are characteristic of impending delivery are determined. At this time, a ratio of the blood coefficient to the collagen coefficient would likely serve as a robust predictor of delivery within 2-4 weeks.

Further mining of this rich data set is likely to identify additional predictive features that can be incorporated into a "delivery time index." Such an index would further facilitate clinical translation into the clinical by offering predictive information to providers that is easily interpretable.

7) Validation of Raman spectral results

Conclusively validating findings from *in vivo* Raman spectroscopy remains a challenge due to the fundamental reason that our understanding cervical remodeling is incompletely understood: biopsy of the cervix is not feasible during pregnancy, particularly serial biopsies throughout pregnancy. This fact is what makes optical technologies so attractive; however validation of optical results must still be performed. I recommend a number of validation methods, ranging from analysis of *ex vivo* cervix tissues from women and mouse models, as well as *in vivo* validation using multiple optical modalities.

In vivo validation*:* Diffuse reflectance is an optical technique that can measure hydration and oxy- and deoxyhemoglobin based on optical absorption. Pairing Raman spectral results with diffuse reflectance will allow comparison of the water and blood signals measured in Raman spectra, and this validation can be performed throughout pregnancy.

Ex vivo validation: The ideal *ex vivo* validation would be from pregnant patients undergoing total hysterectomy for pregnancy complications. This is a rare procedure, and Vanderbilt performs ~3 cases per year. Additional hysterectomies are performed in non-pregnant patients on a much more frequent basis, and important variables such as prior obstetric history,

body mass index, and race can all be investigated using these cervix tissue samples, thus non-pregnant hysterectomies specimens should also be collected. For hysterectomy cases, Raman spectra and diffuse reflectance should be acquired from the cervix prior to surgery at multiple locations on the ectocervix, as well as immediately after the cervix is removed. The orientation of the cervix should be noted, and then put on ice. Once the tissue is brought to the lab, it should be sectioned following a protocol by Myers et al.[48]. A battery of *ex vivo* biochemical assays should then be performed. These should include standard hydroxyproline assays which will measure the collagen content, solubility, and hydration based on pre and post-lyophilized weights. Presence of blood vessels, blood vessel diameter, and blood vessel density will be imaged from hematoxylin and eosin stained slices of cervix tissue, and stains for CD31 will investigate the role of angiogenesis. The Periodic Acid-Schiff histology stain will selectively target glycogen and glycoproteins, and additional slices will be stained for actin, cholesterol, and other phospholipids of interest. Imaging mass spectrometry, a new analytical method that is being heavily investigated at the Vanderbilt Mass Spectrometry Center, has already been performed on mouse cervix tissues, and I recommend this be extended to human cervix tissues. This method allows identification of a number of proteins and lipids with high spatial resolution. Such results should be compared to adjacent tissue sections imaged using a Raman microscope to confirm that the spectral signatures match the histological and imaging mass spectrometry results. Finally, tissue sections should be imaged using the new MANTIS microscope in the Vanderbilt Biophotonics center. This instrument can perform second harmonic generation to monitor collagen structure, and stimulated and coherent anti-stokes Raman imaging to quickly obtain Raman spectral profiles over a large tissue area. These validations methods will confirm

or disprove the current interpretation of the Raman spectral results, and will likely offer new or adjusted interpretations.

7.3 Contributions to the field and societal impact

Contribution to biophotonics/clinical translation of optical technologies

This work presents the first application of Raman spectroscopy for biochemical monitoring of the cervix in pregnant women throughout pregnancy, labor, and post-partum. Through this work, we noninvasively identified multiple biochemical components including lipids, proteins, water, saccharides, and carotenoids that undergo significant change during pregnancy and post-partum, using a technique that doesn't require any exogenous labels. We are the first to report differences in cervical remodeling based on patient parity and body mass index from *in vivo* cervix tisue measurements, demonstrating the utility of this approach for improved basic science understanding.

In a mouse model of delayed parturition, *in vivo* Raman spectroscopy identified delayed cervical remodeling compared to wild type that was validated using *ex vivo* biomechanical tests and biochemical assays. This was the first report of Raman spectroscopy used for understanding cervical remodeling defects during pregnancy.

A custom deep-focused Raman spectroscopy probe was developed for optimized measurement of human cervical stroma, which increased overall signal-to-noise ratio and sensitivity to deep tissue layers. This probe was subsequently integrated into an optical probe designed for speculum-free measurement of the cervix during pregnancy. The design included a NanEye imaging camera and eska illumination fibers for visual confirmation of clean tissue and firm placement during measurements. This Raman spectroscopy probe can be used in other

applications where interrogation of deep tissue layers is desired, or for improved visualization of mesaurement locations. In addition, development of the speculum-free probe provided an important lesson on how to integrate optical technologies into the field of prenatal monitoring in Obstetrics.

Contribution to reproductive biology

In vivo Raman spectral characterization of cervical change in a mouse model of delayed parturition revealed that the absence of Cox-1 causes delayed cervical remodeling compared to wild type, which was validated using *ex vivo* assays. In addition, investigation of uterine contractility in Cox-1 KO mice led by Dr. Jen Herington discovered that Cox-1 KO mice have normal uterine contractility, rejecting the widespread belief that lack of Cox-1 causes impaired uterine contractility. Cox-1 null mice were also found to have elevated cervix progesterone levels at term, which may help explain the cervical remodeling delay.

Broadly, this work helped to educate the field of reproductive biology on emerging biophotonics techniques that can be used for basic and translational research.

Contribution to Obstetrics

As mentioned above, this dissertation is the first report utilizing *in vivo* Raman spectroscopy for study in pregnant women during pregnancy, labor, and post-partum repair. These studies revealed decresaing collagen signals and increasing blood signals as the cervix remodels towards term. In addition, post-partum studies revealed increased signals from actin, cholesterol, and glycogen, indicative of increased immune cell populations and anabolic activity driving repair. In addition, post-partum collagen signals did not return to the early pregnancy

levels as expected, indicating that cervical repair likely takes longer than six weeks. Our Obstetrics collaborators specifically stated that this method should be used to determine the recommended spacing between pregnancies to ensure the cervix is fully healed prior to a second pregnancy. This would ensure that the cervix is fully capable of maintaining its structural function throughout pregnancy.

Furthermore, parity and body mass index were found to affect cervial remodeling during pregnancy. There are few reports in the literature examining the impact of these factors on the cervix, and to our knowledge, there are no reports from *in vivo* optical technologies in this area. Our findings of increased collagen signal at the beginning of pregnancy in nulliparous women were in agreement with *ex vivo* studies which show that prior pregnancy permanently reduces collagen content and stiffness [44,169]. In high BMI patients, our observation of reduced collagen degradation is supported by outcome based studies which show longer gestation, longer labors, and increased rates of cesarean section in high BMI patients [170-174]. Our results suggest that high BMI directly reduces the extent of collagen remodeling prior to delivery, which should be considered during labor or plans of labor augmentation. Finally, the development of a speculum-free optical tool significantly reduces challenges in clinical translation for optical monitoring of the cervix during pregnancy. This approach will facilitate expedited research progress by increased enrollment rates and provider participation in cervical remodeling research using light-based methods. Long term, we hope the results from this dissertation are helpful in better understanding cervical remodeling, that they lead to increased investigation of biochemical monitoring of the cervix throughout pregnancy, labor, and repair, and potentially offer diagnostic information for clinical assessment of preterm birth risk.

APPENDIX 1

IN VIVO RAMAN SPECTRA FROM MOUSE MODELS OF PRETERM BIRTH

A1.1 Abstract

The cervix must undergo significant biochemical remodeling to allow for successful parturition. *In vivo* quantitative assessment of the cervix would be useful in identifying patients at risk of preterm labor and providing increased time for clinical intervention to delay or prevent PTB. To investigate known initiators of preterm birth, mouse models of infection-induced (lipopolysaccharide, induces delivery within 12 hours) and progesterone withdrawal-induced (RU486, induces delivery within 16 hours) PTB were compared to term wildtype mice (full gestation=19.5 days). For treated mice, Raman spectra were acquired prior to treatment on gestation day 15 and every two hours until delivery. Term controls were measured starting at noon on gestation day 19 and then every two hours until natural delivery, and negative controls were measured starting at 8 am on the morning of day 15 for a total of 10 hours. Results were analyzed using generalized estimating equations. RU486-treated mice closely mimicked the changes observed in the term controls. However, the LPS-treated mice displayed significantly different remodeling features compared to the term controls and RU486 mice in regions of the spectrum associated with ECM proteins and water content. Such information could be clinically useful for identifying patients with infection/inflammation-associated preterm labor.

A1.2 Introduction

Cervical integrity is critical for maintenance of a successful pregnancy, and all cases of spontaneous preterm birth are associated with premature cervical remodeling [57]. Cervical remodeling during pregnancy and labor is poorly understood [119], partly due to the lack of *in vivo* investigations aimed at tracking the physiological and biochemical changes that occur in the cervix. As cervical remodeling is required for any successful delivery, elucidating the mechanisms that lead to cervical ripening would provide insight for the development of new treatment options.

Preterm birth is known to have a variety of causes [24], including but not limited to infection, stress, cervical disease, reduced progesterone signaling, and uterine overdistension. Proper etiologic diagnosis is critical for optimium management of preterm labor [57], which likely explains why therapeutic approaches to delay preterm birth are successful for some patients but not others. *Ex vivo* studies in animal models of preterm birth have determined that cervical remodeling may occur differently depending upon the cause [57-61]. Two mouse models of preterm birth have been thoroughly investigated and compared to cervical remodeling at term gestation in wild type (WT) mice.The first treatment model uses lipopolysaccharide (LPS), endotoxins found in the cell wall of Gram-negative bacteria, on day 15 in WT mice to illicit an inflammatory response and cause preterm birth [57,61]. The second treatment model uses subcutaneous injection of mifepristone (RU486, 0.5 mg/200μL solubilized in ethanol) in day 15 WT mice, which acts as a progesterone receptor antagonist, resulting in preterm birth within 13-16 hours [57,58,61]. Mice treated with LPS showed significant signs of inflammation, including increased neutrophils [57], macrophages [61], increased expression of proinflammatory genes (interleukin 6, tumor necrosis factor, Cox-2), and upregulation of cytokines and matrix metalloproteinases [57,58,61,62]; however

progesterone levels reamined high throughout labor and parturition [62] and water content did not change [57]. RU486 treated mice showed signs of expedited term delivery, including decreased progesterone levels, increased tissue wet weight [57], an increase in monocytes [57], with partial upregulation of inflammatory pathways including Cox-1, inflammatory gene interleukin 1 alpha, as well as MMP-8, and Adamts1 & 4. These differences provide a diagnostic opportunity for determining the cause of preterm labor so that targeted treatment can be developed.

A successful diagnostic test must be sensitive to the distinct cervical remodeling features found in LPS and RU486 treated mice without destruction of any tissue. Nearly all published results of PTB mouse model experiments were conducted on excised cervical tissue after sacrifice of the animal. Therefore innovative approaches that can non-invasively probe tissue biochemistry are needed. Optical approaches are well suited to meet these criteria. Multiple methods provide non-invasive monitoring of one or two biochemical components such as collagen content or cross-links, however one method termed Raman spectroscopy is capable of probing a large range of biochemicals including lipids, extracellular matrix proteins, blood, sacharides, carotenoids, and nucleic acids. This technique is sensitive to chemical bond-specific vibrations, resulting in each biomolecule having a unique molecular “fingerprint”. This methods has been successfully applied to the monitoring of cervical remodeling in animal models and human patients during pregnancy, demonstrating its potential for clinical translation.

The goal of this study is to characterize the Raman spectra from the cervix of LPS and RU486 treated pregnant mice in order to establish the potential of this method for discriminating between different preterm labor etiologies. While the mouse model is an imperfect replicate of human pregnancy, it will allow us to study the entire course of pregnancy and labor in a shortened time frame (mouse gestation is 19-21 days, depending on model), as well as

thoroughly analyze the cervix of abnormal pregnancy models *in vivo* and *ex vivo*. By comparing normal WT mouse pregnancy with various models of preterm cervical ripening and delayed cervical ripening, the underlying biochemical differences can be interrogated via Raman spectral features.

A1.3 Methods

Animals

Mice were housed under a 12h light cycle. Timed matings were carried out by placing one male with three females. At the same time each morning, females were evaluated for the presence of a post-copulatory plug, which defined gestation day 1 of a 19.5 day gestation.

The LPS-induced preterm birth mouse model was created by administration of LPS (055:B5, Sigma, St. Louis, MO) via intraperitoneal injection (100 μg/5 μL in PBS) in WT mice on the morning of day 15. Raman spectra were taken prior to the administration of LPS, and every two hours after injection until 8 hours passed afterwhich the mouse was sacrificed for *ex vivo* biomechanical testing of the cervix (n=5), or until the delivery of the first pup (n=10) (Figure A1.1).

The progesterone withdrawal-induced preterm birth mouse model was created by subcutaneous injection of RU-486 (Mifepristone, 500μg in triolene) on day 15 (n=8) to induce labor. Raman spectra were taken prior to the administration of the drug, and every two hours after administration until 12 hours passed afterwhich the mouse was sacrificed for *ex vivo* biomechanical testing (n=5), or until delivery of the first pup (n=10) (Figure A1.1).

Wild type mice were measured on the morning of day 15 and every two hours for a total of 12 hours in order to serve as a negative control. To characterize term labor, Raman spectra

were measured from the cervix of WT mice beginning at noon on day 19 of pregnancy, and were measured every two hours until delivery of the first pup (Figure A1.1).

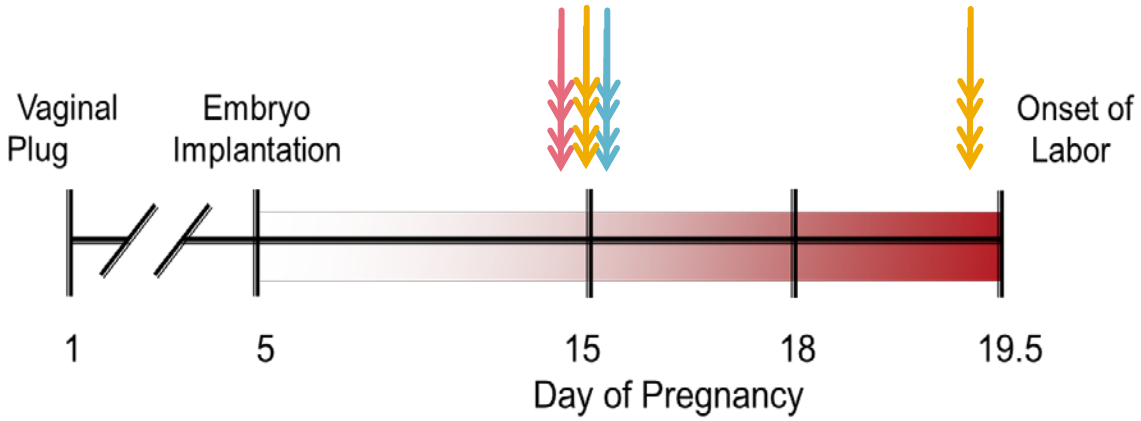

Figure A1.1. Schematic delineating the time points of mouse pregnancy measured in WT (gold), LPS treated (pink), and RU486-treated (blue).

Raman spectral acquisition

The following protocol was used to obtain Raman spectra from the mouse cervix: first the mouse was anesthetized by exposure to isofluorane, after which the mouse vagina and cervix were gently rinsed with saline. A 3-5 mm diameter speculum was inserted into the vagina in order to visualize the cervix (Figure A1.2B). The 2 mm diameter fiber optic probe tip was gently inserted into the mouse vagina and lightly pressed against the cervix for approximately 3-5 seconds to take one Raman measurement. Because this is real-time imaging, signal interference by vaginal secretions or misplacement of the probe tip onto the vaginal wall can be easily recognized and repeat measurements obtained. This protocol was repeated three times at each data collection time point.

A. Illustration of sample orientation for Raman measurements

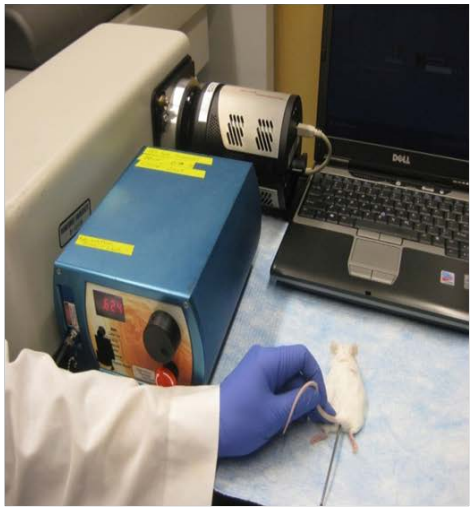

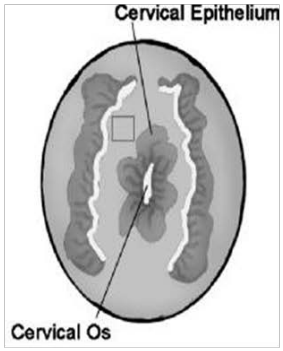

B. Mouse Cervix

from: PMCID: PMC2874049

Figure A1.2. A) Raman fiber optic probe-based system used for mouse experiments. B) Illustration of the mouse cervix and a picture taken of a mouse cervix revealed using a speculum.

Biomechanical testing

After completing the treatment incubation time, mice were sacrificed using overdose of isofluorane and subsequent cervical dislocation. The cervix was immediately dissected out and placed in 37 C oxygenated Krebs buffer. An 8-chamber Radnotti isometric force transduction system was employed to obtain biomechanical measurements. Briefly, the excised cervix was mounted on two stainless steel hooks, one that was fixed, and another that was attached to a mechanical drive providing consistent strain rates and measuring tension using a force transducer. The cervix was stretched in 1 mm every four minutes, during which the tension experienced by the tissue was recorded [138]. Biomechanical testing was used as the standard to stage cervical remodeling [210]. Stress-strain relationships in the toe region, elastic region, yield point (indicative of the structural shift point from elastic-to-plastic phases), break point (tissue failure under tension), and other mechanical properties were determined [144]. Using an effect size

calculated from previous studies, it was determined 5 mice /group would be required to achieve statistical significance.

Data processing and analysis

Raman spectra were calibrated and processed as previously described [2,138]. To minimize spectral cntribution from fat, spectra with a 1440 cm^{-1} peak intensity above 999 wree excluded from analysis, and spectra with counts below 599 were excluded due to signal to noise ratio deterioration. Raman spectra were modeled over the course of labor using a restricted cubic spline with 65 degrees of freedom. Treatment group (day 15 LPS, day 15 RU-486, and day 19 untreated) was included as a model variable, and the spectral changes for each group were plotted separately for comparison.

A1.4 Results

Raman spectra collected over the course of labor

Raman spectra were successfully acquired from the cervix of laboring pregnant mice using a fiber optic probe based Raman spectroscopy system. Measurements were acquired in two hour increments until delivery of the first pup from four cohorts of mice: WT day 15 mice treated with vehicle (served as negative control), WT day 15 mice treated with RU486, WT day 15 mice treated with LPS, and WT day 19 mice. The delivery time of each mouse was recorded, and the time until delivery associated with each set of Raman measurements was calculated.

Spectral models were developed for each group and plotted as a function of hours until delivery (Figure A1.3). In the term group, spectral narrowing as the mice neared delivery was observed in the right shoulder of the 1304 cm^{-1} peak, possibly caused by transition to primarily

lipid contributions. There was reduced signal in the 1003 cm^{-1} phenylalanine peak, consistent with decreasing contribution from extracellular matrix proteins. In the RU486 treated tissues, there appeared to be increased signal from the right shoulder of the 1304 cm^{-1} peak, in constrast to what was observed at term. In addition, peak intensities at 1440 and 1657 cm^{-1} decreased prior to delivery, whereas the 1003 cm^{-1} peak increased, opposite of that observed on day 19. In LPS-treated tissues, narrowing of the 1304 cm^{-1} right shoulder and 1657 cm^{-1} right shoulder was observed, similar to term. Unique to LPS-treated tissues, the intensity of the 1570-1630 band significantly decreased, and the narrow 1304, 1440, and 1657 cm^{-1} peaks increased prior to delivery.

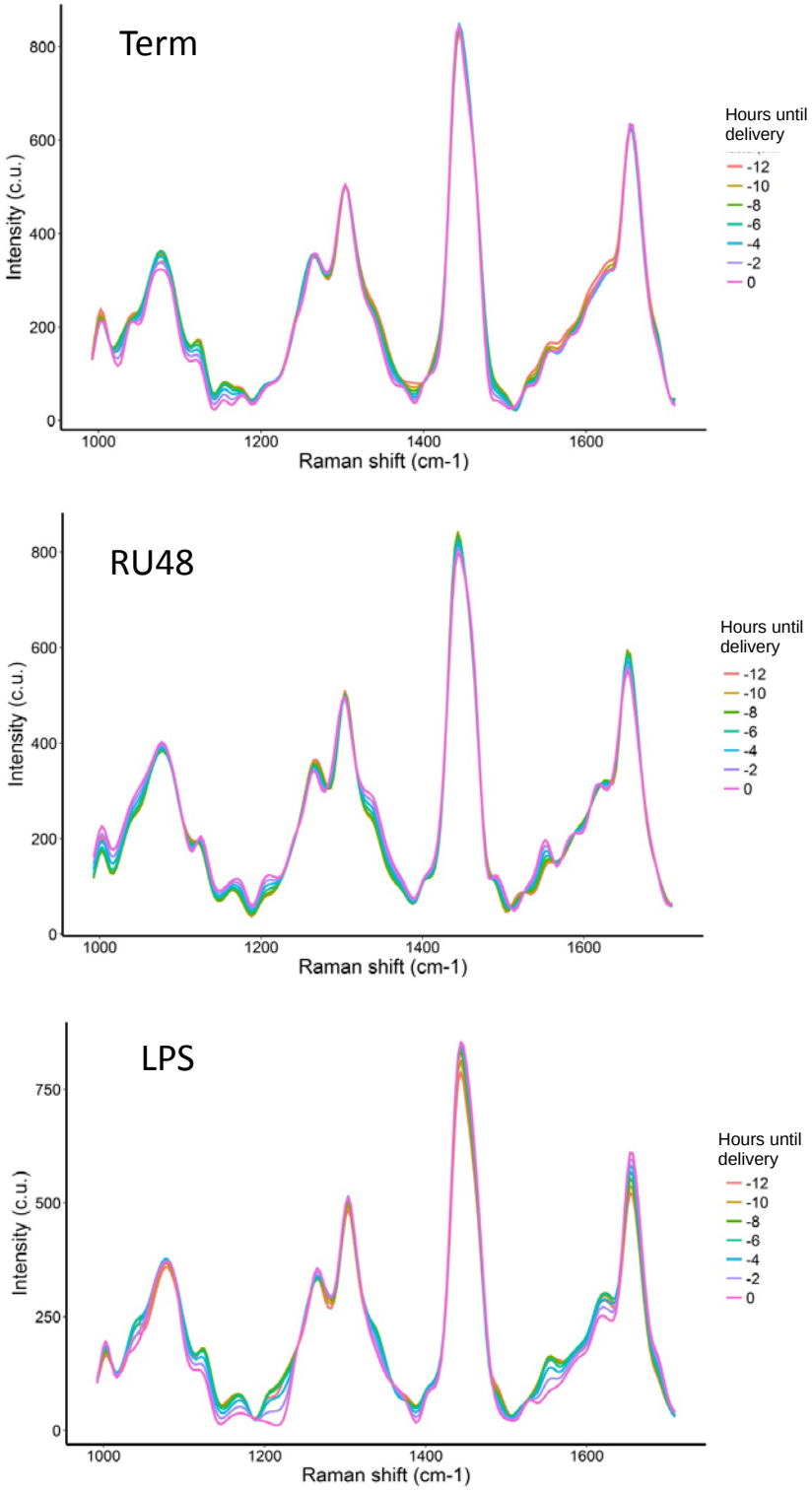

Figure A1.3. Longitudinal analysis of Raman peak ratios over the course of labor in term wild type (WT), LPS-treated day 15 (LPS), and RU486-treatedy day 15 (RU486) pregnant mice. (n=10 per group)

Biomechanics of cervical tissues

A separate cohort of mice were used for biomechanical testing. Similar to the Raman experiment, four groups were tested: WT d15 treated with vehicle for 12 hours, WT day 15 treated with RU486 for 12 hours, WT day 15 treated with LPS for 8 hours, and WT day 19 untreated. Tension measured in grams was plotted against displacement for each mouse cervix tested, and the mean result for each group is displayed in Figure A1.4. The vehicle-treated WT day 15 curve reveals that the cervix tissue became stressed at a much lower displacement compared to the LPS, RU486, and day 19 groups. In addition, the vehicle treated day 15 group had a lower total displacement achieved prior to tissue failure compared to the other three groups. The day 19 group experiences the least amount of tension at any given displacement, and exhibited the highest level of tissue distensibility.

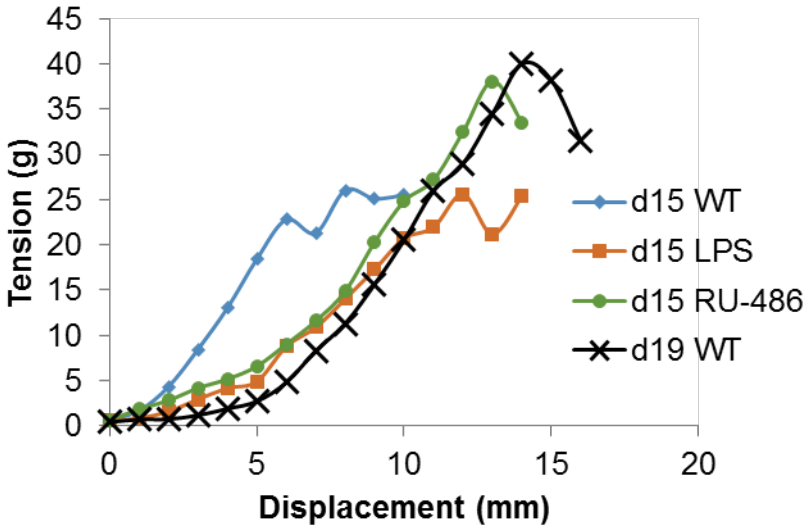

Figure A1.4. Biomechanics results from untreated day 15 WT (n=9), LPS- treated day 15 (n=5), RU486-treated day 15 (n=5), and day 19 WT mouse cervix tissues (n=5).

A1.5 Discussion

The physiology governing cervical remodeling during pregnancy is not fully understood, especially during the transition between ripening and dilation phases. This is further complicated by studies demonstrating that cervical remodeling at term follows distinct pathways and mechanisms compared to preterm, which can be caused by multiple factors that also have unique remodeling physiology. Noninvasive measurement of cervical remodeling during labor has the potential to unveil fundamental physiology that has not yet been observed. In addition, the high rate of change in the cervix throughout the ripening and dilation stages limits the usefulness of measurements taken at a single time point. In the studies presented, a biochemically specifically technique has been used to longitudinally measure the cervix during labor in term and preterm pregnant mouse models. Distinct spectral characteristics were observed in LPS treated, RU486 treated, term mice, demonstrating feasibility of this technique to measure biochemical changes in the cervix of labor mice and distinguish between inflammation-induced and progesterone withdrawal-induced cervical remodeling.

In the Raman spectral models, term mice appeared to undergo the least amount of remodeling in preparation for delivery. The changes observed are attributed to decreased signals from extracellular matrix proteins prior to delivery . As these mice have an additional 4 days to prepare, it is not surprising that the spectral changes were not as dramatic as those seen in the preterm groups. The decreasing lipid contribution and increasing protein contribution observed in RU486 treated mice may be explained by increased collagen synthesis contributing to the increased tissue wet weight observed by Holt et al. [57]. LPS treated tissues had increased lipid contribution prior to delivery, possibly caused by increased levels of prostaglandins and inflammatory cells, resulting in overall higher lipid signals.

Ex vivo biomechanics results confirmed that the RU486 and LPS treatment significantly increased cervix distensibility compared to untreated day 15 tissues, allowing successful passage of pups. These results are similar to those observed by Timmons et al., in which LPS and RU486 treated mouse cervix tissues were significantly more compliant than untreated day 15 controls [211].

The major limitation of this study stems from the high contribution of adipose tissue overwhelming many of the Raman spectra collected from these mice over the course of labor. Multiple fat pads, including inguinal, perigonadal, and lower pelvic fat pads, surround the cervix, and so although the cervix itself is not lipid rich, a large lipid signal is detected from these fat pads deep within the tissue [2,146]. Due to this problem, a large amount of data had to be excluded, limiting the spectra available for analysis. To combat this problem, a new Raman spectroscopy probe is being tested that is designed to selectively collect signal from superficial depths (1-2 mm) and exclude signals originating from adipose tissues surrounding the cervix at greater depths.

Despite contaminant adipose signal contributions to Raman spectra, distinct remodeling features were observed in LPS-treated, RU486-treated, and term mouse cervices in preparation for delivery. Raman spectra were acquired *in vivo* without destruction of tissue, and enabled longitudinal tracking of a single mouse throughout the course of labor. These results having exciting implications for clinical translation, where understanding the etiology of preterm labor would improve patient management. In concludion, *n vivo* Raman spectroscopy has demonstrated its utility as a tool for investigation of cervical remodeling during normal and high risk pregnancy, and has high clinical translation potential for monitoring cervical remodeling in pregnant women.

APPENDIX 2

SUPPLEMENTAL FIGURES FROM CHAPTER 3

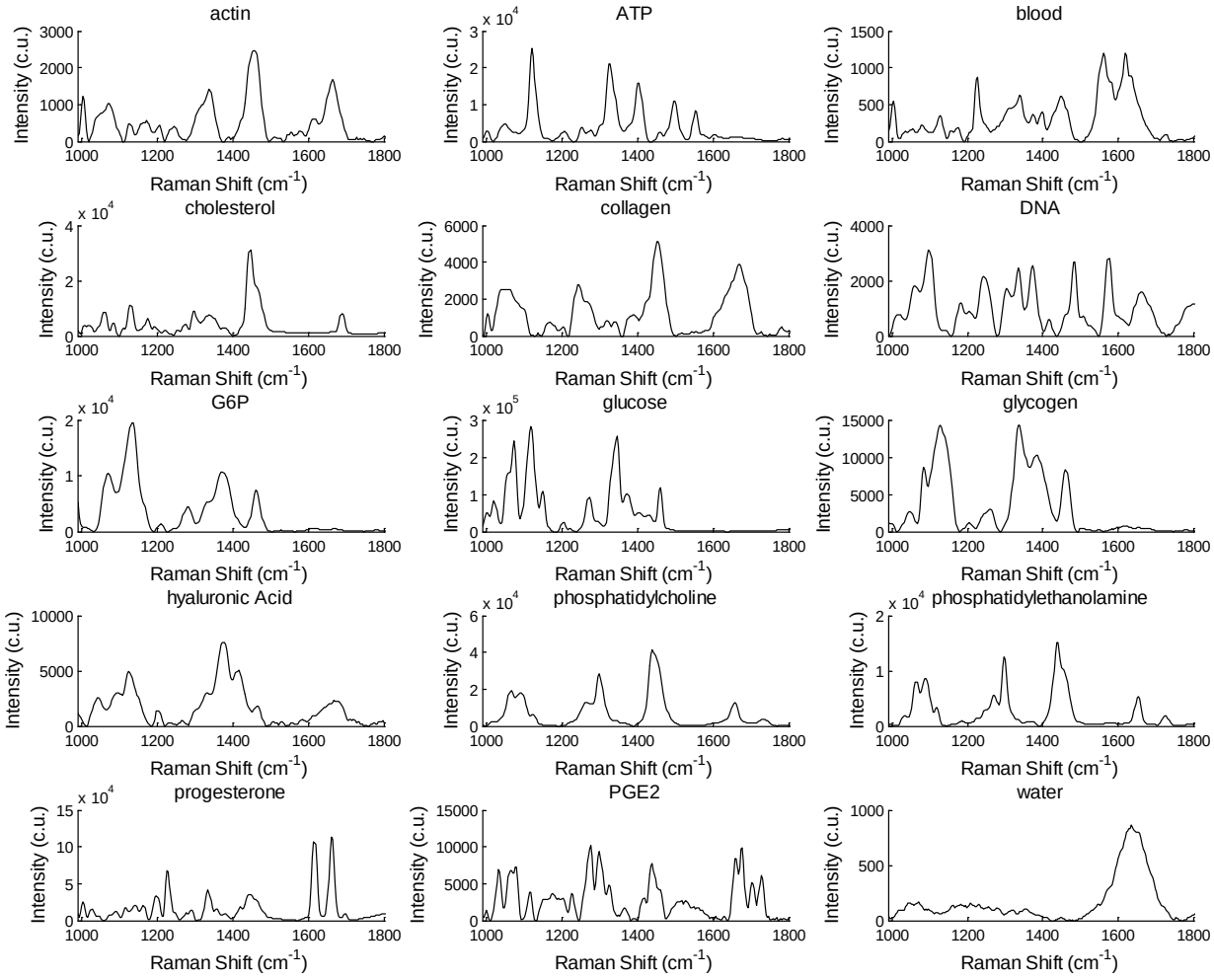

Supplemental Figure 1. Raman spectra of pure chemicals that were evaluated as potential least squares model inputs.

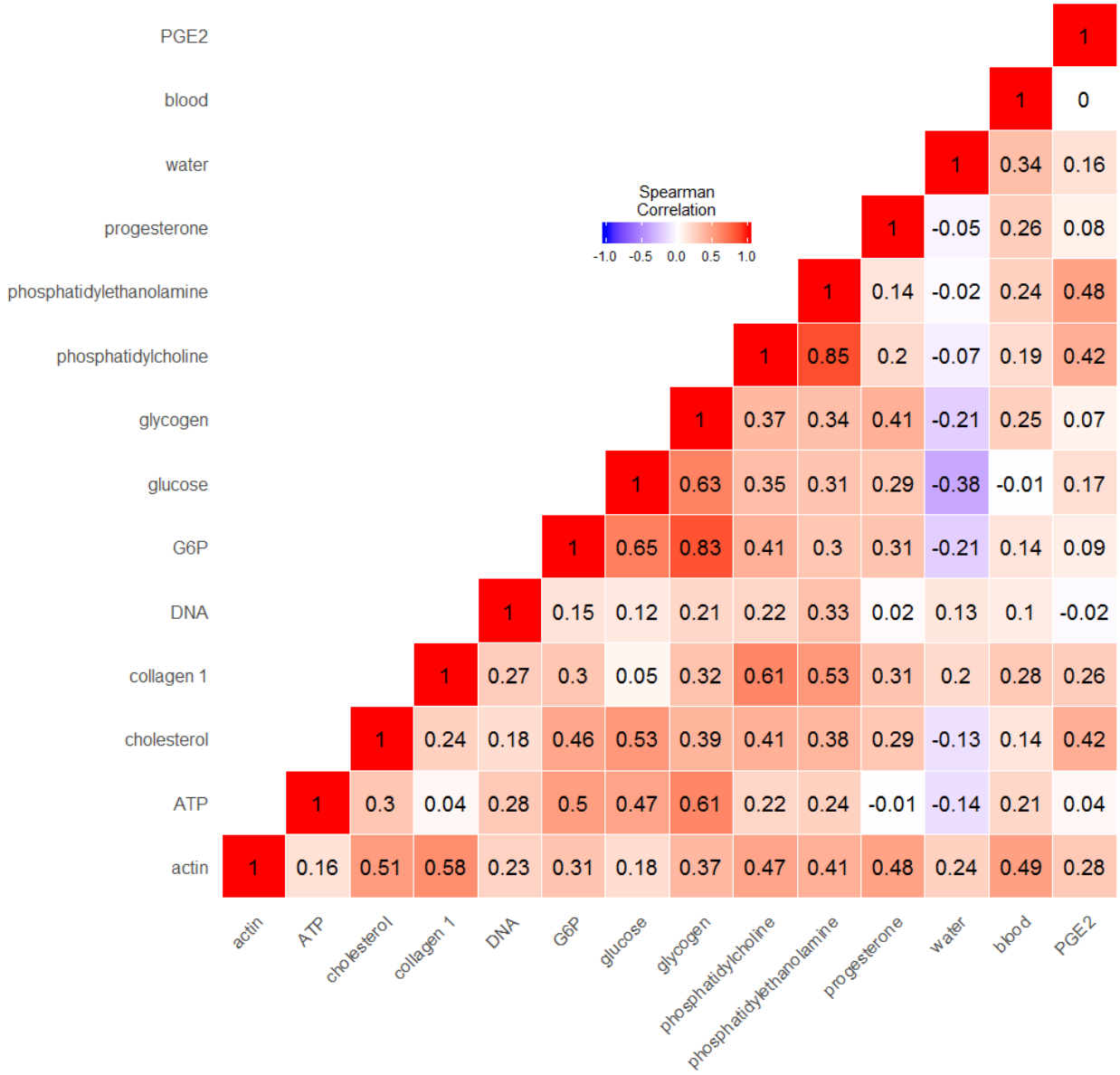

Supplemental Figure 2. Correlation coefficient matrix comparing similarity between pure chemical Raman spectra.

REFERENCES

1. O'Brien CM, Vargis E, Paria BC, Bennett KA, Mahadevan-Jansen A, Reese J. Raman spectroscopy provides a noninvasive approach for determining biochemical composition of the pregnant cervix in vivo. *Acta Paediatr.* 2014;103(7):715-721.
2. O'Brien CM, Herington JL, Brown N, et al. In vivo Raman spectral analysis of impaired cervical remodeling in a mouse model of delayed parturition. *Scientific reports.* 2017;7(1):6835.
3. Blencowe H, Cousens S, Chou D, et al. Born Too Soon: The global epidemiology of 15 million preterm births. *Reproductive Health.* 2013;10(Suppl 1):1.
4. Martin JA, Hamilton BE, Osterman MJ, Curtin SC, Matthews TJ. Births: final data for 2013. *Natl Vital Stat Rep.* 2015;64(1):1-65.
5. Healthcare C, Utilization P. HCUP Facts and Figures. *HCUP Facts and Figures: Statistics on Hospital-Based Care in the United States, 2005*. Rockville (MD): Agency for Healthcare Research and Quality (US); 2007.
6. Behrman RE, Butler AS. *Preterm birth: causes, consequences, and prevention.* National Academies Press; 2006.
7. ACOG Committee Opinion No 579: Definition of term pregnancy. *Obstet Gynecol.* 2013;122(5):1139-1140.
8. Menon R. Spontaneous preterm birth, a clinical dilemma: etiologic, pathophysiologic and genetic heterogeneities and racial disparity. *Acta Obstet Gynecol Scand.* 2008;87(6):590-600.
9. Ruiz RJ, Fullerton J, Dudley DJ. The interrelationship of maternal stress, endocrine factors and inflammation on gestational length. *Obstetrical & gynecological survey.* 2003;58(6):415-428.
10. Robinson JN, Regan JA, Norwitz ER. The epidemiology of preterm labor. Paper presented at: Seminars in Perinatology2001.
11. Macdonald PC, Gant NF, Leveno KJ, Gilstrap LC, Hankins G, Clark SL. *Williams Obstetrics 20th Edition.* Appleton & Lange; 1996.
12. Di Renzo GC, Al Saleh E, Mattei A, Koutras I, Clerici G. Use of tocolytics: what is the benefit of gaining 48 hours for the fetus? *BJOG : an international journal of obstetrics and gynaecology.* 2006;113 Suppl 3:72-77.
13. Hacker NF, Gambone JC, Hobel CJ. *Hacker & Moore's Essentials of Obstetrics and Gynecology.* Saunders; 2009.
14. Iams JD. Prediction and early detection of preterm labor. *Obstetrics & Gynecology.* 2003;101(2):402-412.
15. Catalano PM, Ashikaga T, Mann LI. Cervical change and uterine activity as predictors of preterm delivery. *American journal of perinatology.* 1989;6(02):185-190.
16. Lee HJ, Park TC, Norwitz ER. Management of pregnancies with cervical shortening: a very short cervix is a very big problem. *Reviews in Obstetrics and Gynecology.* 2009;2(2):107.
17. Moroz LA, Simhan HN. Rate of sonographic cervical shortening and the risk of spontaneous preterm birth. *Am J Obstet Gynecol.* 2012;206(3):234. e231-234. e235.

18. Hezelgrave NL, Abbott DS, Radford SK, et al. Quantitative Fetal Fibronectin at 18 Weeks of Gestation to Predict Preterm Birth in Asymptomatic High-Risk Women. *Obstet Gynecol.* 2016;127(2):255-263.
19. Chaemsaithong P, Romero R, Korzeniewski SJ, et al. A rapid interleukin-6 bedside test for the identification of intra-amniotic inflammation in preterm labor with intact membranes. *The Journal of Maternal-Fetal & Neonatal Medicine.* 2016;29(3):349-359.
20. Combs CA, Gravett M, Garite TJ, et al. Amniotic fluid infection, inflammation, and colonization in preterm labor with intact membranes. *Am J Obstet Gynecol.* 2014;210(2):125.e121-125.e115.
21. Chaemsaithong P, Romero R, Korzeniewski SJ, et al. A point of care test for interleukin-6 in amniotic fluid in preterm prelabor rupture of membranes: a step toward the early treatment of acute intra-amniotic inflammation/infection. *The journal of maternal-fetal & neonatal medicine,* 2016;29(3):360-367.
22. Heng YJ, Liong S, Permezel M, Rice GE, Di Quinzio MKW, Georgiou HM. Human cervicovaginal fluid biomarkers to predict term and preterm labor. *Frontiers in Physiology.* 2015;6(151).
23. DeFranco EA, Lewis DF, Odibo AO. Improving the screening accuracy for preterm labor: is the combination of fetal fibronectin and cervical length in symptomatic patients a useful predictor of preterm birth? A systematic review. *Am J Obstet Gynecol.* 2013;208(3):233.e231-233.e236.
24. Romero R, Dey SK, Fisher SJ. Preterm Labor: One Syndrome, Many Causes. *Science.* 2014;345(6198):760-765.
25. Okitsu O, Mimura T, Nakayama T, Aono T. Early prediction of preterm delivery by transvaginal ultrasonography. *Ultrasound in Obstetrics & Gynecology.* 1992;2(6):402-409.
26. Salomon LJ, Diaz-Garcia C, Bernard JP, Ville Y. Reference range for cervical length throughout pregnancy: non-parametric LMS-based model applied to a large sample. *Ultrasound in Obstetrics and Gynecology.* 2009;33(4):459-464.
27. Ludmir J, Sehdev HM. Anatomy and physiology of the uterine cervix. *Clinical Obstetrics and Gynecology.* 2000;43(3):433-439.
28. Nott JP, Bonney EA, Pickering JD, Simpson NAB. The structure and function of the cervix during pregnancy. *Translational Research in Anatomy.* 2016;2:1-7.
29. Leppert PC. Anatomy and physiology of cervical ripening. *Clinical Obstetrics and Gynecology.* 1995;38(2):267-279.
30. Hughesdon PE. The fibromuscular structure of the cervix and its changes during pregnancy and labour. *The Journal of obstetrics and gynaecology of the British Empire.* 1952;59(6):763-776.
31. Vink JY, Qin S, Brock CO, et al. A new paradigm for the role of smooth muscle cells in the human cervix. *Am J Obstet Gynecol.* 2016;215(4):478.e471-478.e411.
32. Yoshida K, Jiang H, Kim M, et al. Quantitative Evaluation of Collagen Crosslinks and Corresponding Tensile Mechanical Properties in Mouse Cervical Tissue during Normal Pregnancy. *PloS one.* 2014;9(11):e112391.
33. Bornstein P, Sage EH. Matricellular proteins: extracellular modulators of cell function. *Curr Opin Cell Biol.* 2002;14(5):608-616.

34. Kokenyesi R, Armstrong LC, Agah A, Artal R, Bornstein P. Thrombospondin 2 Deficiency in Pregnant Mice Results in Premature Softening of the Uterine Cervix. *Biology of Reproduction.* 2004;70(2):385-390.
35. Timmons B, Akins ML, Mahendroo M. Cervical Remodeling during Pregnancy and Parturition. *Trends Endocrinolog Metab.* 2010;21.
36. Akgul Y, Mahendroo M. Cervical changes accompanying birth. *The Guide to Investigation of Mouse Pregnancy.* 2013:391.
37. Myers K, Socrate S, Tzeranis D, House M. Changes in the biochemical constituents and morphologic appearance of the human cervical stroma during pregnancy. *European Journal of Obstetrics & Gynecology and Reproductive Biology.* 2009;144:S82-S89.
38. Asplund J. The uterine cervix and isthmus under normal and pathological conditions; a clinical and roentgenological study. *Acta Radiol Suppl.* 1952;91:1-76.
39. Nallasamy S, Yoshida K, Akins M, Myers K, Iozzo R, Mahendroo M. Steroid Hormones Are Key Modulators of Tissue Mechanical Function via Regulation of Collagen and Elastic Fibers. *Endocrinology.* 2017;158(4):950-962.
40. Herington JL, O'Brien C, Robuck MF, et al. Prostaglandin-endoperoxide synthase 1 (Ptgs1) mediates the timing of parturition in mice despite unhindered uterine contractility. *Endocrinology.* 2017:en.2017-00647-en.02017-00647.
41. Downing S, Sherwood O. The physiological role of relaxin in the pregnant rat. III. The influence of relaxin on cervical extensibility. *Endocrinology.* 1985;116(3):1215-1220.
42. Sherwood OD. Relaxin's physiological roles and other diverse actions. *Endocr Rev.* 2004;25(2):205-234.
43. Word RA, Li X-H, Hnat M, Carrick K. Dynamics of cervical remodeling during pregnancy and parturition: mechanisms and current concepts. Paper presented at: Seminars in reproductive medicine, 2007.
44. Myers KM, Paskaleva A, House M, Socrate S. Mechanical and biochemical properties of human cervical tissue. *Acta Biomaterialia.* 2008;4(1):104-116.
45. House M, Kaplan DL, Socrate S. Relationships Between Mechanical Properties and Extracellular Matrix Constituents of the Cervical Stroma During Pregnancy. *Seminars in Perinatology.* 2009;33(5):300-307.
46. Akins ML, Luby-Phelps K, Bank RA, Mahendroo M. Cervical softening during pregnancy: regulated changes in collagen cross-linking and composition of matricellular proteins in the mouse. *Biology of Reproduction.* 2011;84(5):1053-1062.
47. Rechberger T, Uldbjerg N, Oxlund H. Connective tissue changes in the cervix during normal pregnancy and pregnancy complicated by cervical incompetence. *Obstet Gynecol.* 1988;71(4):563-567.
48. Myers KM, Socrate S, Paskaleva A, House M. A study of the anisotropy and tension/compression behavior of human cervical tissue. *Journal of Biomechanical Engineering.* 2010;132(2):021003-021003.
49. Read C, Word A, Ruscheinsky M, Timmons B, Mahendroo M. Cervical remodeling during pregnancy and parturition: molecular characterization of the softening phase in mice. *Reproduction.* 2007;134.
50. Straach KJ, Shelton JM, Richardson JA, Hascall VC, Mahendroo MS. Regulation of hyaluronan expression during cervical ripening. *Glycobiology.* 2005;15(1):55-65.

51. Akgul Y, Holt R, Mummert M, Word A, Mahendroo M. Dynamic changes in cervical glycosaminoglycan composition during normal pregnancy and preterm birth. *Endocrinology.* 2012;153(7):3493-3503.
52. Timmons BC, Mahendroo MS. Timing of neutrophil activation and expression of proinflammatory markers do not support a role for neutrophils in cervical ripening in the mouse. *Biol Reprod.* 2006;74(2):236-245.
53. Timmons BC, Fairhurst AM, Mahendroo MS. Temporal changes in myeloid cells in the cervix during pregnancy and parturition. *J Immunol.* 2009;182(5):2700-2707.
54. Sakamoto Y, Moran P, Bulmer JN, Searle RF, Robson SC. Macrophages and not granulocytes are involved in cervical ripening. *J Reprod Immunol.* 2005;66(2):161-173.
55. Timmons BC, Mahendroo M. Processes regulating cervical ripening differ from cervical dilation and postpartum repair: insights from gene expression studies. *Reproductive sciences.* 2007;14(8 Suppl):53-62.
56. Hassan SS, Romero R, Haddad R, Hendler I, Khalek N, Tromp G. The transcriptome of the uterine cervix before and after spontaneous term parturition. *Am J Obstet Gynecol.* 2006;195.
57. Holt R, Timmons BC, Akgul Y, Akins ML, Mahendroo M. The molecular mechanisms of cervical ripening differ between term and preterm birth. *Endocrinology.* 2011;152(3):1036-1046.
58. Gonzalez JM, Xu H, Chai J, Ofori E, Elovitz MA. Preterm and term cervical ripening in CD1 mice (Mus musculus): similar or divergent molecular mechanisms? *Biology of Reproduction.* 2009;81(6):1226-1232.
59. Hirsch E, Filipovich Y, Mahendroo M. Signaling via the type I IL-1 and TNF receptors is necessary for bacterially induced preterm labor in a murine model. *Am J Obstet Gynecol.* 2006;194(5):1334-1340.
60. Gonzalez JM, Romero R, Girardi G. Comparison of the mechanisms responsible for cervical remodeling in preterm and term labor. *J Reprod Immunol.* 2013;97(1):112-119.
61. Gonzalez JM, Franzke CW, Yang F, Romero R, Girardi G. Complement activation triggers metalloproteinases release inducing cervical remodeling and preterm birth in mice. *Am J Pathol.* 2011;179(2):838-849.
62. Gonzalez JM, Dong Z, Romero R, Girardi G. Cervical remodeling/ripening at term and preterm delivery: the same mechanism initiated by different mediators and different effector cells. *PLoS One.* 2011;6(11):e26877.
63. Iams JD, Goldenberg RL, Meis PJ, et al. The length of the cervix and the risk of spontaneous premature delivery. *New England Journal of Medicine.* 1996;334(9):567-573.
64. Sotiriadis A, Papatheodorou S, Kavvadias A, Makrydimas G. Transvaginal cervical length measurement for prediction of preterm birth in women with threatened preterm labor: a meta-analysis. *Ultrasound in Obstetrics and Gynecology.* 2010;35(1):54-64.
65. Feltovich H, Hall T, Berghella V. Beyond cervical length: emerging technologies for assessing the pregnant cervix. *Am J of Obstet and Gynecol.* 2012;07.
66. Jokhi R, Brown B, Anumba D. The role of cervical Electrical Impedance Spectroscopy in the prediction of the course and outcome of induced labour. *BMC Pregnancy and Childbirth.* 2009;9(1):40.

67. McFarlin B, Bigelow T, Laybed Y, O'Brien W, Oelze M, Abramowicz J. Ultrasonic attenuation estimation of the pregnant cervix: a preliminary report. *Ultrasound in Obstetrics & Gynecology.* 2010;36(2):218-225.
68. Feltovich H, Nam K, Hall TJ. Quantitative ultrasound assessment of cervical microstructure. *Ultrasonic Imaging.* 2010;32(3):131-142.
69. Swiatkowska-Freund M, Preis K. Elastography of the uterine cervix: implications for success of induction of labor. *Ultrasound in Obstetrics & Gynecology.* 2011;38(1):52-56.
70. Badir S, Mazza E, Zimmermann R, Bajka M. Cervical softening occurs early in pregnancy: characterization of cervical stiffness in 100 healthy women using the aspiration technique. *Prenatal diagnosis.* 2013:1-6.
71. Anthony GS, Walker RG, Robins JB, Cameron AD, Calder AA. Management of cervical weakness based on the measurement of cervical resistance index. *European Journal of Obstetrics & Gynecology and Reproductive Biology.* 2007;134(2):174-178.
72. Myers K, Ateshian GA. Interstitial growth and remodeling of biological tissues: Tissue composition as state variables. *Journal of the mechanical behavior of biomedical materials.* 2013.
73. Maul H, Saade G, Garfield RE. Prediction of term and preterm parturition and treatment monitoring by measurement of cervical cross-linked collagen using light-induced fluorescence. *Acta Obstetricia et Gynecologica Scandinavica.* 2005;84(6):534-536.
74. Maul H, Olson G, Fittkow CT, Saade GR, Garfield RE. Cervical light-induced fluorescence in humans decreases throughout gestation and before delivery: preliminary observations. *Am J of Obstet and Gynecol.* 2003;188(2):537-541.
75. Schlembach D, MacKay L, Shi L, Maner WL, Garfield RE, Maul H. Cervical ripening and insufficiency: From biochemical and molecular studies to in vivo clinical examination. *European Journal of Obstetrics & Gynecology and Reproductive Biology.* 2009;144, Supplement 1(0):S70-S76.
76. Zhang Y, Akins ML, Murari K, et al. A compact fiber-optic SHG scanning endomicroscope and its application to visualize cervical remodeling during pregnancy. *Proc Natl Acad Sci U S A.* 2012;109(32):12878-12883.
77. Reusch LM, Feltovich H, Carlson LC, et al. Nonlinear optical microscopy and ultrasound imaging of human cervical structure. *J Biomed Opt.*. 2013;18(3):031110-031110.
78. Baños A, Wolf M, Grawe C, et al. Frequency domain near-infrared spectroscopy of the uterine cervix during cervical ripening. *Lasers in Surgery and Medicine.* 2007;39(8):641-646.
79. Hornung R, Spichtig S, Baños A, Stahel M, Zimmermann R, Wolf M. Frequency-domain near-infrared spectroscopy of the uterine cervix during regular pregnancies. *Lasers in medical science.* 2011;26(2):205-212.
80. Crow P, Molckovsky A, Stone N, Uff J, Wilson B, Wongkeesong L-M. Assessment of fiberoptic near-infrared Raman spectroscopy for diagnosis of bladder and prostate cancer. *Urology.* 2005;65(6):1126-1130.
81. Grimbergen M, van Swol C, van Moorselaar R, Uff J, Mahadevan-Jansen A, Stone N. Raman spectroscopy of bladder tissue in the presence of 5-aminolevulinic acid. *Photochem Photobiol.* 2009;95(3):170-176.
82. Barr H, Kendall C, Bazant-Hegemark F, Moayyedi P, Shetty G, Stone N. Endoscopic Screening and Surveillance for Barrett's Esophagus–Clinical Implications. *Medscape General Medicine.* 2006;8(2):88.

83. Shetty G, Kendall C, Shepherd N, Stone N, Barr H. Raman spectroscopy: elucidation of biochemical changes in carcinogenesis of oesophagus. *British journal of cancer.* 2006;94(10):1460-1464.
84. Chrit L, Bastien P, Sockalingum G, et al. An in vivo randomized study of human skin moisturization by a new confocal Raman fiber-optic microprobe: assessment of a glycerol-based hydration cream. *Skin pharmacology and physiology.* 2006;19(4):207-215.
85. Sigurdsson S, Philipsen PA, Hansen LK, Larsen J, Gniadecka M, Wulf H-C. Detection of skin cancer by classification of Raman spectra. *Biomedical Engineering, IEEE Transactions on.* 2004;51(10):1784-1793.
86. Haka AS, Shafer-Peltier KE, Fitzmaurice M, Crowe J, Dasari RR, Feld MS. Diagnosing breast cancer by using Raman spectroscopy. *Proc Natl Acad Sci U S A.* 2005;102(35):12371-12376.
87. Bergholt MS, Zheng W, Lin K, et al. Characterizing variability in in vivo Raman spectra of different anatomical locations in the upper gastrointestinal tract toward cancer detection. *J Biomed Opt.*. 2011;16(3):037003-037003-037010.
88. Mahadevan-Jansen A, Mitchell MF, Ramanujam N, Utzinger U, Richards-Kortum R. Development of a Fiber Optic Probe to Measure NIR Raman Spectra of Cervical Tissue In Vivo. *Photochem Photobiol.*. 1998;68(3):427-431.
89. Pence I, Mahadevan-Jansen A. Clinical instrumentation and applications of Raman spectroscopy. *Chemical Society reviews.* 2016;45(7):1958-1979.
90. Mahadevan-Jansen A, Richards-Kortum RR. Raman spectroscopy for the detection of cancers and precancers. *J Biomed Opt.*. 1996;1(1):31-70.
91. Kanter EM, Majumder S, Vargis E, et al. Multiclass discrimination of cervical precancers using Raman spectroscopy. *Journal of Raman Spectroscopy.* 2009;40(2):205-211.
92. Kanter EM, Majumder S, Kanter GJ, Woeste EM, Mahadevan-Jansen A. Effect of hormonal variation on Raman spectra for cervical disease detection. *Am J of Obstet and Gynecol.* 2009;200(5):512.e511-512.e515.
93. Kanter EM, Vargis E, Majumder S, et al. Application of Raman spectroscopy for cervical dysplasia diagnosis. *J Biophotonics.* 2009;2(1-2):81-90.
94. Vargis E, Byrd T, Logan Q, Khabele D, Mahadevan-Jansen A. Sensitivity of Raman spectroscopy to normal patient variability. *J Biomed Opt.* 2011;16(11):117004-117004.
95. Jess PR, Smith DD, Mazilu M, Dholakia K, Riches AC, Herrington CS. Early detection of cervical neoplasia by Raman spectroscopy. *International Journal of Cancer.* 2007;121(12):2723-2728.
96. Vargis E, Tang Y-W, Khabele D, Mahadevan-Jansen A. Near-infrared Raman Microspectroscopy Detects High-risk Human Papillomaviruses. *Translational Oncology.* 2012;5(3):172.
97. Havelock J, Keller P, Muleba N, et al. Human Myometrial Gene Expression Before and During Parturition. *Biol Reprod.* 2005;72:707 - 719.
98. Lyng FM, Faoláin EÓ, Conroy J, et al. Vibrational spectroscopy for cervical cancer pathology, from biochemical analysis to diagnostic tool. *Experimental and molecular pathology.* 2007;82(2):121-129.
99. Kamemoto LE, Misra AK, Sharma SK, et al. Near-Infrared Micro-Raman Spectroscopy for< i> in Vitro</i> Detection of Cervical Cancer. *Appl Spectrosc* 2010;64(3):255-261.

100. Stone N, Kendall C, Shepherd N, Crow P, Barr H. Near-infrared Raman spectroscopy for the classification of epithelial pre-cancers and cancers. *Journal of Raman Spectroscopy.* 2002;33(7):564-573.
101. Vargis E, Brown N, Williams K, et al. Detecting Biochemical Changes in the Rodent Cervix During Pregnancy Using Raman Spectroscopy. *Ann Biomed Eng.* 2012;40(8):1814-1824.
102. Anderson J, Brown N, Mahendroo MS, Reese J. Utilization of Different Aquaporin Water Channels in the Mouse Cervix during Pregnancy and Parturition and in Models of Preterm and Delayed Cervical Ripening. *Endocrinology.* 2006;147(1):130-140.
103. Feltovich H, Ji H, Janowski JW, Delance NC, Moran CC, Chien EK. Effects of selective and nonselective PGE2 receptor agonists on cervical tensile strength and collagen organization and microstructure in the pregnant rat at term. *Am J Obstet Gynecol.* 2005;192(3):753-760.
104. Challis JR, Sloboda DM, Alfaidy N, et al. Prostaglandins and mechanisms of preterm birth. *Reproduction.* 2002;124(1):1-17.
105. Reese J, Paria BC, Brown N, Zhao X, Morrow JD, Dey SK. Coordinated regulation of fetal and maternal prostaglandins directs successful birth and postnatal adaptation in the mouse. *Proc Natl Acad Sci U S A.* 2000;97(17):9759-9764.
106. Reese J, Zhao X, Ma WG, Brown N, Maziasz TJ, Dey SK. Comparative analysis of pharmacologic and/or genetic disruption of cyclooxygenase-1 and cyclooxygenase-2 function in female reproduction in mice. *Endocrinology.* 2001;142(7):3198-3206.
107. Roizen JD, Asada M, Tong M, Tai HH, Muglia LJ. Preterm birth without progesterone withdrawal in 15-hydroxyprostaglandin dehydrogenase hypomorphic mice. *Mol Endocrinol.* 2008;22(1):105-112.
108. Sugimoto Y, Yamasaki A, Segi E, et al. Failure of parturition in mice lacking the prostaglandin F receptor. *Science.* 1997;277(5326):681-683.
109. Yellon SM, Ebner CA, Sugimoto Y. Parturition and recruitment of macrophages in cervix of mice lacking the prostaglandin F receptor. *Biol Reprod.* 2008;78(3):438-444.
110. Cabrol D, Dubois P, Sedbon E, et al. Prostaglandin E2-induced changes in the distribution of glycosaminoglycans in the isolated rat uterine cervix. *Eur J Obstet Gynecol Reprod Biol.* 1987;26(4):359-365.
111. Uldbjerg N, Ekman G, Malmstrom A, Ulmsten U, Wingerup L. Biochemical changes in human cervical connective tissue after local application of prostaglandin E2. *Gynecol Obstet Invest.* 1983;15(5):291-299.
112. Rath W, Osmers R, Adelmann-Grill BC, Stuhlsatz HW, Szevereny M, Kuhn W. Biochemical changes in human cervical connective tissue after intracervical application of prostaglandin E2. *Prostaglandins.* 1993;45(4):375-384.
113. Buhimschi IA, Dussably L, Buhimschi CS, Ahmed A, Weiner CP. Physical and biomechanical characteristics of rat cervical ripening are not consistent with increased collagenase activity. *Am J Obstet Gynecol.*. 2004;191(5):1695-1704.
114. Timmons BC, Reese J, Socrate S, et al. Prostaglandins are essential for cervical ripening in LPS-mediated preterm birth but not term or antiprogestin-driven preterm ripening. *Endocrinology.* 2014;155(1):287-298.
115. Platz-Christensen JJ, Pernevi P, Bokstrom H, Wiqvist N. Prostaglandin E and F2 alpha concentration in the cervical mucus and mechanism of cervical ripening. *Prostaglandins.* 1997;53(4):253-261.

116. Toth M, Rehnstrom J, Fuchs AR. Prostaglandins E and F in cervical mucus of pregnant women. *Am J Perinatol.* 1989;6(2):142-144.
117. Cox SM, King MR, Casey ML, MacDonald PC. Interleukin-1 beta, -1 alpha, and -6 and prostaglandins in vaginal/cervical fluids of pregnant women before and during labor. *J Clin Endocrinol Metab.* 1993;77(3):805-815.
118. Kavanagh J, Kelly AJ, Thomas J. Sexual intercourse for cervical ripening and induction of labour. *The Cochrane database of systematic reviews.* 2001(2):Cd003093.
119. Elovitz M, Mrinalini C. Animal models of preterm birth. *Trends Endocrinol Metab.* 2004;15(10):479 - 487.
120. Mahendroo M. Cervical remodeling in term and preterm birth: insights from an animal model. *Reproduction.* 2012;143(4):429-438.
121. Langenbach R, Morham SG, Tiano HF, et al. Prostaglandin synthase 1 gene disruption in mice reduces arachidonic acid-induced inflammation and indomethacin-induced gastric ulceration. *Cell.* 1995;83(3):483-492.
122. Gross GA, Imamura T, Luedke C, et al. Opposing actions of prostaglandins and oxytocin determine the onset of murine labor. *Proc Natl Acad Sci U S A.* 1998;95(20):11875-11879.
123. Herington J, O'Brien C, Brown N, Paria BC, Reese J. Timing of Embryo Implantation and Uterine Contractility Do Not Account for Delayed Parturition in Cycloxygenase-1 Knockout Mice. *Reproductive Sciences.* 2014;21(3):143A-143A.
124. Hee L. Overview of the methods available for biomechanical testing of the uterine cervix in vivo. *Acta Obstet Gynecol Scand.* 2014;93(12):1219-1237.
125. Lucovnik M, Kuon RJ, Garfield RE. Assessment of Parturition with Cervical Light-Induced Fluorescence and Uterine Electromyography. *Computational and Mathematical Methods in Medicine.* 2013;2013:6.
126. Baños A, Wolf M, Grawe C, et al. Frequency domain near-infrared spectroscopy of the uterine cervix during cervical ripening. *Lasers in Surgery and Medicine.* 2007;39(8):641-646.
127. Matzinger B, Wolf M, Banos A, Fink D, Hornung R. Optical properties, physiologic parameters and tissue composition of the human uterine cervix as a function of hormonal status. *Lasers Med Sci.* 2009;24(4):561-566.
128. Akins ML, Luby-Phelps K, Mahendroo M. Second harmonic generation imaging as a potential tool for staging pregnancy and predicting preterm birth. *J Biomed Opt.* 2010;15(2):026020.
129. Yao W, Gan Y, Myers KM, Vink JY, Wapner RJ, Hendon CP. Collagen Fiber Orientation and Dispersion in the Upper Cervix of Non-Pregnant and Pregnant Women. *PLoS One.* 2016;11(11):e0166709.
130. Rygula A, Majzner K, Marzec K, Kaczor A, Pilarczyk M, Baranska M. Raman spectroscopy of proteins: a review. *Journal of Raman Spectroscopy.* 2013;44(8):1061-1076.
131. Czamara K, Majzner K, Pacia MZ, Kochan K, Kaczor A, Baranska M. Raman spectroscopy of lipids: a review. *Journal of Raman Spectroscopy.* 2015;46(1):4-20.
132. Carey DM, Korenowski GM. Measurement of the Raman spectrum of liquid water. *The Journal of Chemical Physics.* 1998;108(7):2669-2675.

133. Lyng FM, Faoláin EÓ, Conroy J, et al. Vibrational spectroscopy for cervical cancer pathology, from biochemical analysis to diagnostic tool. *Experimental and Molecular Pathology.* 2007;82(2):121-129.
134. Mahadevan-Jansen A, Mitchell MF, Ramanujam N, Utzinger U, Richards-Kortum R. Development of a fiber optic probe to measure NIR Raman spectra of cervical tissue in vivo. *Photochem Photobiol.* 1998;68(3):427-431.
135. Kanter EM, Majumder S, Kanter GJ, Woeste EM, Mahadevan-Jansen A. Effect of hormonal variation on Raman spectra for cervical disease detection. *Am J Obstet Gynecol.* 2009;200(5):512 e511-515.
136. Duraipandian S, Zheng W, Ng J, Low JJH, Ilancheran A, Huang Z. Effect of hormonal variation on in vivo high wavenumber Raman spectra improves cervical precancer detection. 2012:82140A-82140A.
137. Duraipandian S, Zheng W, Ng J, Low JJ, Ilancheran A, Huang Z. Non-invasive analysis of hormonal variations and effect of postmenopausal Vagifem treatment on women using in vivo high wavenumber confocal Raman spectroscopy. *Analyst.* 2013;138(14):4120-4128.
138. Vargis E, Brown N, Williams K, et al. Detecting biochemical changes in the rodent cervix during pregnancy using Raman spectroscopy. *Ann Biomed Eng.* 2012;40(8):1814-1824.
139. Chakraborty I, Das SK, Wang J, Dey SK. Developmental expression of the cyclo-oxygenase-1 and cyclo-oxygenase-2 genes in the peri-implantation mouse uterus and their differential regulation by the blastocyst and ovarian steroids. *J Mol Endocrinol.* 1996;16(2):107-122.
140. Herington JL, Swale DR, Brown N, et al. High-Throughput Screening of Myometrial Calcium-Mobilization to Identify Modulators of Uterine Contractility. *PLoS One.* 2015;10(11):e0143243.
141. Lieber CA, Mahadevan-Jansen A. Automated method for subtraction of fluorescence from biological Raman spectra. *Appl Spectrosc.* 2003;57(11):1363-1367.
142. Shafer-Peltier KE, Haka AS, Fitzmaurice M, et al. Raman microspectroscopic model of human breast tissue: implications for breast cancer diagnosis in vivo. *Journal of Raman Spectroscopy.* 2002;33(7):552-563.
143. Jain R, Calderon D, Kierski PR, et al. Raman spectroscopy enables noninvasive biochemical characterization and identification of the stage of healing of a wound. *Anal Chem.* 2014;86(8):3764-3772.
144. Korhonen R, Saarakkala S. *Biomechanics and Modeling of Skeletal Soft Tissues.* 2011.
145. Rasmussen LE, Buss IO, Hess DL, Schmidt MJ. Testosterone and dihydrotestosterone concentrations in elephant serum and temporal gland secretions. *Biol Reprod.* 1984;30(2):352-362.
146. Mann A, Thompson A, Robbins N, Blomkalns AL. Localization, Identification, and Excision of Murine Adipose Depots. 2014(94):e52174.
147. Lim H, Paria BC, Das SK, et al. Multiple female reproductive failures in cyclooxygenase 2-deficient mice. *Cell.* 1997;91(2):197-208.
148. Vannuccini S, Bocchi C, Severi FM, Challis JR, Petraglia F. Endocrinology of human parturition. *Annales d'Endocrinologie.* 2016;77(2):105-113.

149. Mahendroo MS, Porter A, Russell DW, Word RA. The parturition defect in steroid 5α-reductase type 1 knockout mice is due to impaired cervical ripening. *Mol Endocrinol.* 1999;13(6):981-992.
150. Piekorz RP, Gingras S, Hoffmeyer A, Ihle JN, Weinstein Y. Regulation of progesterone levels during pregnancy and parturition by signal transducer and activator of transcription 5 and 20alpha-hydroxysteroid dehydrogenase. *Mol Endocrinol.* 2005;19(2):431-440.
151. Zeng Z, Velarde MC, Simmen FA, Simmen RC. Delayed parturition and altered myometrial progesterone receptor isoform A expression in mice null for Kruppel-like factor 9. *Biol Reprod.* 2008;78(6):1029-1037.
152. Word RA, Landrum CP, Timmons BC, Young SG, Mahendroo MS. Transgene insertion on mouse chromosome 6 impairs function of the uterine cervix and causes failure of parturition. *Biol Reprod.* 2005;73(5):1046-1056.
153. Yu Y, Cheng Y, Fan J, et al. Differential impact of prostaglandin H synthase 1 knockdown on platelets and parturition. *J Clin Invest.* 2005;115(4):986-995.
154. Chien EK, Macgregor C. Expression and regulation of the rat prostaglandin E2 receptor type 4 (EP4) in pregnant cervical tissue. *Am J Obstet Gynecol.* 2003;189(5):1501-1510.
155. Reese J, Brown N, C. Paria B, Morrow J, K. Dey S. COX-2 compensation in the uterus of COX-1 deficient mice during the pre-implantation period. *Molecular and Cellular Endocrinology.* 1999;150(1–2):23-31.
156. Tsuboi K, Sugimoto Y, Iwane A, Yamamoto K, Yamamoto S, Ichikawa A. Uterine expression of prostaglandin H2 synthase in late pregnancy and during parturition in prostaglandin F receptor-deficient mice. *Endocrinology.* 2000;141(1):315 - 324.
157. De Gelder J, De Gussem K, Vandenabeele P, Moens L. Reference database of Raman spectra of biological molecules. *Journal of Raman Spectroscopy.* 2007;38(9):1133-1147.
158. Silveira L, Silveira FL, Bodanese B, Zângaro RA, Pacheco MTT. Discriminating model for diagnosis of basal cell carcinoma and melanoma in vitro based on the Raman spectra of selected biochemicals. *J Biomed Opt.* 2012;17(7):077003-077001-077003-077011.
159. Mahadevan-Jansen A, Richards-Kortum RR. Raman spectroscopy for the detection of cancers and precancers. *J Biomed Opt.* 1996;1(1):31-70.
160. Rimmer DM. The effect of pregnancy on the collagen of the uterine cervix of the mouse. *J Endocrinol.* 1973;57(3):413-418.
161. Myers KM, Feltovich H, Mazza E, et al. The mechanical role of the cervix in pregnancy. *J Biomech.* 2015;48(9):1511-1523.
162. Myers KM, Hendon CP, Gan Y, et al. A continuous fiber distribution material model for human cervical tissue. *J Biomech.* 2015;48(9):1533-1540.
163. Bergholt MS, Zheng W, Ho KY, et al. Fiber-optic Raman spectroscopy probes gastric carcinogenesis in vivo at endoscopy. *J Biophotonics.* 2013;6(1):49-59.
164. Matousek P, Clark I, Draper E, et al. Subsurface probing in diffusely scattering media using spatially offset Raman spectroscopy. *Appl Spectrosc.* 2005;59(4):393-400.
165. Hanlon EB, Manoharan R, Koo TW, et al. Prospects for in vivo Raman spectroscopy. *Physics in Medicine and Biology.* 2000;45(2):R1-59.
166. Friedman EA, Kroll BH. Computer analysis of labor progression. 3. Pattern variations by parity. *J Reprod Med.* 1971;6(4):179-183.
167. Vahratian A, Hoffman MK, Troendle JF, Zhang J. The impact of parity on course of labor in a contemporary population. *Birth.* 2006;33(1):12-17.

168. Harper LM, Caughey AB, Odibo AO, Roehl KA, Zhao Q, Cahill AG. Normal progress of induced labor. *Obstet Gynecol.* 2012;119(6):1113-1118.
169. Petersen LK, Uldbjerg N. Cervical collagen in non-pregnant women with previous cervical incompetence. *Eur J Obstet Gynecol Reprod Biol.* 1996;67(1):41-45.
170. Ovesen P, Rasmussen S, Kesmodel U. Effect of prepregnancy maternal overweight and obesity on pregnancy outcome. *Obstet Gynecol.* 2011;118(2 Pt 1):305-312.
171. Vahratian A, Zhang J, Troendle JF, Savitz DA, Siega-Riz AM. Maternal prepregnancy overweight and obesity and the pattern of labor progression in term nulliparous women. *Obstet Gynecol.* 2004;104.
172. Gauthier T, Mazeau S, Dalmay F, et al. Obesity and cervical ripening failure risk. *The journal of maternal-fetal & neonatal medicine* 2012;25(3):304-307.
173. Lassiter JR, Holliday N, Lewis DF, Mulekar M, Abshire J, Brocato B. Induction of labor with an unfavorable cervix: how does BMI affect success? *The Journal of Maternal-Fetal & Neonatal Medicine.* 2016;29(18):3000-3002.
174. Carlson NS, Hernandez TL, Hurt KJ. Parturition dysfunction in obesity: time to target the pathobiology. *Reproductive Biology and Endocrinology.* 2015;13(1):135.
175. Qian X, Jiang Y, Liu L, Shi SQ, Garfield RE, Liu H. Changes in ectocervical surface area in women throughout pregnancy compared to non-pregnant and postpartum states. *The journal of maternal-fetal & neonatal medicine* 2016;29(22):3677-3681.
176. Mo J, Zheng W, Low JJ, Ng J, Ilancheran A, Huang Z. High wavenumber Raman spectroscopy for in vivo detection of cervical dysplasia. *Analytical Chemistry-Columbus.* 2009;81(21):8908.
177. Duraipandian S, Zheng W, Ng J, Low JJ, Ilancheran A, Huang Z. In vivo diagnosis of cervical precancer using Raman spectroscopy and genetic algorithm techniques. *Analyst.* 2011;136(20):4328-4336.
178. Duraipandian S, Zheng W, Ng J, Low JJ, Ilancheran A, Huang Z. Simultaneous fingerprint and high-wavenumber confocal raman spectroscopy enhances early detection of cervical precancer in vivo. *Analytical chemistry.* 2012;84(14):5913-5919.
179. Krishna CM, Prathima N, Malini R, et al. Raman spectroscopy studies for diagnosis of cancers in human uterine cervix. *Vibrational Spectroscopy.* 2006;41(1):136-141.
180. Shaikh R, Dora TK, Chopra S, et al. In vivo Raman spectroscopy of human uterine cervix: exploring the utility of vagina as an internal control. *J Biomed Opt.* 2014;19(8):087001.
181. Liang K-Y, Zeger SL. Longitudinal data analysis using generalized linear models. *Biometrika.* 1986;73(1):13-22.
182. Hanley JA, Negassa A, Edwardes MD, Forrester JE. Statistical analysis of correlated data using generalized estimating equations: an orientation. *American journal of epidemiology.* 2003;157(4):364-375.
183. Vargis E, Byrd T, Logan Q, Khabele D, Mahadevan-Jansen A. Sensitivity of Raman spectroscopy to normal patient variability. *J Biomed Opt.* 2011;16(11):117004.
184. Mandair GS, Morris MD. Contributions of Raman spectroscopy to the understanding of bone strength. *BoneKEy Rep.* 2015;4.
185. Gasior-Glogowska M, Komorowska M, Hanuza J, Ptak M, Kobielarz M. Structural alteration of collagen fibres--spectroscopic and mechanical studies. *Acta of bioengineering and biomechanics.* 2010;12(4):55-62.

186. Koyama Y, Takatsuka I, Nakata M, Tasumi M. Raman and infrared spectra of the all-trans, 7-cis, 9-cis, 13-cis and 15-cis isomers of β-carotene: Key bands distinguishing stretched or terminal-bent configurations form central-bent configurations. *Journal of Raman Spectroscopy.* 1988;19(1):37-49.
187. Hata TR, Scholz TA, Pershing LK, et al. Non-Invasive Raman Spectroscopic Detection of Carotenoids in Human Skin. *J Invest Dermatol.* 2000;115(3):441-448.
188. Wendremaire M, Goirand F, Barrichon M, Lirussi F, Peyronel C, Dumas M. Leptin prevents MMP activation in an in vitro model of myometrial inflammation. *Fundam Clin Pharmacol.* 2012;26.
189. Wendremaire M, Mourtialon P, Goirand F, Lirussi F, Barrichon M, Hadi T. Effects of leptin on lipopolysaccharide-induced remodeling in an in vitro model of human myometrial inflammation. *Biol Reprod.* 2013;88.
190. Wendremaire M, Bardou M, Peyronel C, Hadi T, Sagot P, Morrison JJ. Effects of leptin on lipopolysaccharide-induced myometrial apoptosis in an in vitro human model of chorioamnionitis. *Am J Obstet Gynecol.* 2011;205.
191. Lui H, Zhao J, McLean D, Zeng H. Real-time Raman spectroscopy for in vivo skin cancer diagnosis. *Cancer Res.* 2012;72(10):2491-2500.
192. Bergholt MS, Zheng W, Ho KY, et al. Fiberoptic confocal raman spectroscopy for real-time in vivo diagnosis of dysplasia in Barrett's esophagus. *Gastroenterology.* 2014;146(1):27-32.
193. Thekkek N, Richards-Kortum R. Optical Imaging for Cervical Cancer Detection: Solutions for a Continuing Global Problem. *Nature reviews Cancer.* 2008;8(9):725-731.
194. Orfanoudaki IM, Kappou D, Sifakis S. Recent advances in optical imaging for cervical cancer detection. *Arch Gynecol Obstet.* 2011;284(5):1197.
195. Bates CK, Carroll N, Potter J. The challenging pelvic examination. *Journal of general internal medicine.* 2011;26(6):651-657.
196. Sandelowski M. This Most Dangerous Instrument Propriety, Power, and the Vaginal Speculum. *Journal of Obstetric, Gynecologic & Neonatal Nursing.*29(1):73-82.
197. Rossmann JS. Built to spec?: The vaginal speculum as a case study of inadequate design. Ambidextrous; 2008.
198. Asiedu MN, Agudogo J, Krieger MS, et al. Design and preliminary analysis of a vaginal inserter for speculum-free cervical cancer screening. *Plos one.* 2017;12(5):e0177782.
199. Lam CT, Krieger MS, Gallagher JE, et al. Design of a novel low cost point of care tampon (POCkeT) colposcope for use in resource limited settings. *PloS one.* 2015;10(9):e0135869.
200. Gardner R, Raemer DB. Simulation in Obstetrics and Gynecology. *Obstetrics and Gynecology Clinics of North America.* 2008;35(1):97-127.
201. Bland JM, Altman D. Statistical methods for assessing agreement between two methods of clinical measurement. *The lancet.* 1986;327(8476):307-310.
202. Organization WH. Guidelines for screening and treatment of precancerous lesions for cervical cancer prevention. WHO guidelines. 2015.
203. Sutton EF, Cain LE, Vallo PM, Redman LM. Strategies for Successful Recruitment of Pregnant Patients Into Clinical Trials. *Obstet Gynecol.* 2017;129(3):554-559.
204. Obstetricians ACo, Gynecologists. Medically indicated late-preterm and early-term deliveries. ACOG Committee opinion no. 560. *Obstet Gynecol.* 2013;121:908-910.

205. Doldan A, Otis CN, Pantanowitz L. Adipose tissue: a normal constituent of the uterine cervical stroma. *Int J Gynecol Pathol.* 2009;28(4):396-400.
206. Makowski AJ, Patil CA, Mahadevan-Jansen A, Nyman JS. Polarization control of Raman spectroscopy optimizes the assessment of bone tissue. *J Biomed Opt.* 2013;18(5):55005.
207. Wang J, Bergholt MS, Zheng W, Huang Z. Development of a beveled fiber-optic confocal Raman probe for enhancing in vivo epithelial tissue Raman measurements at endoscopy. *Optics letters.* 2013;38(13):2321-2323.
208. Hendler I, Goldenberg RL, Mercer BM, et al. The Preterm Prediction study: Association between maternal body mass index and spontaneous and indicated preterm birth. *Am J Obstet Gynecol.* 2005;192(3):882-886.
209. Frey HA, Klebanoff MA. The epidemiology, etiology, and costs of preterm birth. *Seminars in Fetal and Neonatal Medicine.* 2016;21(2):68-73.
210. Harkness ML, Harkness R. Changes in the physical properties of the uterine cervix of the rat during pregnancy. *The Journal of physiology.* 1959;148(3):524-547.
211. Timmons BC, Reese J, Socrate S, et al. Prostaglandins Are Essential for Cervical Ripening in LPS-Mediated Preterm Birth But Not Term or Antiprogestin-Driven Preterm Ripening. *Endocrinology.* 2013:en. 2013-1304.